Microfluidics for Electrochemical Energy Conversion

Omar A. Ibrahim[a,b], Marina Navarro-Segarra[c], Pardis Sadeghi[a], Neus Sabate[c,d], Juan Pablo Esquivel[c,e,f], Erik Kjeang[a*]

[a] Fuel Cell Research Lab., School of Mechatronic Systems Engineering, Simon Fraser University, V3T 0A3, Surrey, BC, Canada

[b] Fuelium S.L., Edifici Eureka. Av. Can Domènech S/N. 08193 Bellaterra, Barcelona, Spain

[c] Instituto de Microelectrónica de Barcelona, IMB-CNM (CSIC), C/ dels Til·lers sn, Campus UAB, 08193 Bellaterra Barcelona, Spain

[d] Catalan Institution for Research and Advanced Studies (ICREA), Passeig Lluís Companys 23, 08010 Barcelona, Spain

[e] BCMaterials, Basque Centre for Materials, Applications and Nanostructures, UPV/EHU Science Park, 48940 Leioa, Spain

[f] IKERBASQUE, Basque Foundation for Science, 48009 Bilbao, Spain

[*]Corresponding Author: Dr. Erik Kjeang – ekjeang@sfu.ca

Abstract

Electrochemical energy conversion is an important supplement for storage and on-demand use of renewable energy. In this regard, microfluidics offers prospects to raise the efficiency and rate of electrochemical energy conversion through enhanced mass transport, flexible cell design, and ability to eliminate the physical ion-exchange membrane, an essential yet costly element in conventional electrochemical cells. Since the 2002 invention of the microfluidic fuel cell, the research field of *microfluidics for electrochemical energy conversion* has expanded into a great variety of cell designs, fabrication techniques, and device functions with a wide range of utility and applications. The present review aims to comprehensively synthesize the best practices in this field over the past 20 years. The underlying fundamentals and research methods are first summarized, followed by a complete assessment of all research contributions wherein microfluidics was proactively utilized to facilitate energy conversion in conjunction with electrochemical cells, such as fuel cells, flow batteries, electrolysis cells, hybrid cells, and photoelectrochemical cells. Moreover, emerging technologies and analytical tools enabled by microfluidics are also discussed. Lastly, opportunities for future research directions and technology advances are proposed.

Table of Contents:

1 - Introduction

Access to affordable, on-demand energy is a cornerstone of modern society. It facilitates technological progress and enables development of products and services which can greatly enhance our quality of life. Despite encouraging technological progress, the global energy supply is still dominated by fossil fuels such as coal and petroleum, which are the main underlying factor for climate change and many other forms of environmental degradation.[1] Renewable sources of electrical energy (*e.g.*, solar and wind) with zero harmful greenhouse gas emissions and renewable or hydrogen-based fuels are quoted to be a necessary turning point in the history of energy[2] towards the goal of net zero emissions by 2050.[3] Given the recent cost reduction trajectory of such sustainable-energy technologies, it is envisaged that the first (*i.e.*, inventing coal-fired steam engines) and second (*i.e.*, switching from coal to petroleum) energy revolutions will soon be followed by a third energy revolution based on green energy. It is notable however that mass adoption of renewable energy will not only require new and improved technologies for energy harvesting but also a variety of new forms of energy storage and transport in order to accommodate the intermittency of the sources and the delivery to the user.

Electrochemical energy storage and conversion[4] is a viable solution to this dilemma, as it facilitates conversion of electricity into chemical energy that can be stored, transported, and used on demand. In an electrochemical cell, electrons extracted through oxidation at one electrode are balanced by reduction at the other electrode, thus facilitating energy conversion between electrical and chemical forms. Electrochemical devices have been developed across a wide range of power and energy scales; departing from button cells and conventional alkaline batteries that power portable electronic devices, lithium-ion batteries and fuel cells designed for transportation, up to large-scale electrolyzers and redox flow batteries, being actively developed for stationary energy conversion and storage. The latter cells are also progressively being considered for energizing a variety of small-scale devices. In recent history, the energy needs of portable electronic devices have created a significant demand for conventional batteries, which benefit from electrochemical technologies originating from the 1800s. The introduction of the lithium-ion battery in 1991 is undoubtedly a major breakthrough in battery technology advancement and is currently the norm within the consumer-electronics market. However, its dependence on critical raw materials currently represents one of the major challenges to be solved for their wide-spread implementation in e-mobility and large-scale energy storage applications. In this sense, fuel cells and flow batteries have emerged as a suitable complement to lithium-ion cells for a variety of reasons, most notably the practical scalability achieved by energy storage in liquid or gaseous fluids. Their growing popularity also stems from the notion that their energy capacity (which is a function of reactant volume) and power (which is a function of electrode

surface area) can be decoupled and independently tuned through the flow of energy carrying fluids. Fluid mechanics is thus a critical requirement for the function and performance of these devices.

Microfluidics[5] is the science of manipulating minute amounts of fluids in small conduits having at least one sub-millimeter dimension, *i.e.*, the thickness of a human hair. The technology spans a wide range of applications from early developments of inkjet printing, chromatography, and biological analyses to more recent advances on diagnostics, pharmaceutical synthesis, and soft robotics.[6] Microfluidics is nature's way of facilitating mass transport in conjunction with biological processes. For example, the water supply for photosynthesis in plants and nutrient supply within the human body rely on microfluidics through capillary- and pressure-driven flow, respectively. Evolution has optimized these processes based on microfluidic principles as the most effective means of mass transport to reactive sites. By the same token, microfluidics is the ideal tool for efficient mass transport within electrochemical cells. The emergence of microfluidics as a research field has therefore enabled tremendous opportunities for improved electrochemical energy conversion, which is the focus of this review. In this context, microfluidics provides convective mass transport at much higher rates than purely diffusive processes such as those encountered in solid state batteries. Electrochemical reactions also benefit from the intrinsically high surface-area-to-volume ratio of microfluidic systems compared to larger conduits. Furthermore, microfluidics may offer other benefits for electrochemical energy conversion devices such as precise flow control, selective species manipulation to desired locations, optimal thermodynamic equilibrium, and the possibility of pressurized operation, thus improving efficiency and power density.

The new research field of *microfluidics for electrochemical energy conversion* was first created with the pioneering invention of the co-laminar microfluidic fuel cell in 2002,[7,8] wherein microfluidics was used to control reactant flows in a membrane-less cell architecture. More generally, fluid flow at low Reynolds numbers has enabled the design of co-laminar electrochemical flow cells which eliminate the need for a physical ion-exchange membrane — an essential but costly component of conventional electrochemical cells.[9] The progress on microfluidic fuel cells was first reviewed by Kjeang *et al.* in 2009.[10] Similarly, the evolution of co-laminar flow cells was reviewed in 2014.[11,12] Since then, this field of research has expanded significantly into a greater variety of microfluidic cell designs and functions, with utility and application in a wide range of energy conversion devices and systems. Although certain portions of these advances have been reviewed elsewhere,[13–16] there is currently a lack of a more comprehensive review that covers all aspects of microfluidics-enhanced or microfluidics-facilitated electrochemistry for energy systems. The objective of the present review article is therefore to portray a complete picture of the advantages and opportunities created using microfluidics for electrochemical energy conversion. The review covers all research contributions to date wherein microfluidics was

proactively utilized in conjunction with electrochemical cells to facilitate energy conversion. In terms of devices, this includes fuel cells, flow batteries, electrolysis cells, hybrid cells, and other emerging devices. The main purpose of this review is to synthesize the best practices from the past 20 years of research in this field, and to inform the research community on the potential future use of microfluidics for enhanced electrochemical energy conversion as a core technological component of the impending renewable energy transition. The review is structured as follows. Section 2 describes the essential fundamental theory of electrochemical cells, mass transfer, and microfluidics, whereas Section 3 outlines appropriate methods for cell design, fabrication, and experimentation. Key contributions to this field are summarized in Section 4. Opportunities for further research and technology outlook are discussed in Section 5.

2 - Fundamentals

2.1 Electrochemical Cells for Energy Conversion

Electrochemistry is a branch of physical chemistry which studies chemical species and their reactions at the interface between an electronic conductor (electrode) and an ionic conductor (electrolyte). Devices in which such reactions take place are called electrochemical cells.[17] They normally comprise of two electrodes**,** an electrolyte, and an external load-carrying circuit as their main components. In electrochemical cells, the chemical reactions are of oxidation-reduction type wherein the electrons extracted from a species undergoing oxidation at one electrode are balanced by the uptake of electrons of a species undergoing reduction at the other electrode. Common examples are 1.5-volt dry cells and lithium-ion batteries which are widely used for consumer electronics. Other types of electrochemical cells used for energy conversion include fuel cells, electrolysis cells, and flow batteries which, unlike dry cells, rely on continuous flow of reactants, products, and/or electrolytes for their functioning.[18] These cells, commonly referred to as *flow cells*, have a wide variety of potential utility ranging from small-scale electronics such as diagnostic kits to transportation and grid-scale energy storage.[19] Flow cells can function galvanically in order to generate electricity or electrolytically in order to regenerate the reactants by simply reversing the redox reactions. In *galvanic* mode, spontaneous reactions occur at the electrodes that convert chemical energy from the reactants into electrical energy. By contrast, in *electrolytic* mode, electrochemical reactions are initiated by the application of an external voltage to generate or re-generate chemical species of higher enthalpy. In both modes, the flow of electronic current through the electrodes is balanced by a simultaneous flow of ionic current through the electrolyte to satisfy conservation of charge within the cell. Figure 1 shows a generalized electrochemical cell, featuring two electrodes separated by an ion-conductive membrane or liquid

electrolyte. The electrodes can be made of inert, conductive materials such as carbon fibers with optional electrocatalysts. For such electrodes, the charge is normally stored in the electrolytes or liquid/gas reactants, as in most flow batteries and electrolyzers. Alternatively, the electrode may itself embody reactant or product species, which is the case of metal-air cells and hybrid flow-batteries, among others, as reported in the review by Soloveichik.[20]

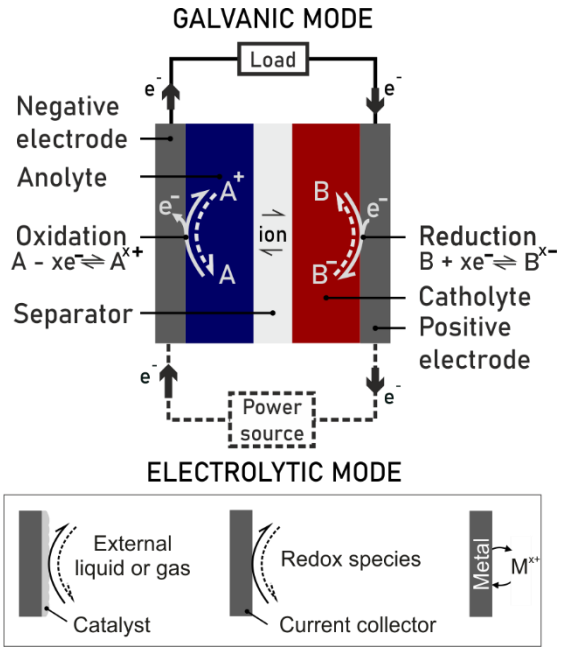

Figure 1: A general schematic of an electrochemical cell, showing its main components and possible electrode configurations. The flow of charge is shown for both galvanic (solid lines) and electrolytic (dashed lines) modes, whereas the naming convention is based on galvanic mode.

In generic form, the electrochemical reactions which take place at the surface of the electrodes in a typical flow cell can be written as:

$$\text{Negative half-cell: } \boldsymbol{A^{m+} \rightleftharpoons A^{(m+x)+} + xe^{-}} \quad (1)$$

$$\text{Positive half-cell: } \boldsymbol{B^{n+} + xe^{-} \rightleftharpoons B^{(n-x)+}} \quad (2)$$

The reversible equilibrium potential of the redox couple in each half-cell, $\boldsymbol{E_r}$, can be determined according to the Nernst equation:

$$\boldsymbol{E_r = E^0 - \frac{\bar{R}T}{zF} ln\left[\frac{\Pi\, a_{products}^{\nu_i}}{\Pi\, a_{reactants}^{\nu_i}}\right]} \quad (3)$$

where $\boldsymbol{\bar{R}}$ is the universal gas constant, $\boldsymbol{T}$ is the temperature, $\boldsymbol{z}$ is the number of electrons transferred per molecule, $\boldsymbol{F}$ is Faraday's constant, and $\boldsymbol{a}$ is the activity of each species by its corresponding stoichiometric coefficient, $\boldsymbol{\nu_i}$. In this equation, $\boldsymbol{E^0}$ is the *standard-state* (*i.e.*, thermodynamically determined) electrode potential, which is related to the Gibbs free energy, $\boldsymbol{\Delta G}$, as:

$$E^0 = -\frac{\Delta G}{zF} \tag{4}$$

The reversible cell potential can then be obtained as:

$$E_{cell} = E_c - E_a \tag{5}$$

where subscripts c and a refer to the cathode and anode, respectively. Similarly, the open-circuit voltage (OCV) of the cell, commonly denoted as E_{OCV}, is the measured potential difference between the two electrodes when no electric current is drawn or supplied. It represents the maximum voltage a cell can generate in galvanic mode, and conversely, the minimum voltage which must be supplied to charge the cell in electrolytic mode. As a thermodynamic system, flow cells are subjected to various irreversibilities that arise from the different transport processes involved, namely mass, momentum, and charge transport. As a result, flow cells operate at potentials significantly different from their reversible potentials. This difference between actual potential and reversible potential is called overpotential. While in a galvanic cell, overpotential means that less energy is recovered than thermodynamically determined, in an electrolytic cell it means more energy must be supplied to drive a redox reaction. In both cases, the missing or extra energy is lost as heat. The relationship between cell voltage and electric current is called polarization or performance curve. Figure 2 shows a typical polarization curve in galvanic mode. The actual cell voltage is seen to be significantly lower than the reversible (or ideal) cell potential in this mode of operation. As mentioned above, irreversibities are responsible for this drop in potential. There are four main sources for potential loss of an electrochemical cell as listed below and detailed in Figure 2:

1. **Activation overpotential** due to irreversibility in the reaction kinetics at both electrodes (η_A). Activation losses are significant for electrochemical reactions with slow to moderate kinetics and can be reduced through appropriate electrocatalyst selection. This type of loss is more important at low current densities and is a non-linear function of current density.
2. **Ohmic overpotential** due to ohmic resistance of the electrodes to the mobility of electrons and the resistance of electrolytes to the transport of ions (η_R). The resistance of connectors, terminals, and wirings also contribute to this loss. The ohmic loss is a linear function of current density.
3. **Mass transport overpotential** due to mass transport limitations at both electrodes (η_M). This loss occurs when the reaction rate approaches the maximum rate of reactant (or product) transport to (or from) the active sites. In practice, this phenomenon gives rise to depletion of reactants or accumulation of products at the surface of the electrode. This type of loss varies non-linearly with current density.

4. **OCV overpotential** due to mixed potential arising from reactant crossover to the opposite electrode, current leakage, catalyst impurities, and other parasitic losses. Such losses are often collectively denoted by $\boldsymbol{\eta_x}$.

The net effect of all these losses is a cell voltage departure from the thermodynamically predicted value ($\boldsymbol{E^0}$) according to:

$$\boldsymbol{E_{Cell} = E_r \pm (|\eta_A| + |\eta_R| + |\eta_M| + |\eta_x|)} \quad (6)$$

where the losses are subtracted for galvanic mode and added for electrolytic mode.

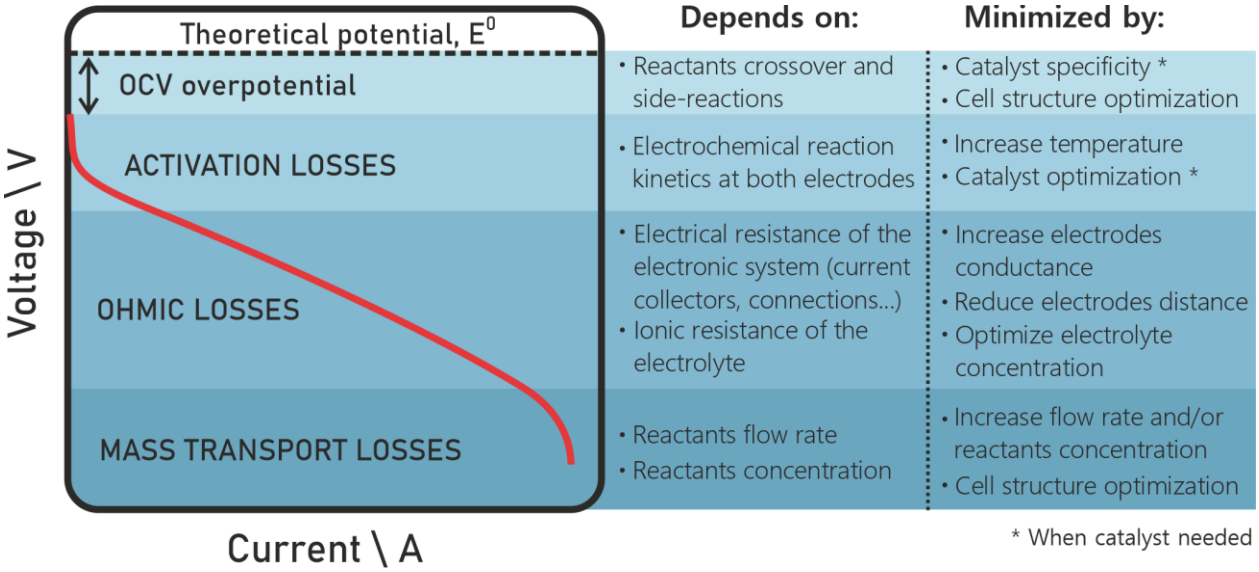

Figure 2: Flow cell polarization curve in galvanic mode indicating sources of overpotential and performance losses.

2.2 Mass Transfer Phenomena

Understanding the relevant mass transfer phenomena is of crucial importance for design and optimization of electrochemical cells. This is because for the reactions to take place at the surface of the electrode, for instance at the internal surfaces of a porous electrode, each reactant species must first diffuse from the bulk medium to the active surface. Based on thin-film theory of mass transfer, a species suspended in the bulk fluid can reach the active surface by diffusing through a thin layer of fluid adjacent to the surface. The theory then asserts that the rate of species transfer from the bulk fluid to the surface of the electrode is proportional to the specific surface area of the electrode, $\boldsymbol{a}$, and the difference in concentration between the bulk fluid and the surface of the electrode. Therefore, for each species, $\boldsymbol{i}$;

$$\boldsymbol{\mathcal{R} = aK_m(c^s - c^b)} \quad (7)$$

where $\mathcal{R}$ is the rate of reaction, K_m is the mass transfer coefficient for each species, and c is the concentration of the respective species with superscripts s and b denoting surface and bulk values, respectively. This equation is valid for both stationary and moving fluids with the difference being that for the former case, K_m is a constant while for the latter case it is an increasing function of the Reynolds number (see Section 2.3).

For dilute systems, the net molar flux (N) of a species (i) is the sum of the contributions from advection, diffusion, and migration, as described by the Nernst-Planck equation. The electrolyte potential is a function of the charge density and concentration of ions, as represented by the Poisson equation. The generalized Nernst-Planck-Poisson equations for species transport in microfluidic electrochemical cells can thus be written as:

$$N_i = c_i u - D_i \vec{\nabla} c_i - z_i \frac{F}{RT} D_i c_i \vec{\nabla} \varphi \tag{8a}$$

$$\nabla^2 \varphi = -\frac{F}{\varepsilon_P} \sum_i z_i c_i \tag{8b}$$

where u is the velocity field, D is the diffusion coefficient of each species (i), φ is the electrolyte potential, and ε_P is the permittivity. The local current density, j, generated by the electrochemical reactions, can be described by the Butler-Volmer equation (Eq. 9) of electrochemical kinetics. This equation, which is one of the most fundamental relationships in the field of electrochemistry, relates the electrical current of an electrode to the voltage difference between the electrode and the bulk electrolyte at their interface, together with several other parameters such as the bulk and surface concentrations of the species. Considering that simultaneous oxidation (denoted by subscript o) and reduction (denoted by subscript r) reactions are occurring on the same electrode, the equation contains two terms for forward and reverse current:

$$j = j_0 \left[\frac{c_o^s}{c_o^b} exp\left(\frac{-\alpha z F}{RT} \eta_A \right) - \frac{c_r^s}{c_r^b} exp\left(\frac{(1-\alpha) z F}{RT} \eta_A \right) \right] \tag{9}$$

where j_0 is the exchange current density and α is the charge transfer coefficient. It shall be understood that one can enter the electrochemical reaction as either a boundary condition or source term, depending on the electrode configuration. For each electrode, the reaction current density is related to the ionic current density in the electrolyte via Ohm's law:

$$\nabla \cdot \vec{i}_f = \sigma_f \nabla^2 \varphi_f = \mathcal{R} = aj \tag{10}$$

From conservation of charge, we also have:

$$\nabla \cdot \vec{i}_s = \sigma_s \nabla^2 \varphi_s = -\nabla \cdot \vec{i}_f \tag{11}$$

where $\vec{\boldsymbol{\imath}}$ is the current density vector, $\boldsymbol{\sigma}$ is the ionic or electrical conductivity, and $\boldsymbol{\varphi}$ is the potential with subscripts $\boldsymbol{f}$ and $\boldsymbol{s}$ referring to the fluid and solid phases, respectively. For porous electrodes, the physical properties of the fluid occupying the pores are corrected for by the porosity of the electrode, $\boldsymbol{\varepsilon}$ by applying the Bruggeman correction. For example, the *effective* diffusion coefficient, $\boldsymbol{D_{eff}}$ is obtained by:[21]

$$\boldsymbol{D_{eff} = \varepsilon^{3/2} D} \tag{12}$$

The obtained set of partial differential equations can be solved numerically, subject to appropriate initial and boundary conditions for the concentration and potential fields. For a given cell voltage, the corresponding current density can be calculated to construct a complete polarization curve for the cell.

2.3 Microfluidics

Microfluidics is the science of manipulating minute amounts of fluids in networks of tiny channels with at least one sub-millimeter dimension.[5] In recent years, it has emerged as an active field of research owing to its application in many branches of science and technology. Like macro-channels, steady-state flow is governed by the continuity (Eq. 13a) and Navier-Stokes (Eq. 13b) equations which represent conservation of mass and momentum, respectively. However, the gravitational body force and the inertial force terms are generally neglected in microfluidic flow regime problems. Thus, for incompressible fluids and iso-thermal flows, the momentum equations can be reduced to Stokes equations (Eq. 13c):[22]

$$\boldsymbol{\nabla \cdot \vec{u} = 0}, \tag{13a}$$

$$\boldsymbol{\rho\left((u.\vec{\nabla})u\right) = -\vec{\nabla}p + \mu\nabla^2 u + \vec{f}_g + \vec{f}_e}, \tag{13b}$$

$$\boldsymbol{0 = -\vec{\nabla}p + \mu\nabla^2 u + \vec{f}_e} \tag{13c}$$

where $\boldsymbol{\rho}$ is the density of the fluid, $\boldsymbol{p}$ is the thermodynamic pressure, $\boldsymbol{\mu}$ is the dynamic viscosity, $\vec{\boldsymbol{f}}_{\boldsymbol{g}}$ represents the gravitational body force density, and $\vec{\boldsymbol{f}}_{\boldsymbol{e}}$ represents the electrostatic body force density. The latter term may be dropped from the momentum equations (Eq. 13c) on the account that electro-neutrality approximation holds throughout the electrolyte domain. Lastly, the momentum equations written in this form are used for micro-channels. However, when dealing with porous material (*e.g.*, flow-through electrodes), Darcy's equation should be used instead:

$$\boldsymbol{\vec{\nabla}p = -\frac{\mu}{k}\nabla u} \tag{14}$$

where $\boldsymbol{k}$ is the permeability of the porous medium. Note that in either form, the momentum equations are valid only for laminar flows, where dynamic viscosity is adequate to represent momentum transfer between fluid layers. Fortunately, flow in microfluidic systems is often realized to be laminar, as the Reynolds number in micro-channels is normally much smaller than the critical Reynolds number for

transition to turbulence. For duct flow, the critical Reynolds number is ~2,000, where the Reynolds number (*i.e.*, the ratio between inertial to viscous forces) is defined as:

$$\boldsymbol{Re} = \frac{\boldsymbol{\rho U d_h}}{\boldsymbol{\mu}} \tag{15}$$

where $\boldsymbol{U}$ is the mean velocity and $\boldsymbol{d_h}$ is the hydraulic diameter. Since laminar flow is dominated by viscous forces, it is important to estimate the flow resistance arising from shear stress and estimate the necessary pumping power. The flow resistance depends on fluid properties and channel dimensions. For example, for a rectangular microchannel, the flow resistance ($\boldsymbol{R_h}$) can be estimated as a function of the channel length ($\boldsymbol{L}$), width ($\boldsymbol{W}$), and height ($\boldsymbol{H}$), according to Eq. 16. Other external flow resistances such as fittings and tubing also need to be overcome by the pumping system. The pumping power can be estimated by multiplying the pressure drop by the flow rate ($\boldsymbol{Q}$) or by multiplying the overall flow resistance by the square of the flow rate ($\boldsymbol{P_{pump} = \Delta P\, Q = R_h\, Q^2}$), resembling an equivalent circuit model.

$$\boldsymbol{R_h} = \frac{\boldsymbol{12\mu L}}{\boldsymbol{H^3 W}} \left(\frac{\boldsymbol{1}}{\boldsymbol{1 - 0.63\left(H/W\right)}} \right) \tag{16}$$

In flow-through fibrous electrodes, the fiber diameter, $\boldsymbol{d_f}$ and intrinsic velocity, $\boldsymbol{U_f}$ are often used in the definition of the Reynolds number. In such electrodes, the Reynolds number together with the Schmidt number closely control mass transfer of species from the bulk electrolyte to the surface of the fibers. The Schmidt number represents the ratio of momentum diffusion to mass diffusion; that is:

$$\boldsymbol{Sc} = \frac{\boldsymbol{\nu}}{\boldsymbol{D}} \tag{17}$$

where $\boldsymbol{\nu}$ is the kinematic viscosity. The dimensionless mass transfer coefficient, also known as the Sherwood number, correlates with ***Re*** and ***Sc*** as follows:[23]

$$\boldsymbol{Sh} = \frac{\boldsymbol{K_m d_f}}{\boldsymbol{D}} = \boldsymbol{m + n\, Re^{\gamma_1} \cdot Sc^{\gamma_2}} \tag{18}$$

where $\boldsymbol{m}$, $\boldsymbol{n}$, γ_1, and γ_2 are empirical parameters.

A key feature of microfluidic systems is that, in addition to being laminar, their Reynolds number is well within the creeping flow limit. Under this condition, all convective inertial terms can be dropped from the Navier-Stokes equations, thereby dramatically simplifying these equations. With non-linear convective terms dropped from the equations of motion, the interface between two fluid layers remains flat (*i.e.*, stable), provided the two fluids have the same density and viscosity. Otherwise, exponentially growing interfacial waves may emerge at the interface, which can give rise to unwanted chaotic mixing between two liquid streams. This feature of creeping flow has been embraced in

microfluidic flow cells as it implies that a physical membrane may not be required to separate anolyte and catholyte streams. At the resulting fluid-fluid interface, as shown in Figure 3, mixing is controlled by cross-stream diffusion rather than advection. Fortunately, since diffusion is a relatively slow process, the thickness of the interfacial diffusion layer generally remains within a tolerable range. With the anolyte and catholyte flowing co-laminarly (*i.e.*, side-by-side) in a stable flow configuration, ions can be exchanged at the interface between the two streams whilst curbing reactant crossover. To ensure that crossover is avoided, the residence time of the reactants in the electrochemical zone, $\boldsymbol{t_{res} = L/U}$ where $\boldsymbol{L}$ is the length of the electrode, must be shorter than their diffusion time, $\boldsymbol{t_{dif}}$ across the interface, which correlates with the thickness of the diffusion layer, $\boldsymbol{\delta = \sqrt{Dt_{dif}}}$. To avoid fuel crossover, $\boldsymbol{\delta}$ should be less than the width of the channel, $\boldsymbol{W}$, *i.e.*:

$$\boldsymbol{t_{res} < t_{dif} \Rightarrow \frac{L}{U} < \frac{W^2}{D}} \tag{19}$$

The ratio of residence and diffusion times is related to the Peclet number, ***Pe***, which is defined by the ratio of convective to diffusive mass transport. Assuming that ***W*** and ***L*** are of the same order for the channel depicted in Figure 3, the Peclet number can be defined as:

$$\boldsymbol{Pe = \frac{UL}{D}}. \tag{20}$$

For sufficiently large Peclet numbers (***Pe >> 1***), heterogeneous crossover can be ignored. However, certain bulk chemical reactions may still occur near the interface.

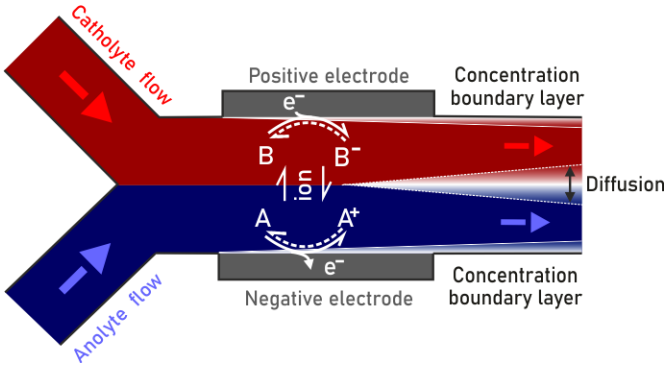

Figure 3. Schematic representation of a microfluidic flow cell. The electrolyte naming convention is based on galvanic mode (microfluidic fuel cell).

Figure 3 also illustrates the formation of concentration boundary layers or reactant depletion layers at the surface of each electrode. This is caused by rapid electrochemical kinetics while having mass transport limitations.[12]

2.4 Paper-Based Systems

Evidently, eliminating the need for a physical membrane was a design breakthrough that motivated the development of microfluidic flow cells. Another breakthrough in design was the introduction of self-primed, paper-based systems which eliminate the need for mechanical pumps to drive the flow through the microchannels. Paper-based systems rely on capillary forces for establishing the flow of electrolytes using the wicking effect of porous materials. The wicking force is created by a pressure imbalance at the curved interface between two immiscible fluids (*e.g.*, air/water) causing the wetting fluid (water) to displace the non-wetting fluid (air). Similarly, most liquid electrolytes used in electrochemical flow cells can readily be imbibed by cellulosic papers through capillary action. For this reason, paper-based systems are increasingly being considered for use in microfluidic flow cells.[24] The amount of liquid imbibed by a porous medium can be estimated using the Lucas-Washburn method.[25,26] They experimentally showed that the time-evolution of capillary rise, $\boldsymbol{L}$ of a liquid into an empty capillary tube scales as $\boldsymbol{L(t) = \sqrt{D \times t}}$, where the diffusion coefficient depends on the properties of the penetrating fluid and the capillary tube. To theoretically model this phenomenon, they started from the Poiseuille equation in pipe flow and replaced the driving pressure, $\boldsymbol{\Delta p}$, by the capillary pressure, $\boldsymbol{p_c}$:

$$\boldsymbol{Q(t) = \frac{\pi {d_c}^4}{128\mu}\frac{\Delta p}{L} = \frac{\pi {d_c}^4}{128\mu}\frac{p_c}{L(t)}} \tag{21}$$

where $\boldsymbol{Q}$ is the flow rate and $\boldsymbol{d_c}$ is the diameter of the representative capillary tube. The time-dependent flow rate can be related to the mean velocity at a given time:

$$\boldsymbol{Q(t) = A \times U(t) = \frac{\pi d^2}{4}\frac{dL}{dt}} \tag{22}$$

By combining these two equations, they obtained the following expression for $\boldsymbol{L(t)}$:[25,26]

$$\boldsymbol{LdL = p_c\left(\frac{d^2}{32\mu}\right)dt \Rightarrow L(t) = \sqrt{\left(\frac{\sigma d \cos\theta}{4\mu}\right)t}} \tag{23}$$

wherein the capillary pressure was denoted by $\boldsymbol{4\sigma \cos\theta \,/\, d}$ in which $\boldsymbol{\sigma}$ is the surface tension and $\boldsymbol{\theta}$ is the contact angle. In spite of its apparent simplicity, this equation was found to be accurate for one-dimensional liquid imbibition in mono-dispersed, fully saturated porous media. For two- or three-dimensional, poly-dispersed, unsaturated or partially saturated systems typical of those encountered in paper-based devices, one can employ Richards' equation for design purposes. This robust model is obtained by combining the continuity equation for moisture content (or saturation) with a modified version of Darcy's law in which the pressure term is replaced by a saturation-dependent capillary

pressure, $\boldsymbol{p_c(S)}$. By allowing permeability to be a function of saturation, $\boldsymbol{k(S)}$, Richards obtained the following nonlinear partial differential equation for the saturation, ***S***:[27]

$$\frac{\partial S}{\partial t} = \frac{\partial}{\partial x}\left(D(S)\frac{\partial S}{\partial x}\right) + \frac{\partial}{\partial y}\left(D(S)\frac{\partial S}{\partial y}\right) + \frac{\partial}{\partial z}\left(D(S)\frac{\partial S}{\partial z}\right) \tag{24}$$

where ***S*** is the degree of saturation of the wetting phase defined as $\boldsymbol{S = \beta / V_\varepsilon}$ with $\boldsymbol{\beta}$ being the volume of liquid imbibed and $\boldsymbol{V_\varepsilon}$ the total volume of the pores. Note that in Richards' equation, ***D(S)*** is the viscosity-scaled diffusivity defined as:

$$D(S) = \left(\frac{k(S)}{\mu V_\varepsilon}\right)\left(\frac{\partial p_c(S)}{\partial S}\right) \tag{25}$$

Based on Brooks-Corey model, it can also be expressed as:

$$D(S) = D_0 S^n \tag{26}$$

where $\boldsymbol{D_0}$ corresponding to the fully saturated condition, ***S = 1*** is related to the fluid/solid properties as follows:

$$D_0 = \left(\frac{\sigma}{\mu}\right)\left(\frac{4\, d_{max}\, \cos\theta}{\lambda}\right)\left(\frac{\varepsilon^2}{180(1-\varepsilon)^2}\right) \tag{27}$$

where $\boldsymbol{\lambda}$ is a parameter related to the pore size distribution and connectivity and $\boldsymbol{d_{max}}$ is the maximum pore size, also known as retention size. Richards' equation is thus a two-parameter $(\boldsymbol{n, D_0})$, highly nonlinear, unsteady partial differential equation which can be solved numerically. Having solved Richards' equation for ***S(x,t)***, one can obtain the flow rate by:

$$Q(t) = \frac{d\forall}{dt} = \iiint_{\forall} \varepsilon\left(\frac{dS}{dt}\right) d\forall, \tag{28}$$

where $\forall(t)$ is the volume of absorbed liquid. Provided the Reynolds number is sufficiently smaller than one, the saturation field can be used to find the velocity field using the modified Darcy's law:[27]

$$u = -\frac{k(x,S)}{\mu}[\nabla p_c(x,S)] \tag{29}$$

where, as mentioned above, $\boldsymbol{k}$ and $\boldsymbol{p_c}$ are known functions of the saturation ***S*** for a given porous material. Once the velocity field is known, it can be combined with the aforementioned equations for mass transport and electrochemical kinetics to solve for the performance of paper-based microfluidic electrochemical cells.

3 - Methods

As previously mentioned, microfluidics offers significant benefits for electrochemical flow cells such as simplicity, low cost, and elimination of the need for a physical separator between the two half-cells. These benefits led to the start of a new class of microfluidic electrochemical flow cells, wherein the cell reaction is aided by microfluidics. Typically, these cells are designed to operate without a membrane by means of microfluidics enabled control of reactant dynamics. Therefore, they are commonly referred to as membrane-less flow cells. Since the mixing under the laminar flow regime in microfluidics is governed by diffusion, two liquid streams will flow in a microchannel separated by the diffusion interface. The cells are hence also referred to as co-laminar flow cells (CLFCs). In this section, the research methods applied to microfluidic electrochemical flow cells are presented. The different cell designs as well as cell fabrication and characterization techniques are summarized.

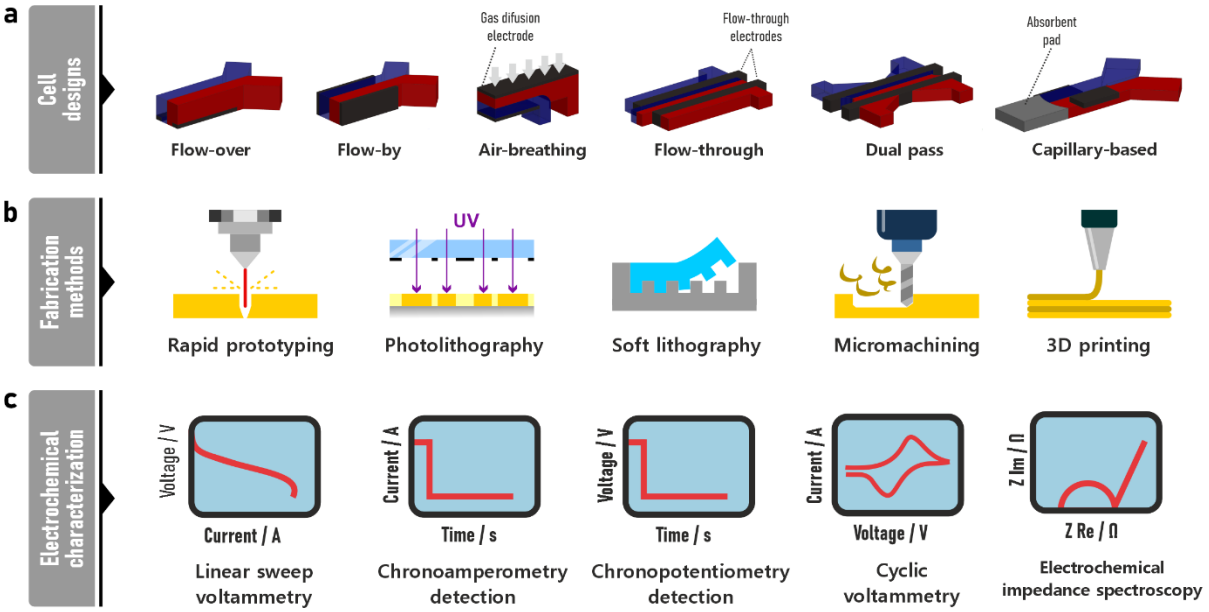

Figure 4: Microfluidic flow cells: a) design, b) fabrication, and c) characterization methods.

3.1 Cell Design

The most basic design of a microfluidic electrochemical flow cell has a single microchannel that separates the two electrodes. The microchannel may have two separate inlets for the two half-cell reactant streams and thus a Y-shaped or T-shaped channel. However, other configurations with one or three inlets have also been reported. Other microchannel designs were also presented such as F-shaped, H-shaped, and Ψ-shaped channels. Cell designs may also vary according to the electrode configuration. Figure 4a presents a schematic for a Y-shaped channel with different electrode configurations: flow-over, flow-by, air-breathing, and flow-through electrodes.

The pioneering works of microfluidic electrochemical flow cells by Ferrigno *et al.*[7] and Choban *et al.*[8] relied on the so-called flow-over and flow-by architectures, respectively. In these cells, the reactant streams merge horizontally in a Y- or T-channel to flow over positive and negative planar electrodes placed on the bottom or on the side walls of the microchannel. These CLFCs used a simple monolithic T-shaped or Y-shaped design that had two inlets and one outlet and demonstrated the stability of the microfluidic co-laminar interface to control reactant crossover, resulting in robust electrochemical energy conversion within the device. Many derivative studies inspired by these simple flow-over designs have followed.[28–33] However, the cell performance with this cell design was generally hindered by mass transport limitations due to the formation of the concentration boundary layer at the planar electrode surface.

Gas diffusion electrodes (GDEs) were also utilized in microfluidic electrochemical flow cells for gaseous reactants, as breathing electrode architectures, to address the mass transport issues from poor gas solubility and slow transport in aqueous media. The design was adapted from conventional electrochemical cells such as polymer electrolyte membrane (PEM) fuel cells and metal-air batteries. This was first applied as an air-breathing microfluidic fuel cell by Jayashree *et al.* in an F-shaped design (Figure 4a), with a blank electrolyte flowing over the GDE introduced from the first inlet.[34] The breathing electrode structure has been widely used in many other studies for different gaseous reactants, as discussed in the next section.[35–39] A key advancement in CLFC structures was introduced by Kjeang *et al.* in 2008, by presenting the flow-through porous electrode architecture, which enabled high-performance cells.[40] In this cell design (Figure 4a), the reactants are forced inside the three-dimensional pore-network in the electrode, eliminating the concentration boundary layer issues by continuously replenishing the reactant electrolytes. The baseline design of flow-through architecture by Kjeang *et al.* was subsequently modified by Lee *et al.* to form the so-called dual-pass architecture with two outlets (Figure 4a), resembling an X-shaped channel design to facilitate reactant recirculation and regeneration under electrolytic operation.[41] Overall, the high-performance flow-through cell design has been mostly applied to liquid-based fuel cells and flow batteries but have recently been extended for microfluidic electrolyzers,[42–45] metal-air batteries,[46] and organic batteries.[47] Other cell architectures have also been reported such as the orthogonal flow by Hayes *et al.*,[48] the radial[49] and counter flow designs[50] by Salloum *et al.*, the H-shaped or bridge designs[51–56] that use a shallow channel portion to reduce mixing, and the Ψ-shaped design by Sun *et al.*, where a third inlet stream with blank electrolyte was introduced in the microchannel.[57]

More recently, paper-based microfluidics technology was also adapted to microfluidic electrochemical flow cells including CLFCs to utilize passive self-pumping by capillary forces in lieu of active micro-pumping of reactant flows. These specialized cells can be promising power sources for paper-based

diagnostics to satisfy the *ASSURED criteria by the* World Health Organization*:* Affordable, Sensitive, Specific, User friendly, Rapid and Robust, Equipment free, and Deliverable to end users.[16,58,59] Esquivel *et al.* pioneered this concept and presented a lateral flow paper-based CLFC which had flow-over and air-breathing electrodes (Figure 4a).[60] The paper-based cells support a capillary-driven flow rate until the absorbent pad is fully saturated with the liquid, which hence matches single-use applications. The concept was initially reported using flow-over electrodes but was later extended to high performance flow-through porous electrodes[47,61] and other porous substrates.[62,63]

3.2 Cell Fabrication

Most conventional microfabrication techniques used for microfluidic applications are generally also applied for fabrication of microfluidic electrochemical flow cells. Fabrication can be categorized into monolithic or multi-layer systems depending on how the cell structure is formed.[11] Microchannels are generally made by rapid prototyping using photolithography, soft lithography, laser etching, computer numerical control (CNC) machining, or additive manufacturing techniques, as depicted in Figure 4b. The pioneering works relied on standard microfabrication and lithography techniques to form monolithic systems that are well suited for system integration.[7,31] CNC machining has also been applied to create millimeter-scale channels for microfluidic fuel cells.[64] Soft lithography in poly(dimethylsiloxane) (PDMS), also referred to as micromolding, has been widely used because of its precision, easy replication from the master mold, and compatibility with many solvents and electrolytes.[40,65] In these cells, the produced PDMS part is subsequently bonded with a solid substrate. For example, the PDMS can be irreversibly sealed with a glass lid or another PDMS part using plasma bonding. Moreover, laser etching has been used to create microfluidic channels in plastic materials such as poly(methyl methacrylate) (PMMA), with precise control on geometry using laser rastering power and speed.[34,37] Laser patterning was also applied to precisely cut-through different multi-layers designed for channels, fluidic ports, and electronic ports, that were then assembled or laminated to form the final device.[28,29] For example, the channel design can be cut into thin plastic substrates or flexible compressible materials that are then mechanically sealed into top and bottom parts.[66,67] This technique may be more favorable for reversible sealing, particularly in studies that require further electrode analysis post-measurements in a non-destructive manner. The device parts may also be sealed using adhesives as shown by Shyu *et al.* who bonded PMMA and PDMS parts.[68] Lastly, paper-based devices have also relied on laser-patterning or die-cutting for precise production of Y-shaped channels.[60,69,70]

More recently, 3D printing has been gaining popularity in both electrochemical[71–75] and microfluidic applications,[76–78] owing to advances in increased precision and layer resolution. Several reviews summarized the potential uses of additive manufacturing technology for electrocatalytic

applications,[72] electrochemical flow systems,[73] and electrochemical microfluidic platforms.[79] Different microfluidic cell components such as device structure,[80–82] fluidic networks,[83–85] or electrodes[71,86,87] have been reported using 3D printing technology. Martins *et al.* showed significant reduction in device production time using 3D printing in polylactic acid (PLA) material.[82] In general, the advent in higher resolution additive manufacturing will make it easier to produce different designs and facilitate parametric studies in this field of research.

Electrodes and current collectors may be pre-patterned on the substrate using microfabrication techniques such as vapor deposition, sputtering, and photolithography etching or lift-off.[7,35,88] Self-contained electrodes can also be employed such as graphite rods,[64] carbon papers,[40] carbon foams,[65] metals,[89] or metal meshes[43] as combined electrodes and current collectors for microfluidic flow cells. Such electrodes are generally placed in prefabricated positions or grooves designed in the corresponding device layer. In paper-based systems, the electrodes can also be self-contained, whereas some authors have deposited graphite electrodes on the paper substrates using pencils.[90–94] In general, the chemical composition, structure, and morphology of the electrode are important characteristics that may significantly influence the overall performance of electrochemical cells including microfluidic cells. Electrocatalytic activity can be enhanced by increasing the electrochemical surface area or applying a catalyst. Both *ex-situ* and *in-situ* methods have been applied for this purpose including electrochemical deposition,[7,95] electron-beam evaporation,[30,31,96] dip or spray coating of catalyst inks,[28,29,97] *in-situ* flowing deposition,[98] and *in-operando* deposition.[99]

3.3 Reactant Chemistry

The simplest and most convenient form of a microfluidic electrochemical flow cell relies on two liquid streams which contain supporting electrolyte with or without dissolved reactant species. A great variety of liquid,[7] gas,[34] solid,[46] and two-phase reactants[100] have been reported, which will be further detailed in Section 4. Supporting electrolytes (*e.g.,* 1 M H_2SO_4 or 1 M KOH) increase the freely available ions such as hydronium or hydroxide ions and enhance the ionic charge transfer and hence reduce the ohmic resistance of the cell. Typically, in a conventional electrochemical cell, the ionomer membrane is designed to conduct a specific ion and therefore dictates the media of operation as it cannot operate effectively in both alkaline and acidic conditions. Conversely, the operation of microfluidic cells with different pH conditions is feasible, as shown by Cohen *et al.*[31] wherein the voltage of a H_2/O_2 fuel cell was raised by using alkaline and acidic media within the respective half-cells. This unique feature is often referred to as mixed-media or dual-electrolyte operation. The flexibility of tuning the operating medium allows the pH to be tailored to maximize each half-cell potential and hence the overall potential difference (cell voltage). Therefore, this operation scheme has been widely applied in many different microfluidic electrochemical flow cells, as will be shown in Section 4.

3.4 Cell Testing

Testing of microfluidic electrochemical flow cells requires lab-based methods to drive fluid flow and take electrochemical measurements, as depicted in Figure 4c. In most works reported to date, the fluid streams were pumped into the cell by means of syringe pumps with tubes connected to the inlets. Syringe pumps offer a wide range of pulse-free flow rates with precise control and possibility to hold multiple syringes. Peristaltic pumps with pulse dampeners were also used.[101] Some works with gaseous reactants also relied on vapor-fed electrodes.[89,102–105] A potentiostat is commonly employed for electrochemical measurements, which enables cell potential or current measurement through galvanostatic or potentiostatic control, respectively. Cell polarization curves (see Figure 2) are generally recorded by stepwise measurement of steady-state current at different cell potentials. Alternatively, a linear voltage sweep can be applied, provided that the scan rate is slow enough to ensure pseudo steady-state conditions. In the absence of a potentiostat, a simple combination of load bank and multimeters may alternatively be used by applying Ohm's law to calculate point-by-point current at each load resistance. Power density is estimated by multiplying the cell potential with the current density normalized by the active electrode area. However, for generalization and scalability, volumetric power density is considered a preferred metric to normalize the power output by the overall volume of the cell.[11,106] Individual electrode performance data may also be recorded by incorporating a reference electrode (usually Ag/AgCl, saturated calomel, or pseudo reference electrode) in the flowing electrolyte. This method has been applied to measure individual electrode polarization behavior with two-electrode[29,40] or three-electrode configurations[66,107,108] in flow cells with liquid reactants, but is more challenging for gaseous reactants.

The ohmic cell resistance is an important factor for the overall cell performance and depends on the ionic resistance of the electrolyte as well as the electrical resistance of the electrodes, contacts, and current collectors. The combined ohmic cell resistance can be measured from the high frequency real-axis intercept of the Nyquist plot of impedance obtained by electrochemical impedance spectroscopy (EIS), by applying a small sinusoidal voltage perturbation and measuring resulting current over a range of frequencies. To isolate ohmic resistance effects, IR-compensated polarization curves may be obtained by adding the ohmic overpotential (η_R) to the measured cell voltage. The area-specific resistance (ASR) is the product of the resistance and the active area and is used for normalized ohmic polarization. Some studies have also estimated the cell resistance by measuring the slope of the polarization curve at the linear zone, *i.e.*, the ohmic losses region in Figure 2. While this can be used to provide a rough estimate, it should only be considered valid in highly ohmic-limited cells, for example, in cells with rapid kinetics and high flow rates, so that the activation and mass transport polarizations are comparatively much lower. In electrolytic cells, the methods of testing using potentiostat-

supported current and cell potential measurements mentioned above are also applicable with no major differences.

Lastly, the efficiency metrics for electrochemical energy conversion are also important to characterize. For galvanic cells, the voltage efficiency, ϵ_V at a given current density is estimated as the ratio of the measured cell voltage over the reversible cell potential (E^0), whereas in electrolytic operation, it is the ratio of the reversible potential over the operating voltage. For cells with reversible operation modes such as redox flow batteries or regenerative fuel cells, round-trip voltage efficiency is estimated as the ratio of discharge voltage to the charge voltage at a given current density. Another important parameter is the fuel utilization factor or reactant conversion efficiency, ϵ_F, also referred to as faradaic or coulombic efficiency. It is estimated as the ratio of measured current at a given cell potential over the theoretical faradaic current from the reactant supplied to the cell. The faradaic efficiency is estimated as given in Eq. 30a and 30b for flowing reactants and static reactants, respectively, where i is the current density, A is the electrode area, Q is the flow rate, m is the mass of reactant, and MW is the molar mass of the reactant. Finally, the overall energy efficiency of the cell is the product of the voltage efficiency and the coulombic or faradaic efficiency, $\epsilon_E = \epsilon_V \times \epsilon_F$.

$$\epsilon_{F,flow} = \frac{i\,A}{z\,c\,F\,Q} \tag{30a}$$

$$\epsilon_{F,static} = \frac{\int i\,A\,dt}{z\,F\,{}^{m}/_{MW}} \tag{30b}$$

4 - Devices and Applications

In this section, the progress and research contributions reported in the literature for microfluidic electrochemical energy conversion devices are summarized. Since the first published microfluidic fuel cells (µFCs) by Ferrigno *et al.*[7] and Choban *et al.*,[8] the field of microfluidic electrochemical flow cells has significantly grown. Section 3.1 discussed the overall cell design requirements and strategies, showing a range of membrane-less device architectures with different channel designs and electrode configurations. A timeline highlighting the major developments and evolution in this research domain is depicted in Figure 5. As shown in this figure, the field has evolved beyond µFCs to incorporate paper-based microfluidics technology, resulting in the development of self-pumping paper-based µFCs. On a parallel path, the research domain has also evolved to include other microfluidic electrochemical flow cells such as redox flow batteries (µRFBs), electrolyzers, and photoelectrochemical cells.

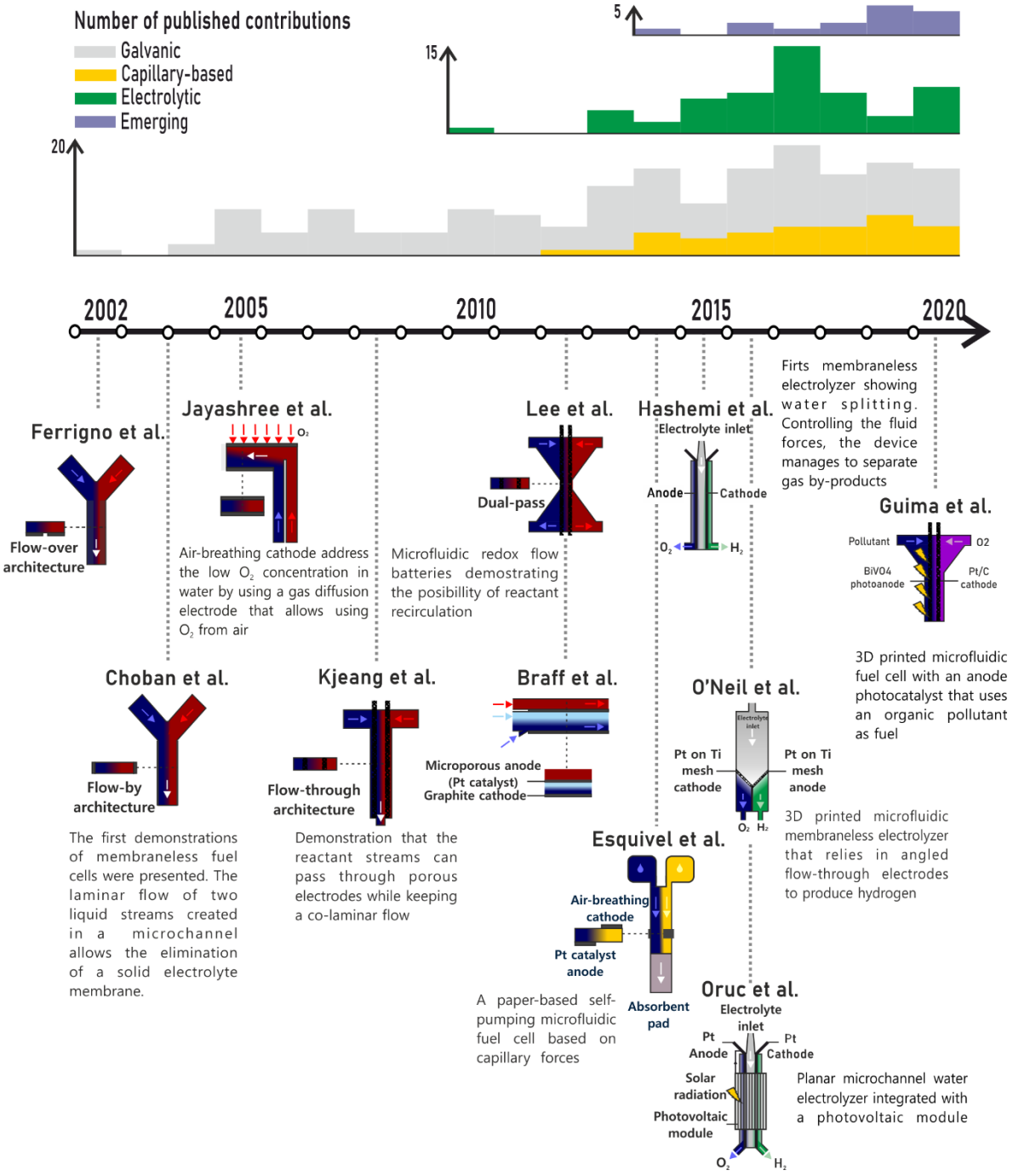

Figure 5. Timeline highlighting the major developments and evolution in microfluidic electrochemical energy conversion devices.

This section categorizes the devices according to their mode of operation into two subsections: *galvanic cells* and *electrolytic cells*. Galvanic cells are discussed in Section 4.1 and include works on µFCs, paper-based µFCs, microfluidic metal-air cells, and other microfluidic primary batteries. These galvanic cells are typically reported as portable power sources and have mostly focused on enhancing the overall cell performance in terms of output power density and fuel utilization efficiency. Electrolytic cells are discussed in Section 4.2 which includes works on µRFBs reported for energy storage applications, wherein the contributions not only address cell discharge performance aspects

but also report cell charging or cycling performance characteristics typically needed for the electrolytic operation. In addition, rather than a mere single-pass performance typical of fuel cells in galvanic mode, a means of closed-loop reactant recirculation is commonly reported in such contributions. Electrolytic cells also include microfluidic electrolyzers reported for hydrogen (H_2) generation, carbon dioxide electrochemical reduction (CO_2RR), or other purposes. Section 4.3 describes some of the emerging concepts and applications for microfluidic flow cell technology such as photoelectrochemical cells and cogeneration of power and chemicals. Lastly, Section 4.4 summarizes the works that utilized microfluidic flow cells as analytical platforms for electrochemical energy applications with an outcome which is generally beneficial and applicable to conventional electrochemical devices.

4.1 Galvanic Cells

Among different types of microfluidic galvanic cells, research on µFCs has undoubtedly attracted the most scientific contributions to date, with key representative developments illustrated in Figure 6. The microfluidics aided miniaturization of fuel cells was primarily motivated by the development of a low-cost and portable power source, whereas the strategic use of the microfluidic scale eliminated the need for a physical separator or ion exchange membrane. Indeed, the membrane elimination has offered many promising advantages related to cost reduction and simplicity. This breakthrough encouraged many research works to investigate cell performance and address the different sources of overpotential losses found in a typical polarization curve (Figure 2): activation overpotential, ohmic overpotential, mass transport overpotential, and OCV overpotential. The cells have been operated with various reactant fuels, generally pursuing the highest OCV, power density, or energy density; and several types of catalysts have also been developed and integrated within the cells. Cell architectures have noticeably evolved over the years to diminish the ohmic resistance. Electrode materials, configurations, and microstructures have also evolved to increase the electrochemically active surface area and enhance the electrochemical reaction kinetics. Various investigations have been performed to enhance fuel utilization efficiencies by addressing mass transport losses. Lastly, the motivation to reach the market has also led to several attempts of stacking and system level integration, taking into consideration practical features such as portability, affordability, or manufacturability. In this subsection, the galvanic cell contributions are therefore categorized in a similar manner, discussing sources affecting cell performance and overpotentials, and ending with a summary of stacking methods and practical features.

4.1.1 Reactants

The fuel and oxidant choice will chiefly determine the microfluidic fuel cell OCV and pose theoretical limits on the cell performance in terms of different overpotentials and the overall energy density of

the device. A wide variety of liquid, gas, and solid phase reactants have been reported for microfluidic galvanic cells. The pioneering miniaturization works used liquid fuels including organic fuels such as formic acid (HCOOH),[8,34] alcohols such as methanol (CH_3OH),[37] and redox flow reactants such as vanadium redox species (V^{2+} and VO_2^+).[7] Gaseous fuels have also been reported in early works, such as hydrogen (H_2) used either in the gas phase or as a dissolved gas in the supporting electrolyte.[31,109–111] However, the challenges associated with the storage of hydrogen has made liquid fuel alternatives more attractive for portable applications.

In addition to CH_3OH,[28,29,35,112,113] oxidation of other alcohols such as ethanol,[114,115] glycerol,[116–119] and ethylene glycol[116,120–122] has been also reported. Their low toxicity when compared to CH_3OH, higher boiling points, and comparable energy density make them interesting candidates for electro-oxidation. Other reported fuels which also benefit from dense liquid phase storage and transportation include formic acid,[55,123–130] formate,[95,131–134] hydrogen peroxide (H_2O_2),[135–137] sodium borohydride,[138–140] hydrazine,[138,141,142] and urea.[143,144] Many biofuels such as glucose and lactate have also been directly used as fuel or harvested from sample analytes.[145–155] Furthermore, some authors have explored the possibility of interchangeably feeding the same cell with different aforementioned fuels, proving the μFC capability of being fuel-flexible.[115,116,138] Maya-Cornejo *et al.* showed a multi-fuel membrane-less nanofluidic fuel cell based on Cu@Pd catalysts for the successful oxidation of methanol, ethanol, ethylene glycol, glycerol, and a mixture of fuels together (Figure 6a).[115] Lastly, some works have also utilized solid metals as anodes such as aluminum[89,156–160] or zinc.[46]

Regarding oxidants, most μFCs relied on the oxygen reduction reaction (ORR), employing oxygen (O_2) either in gaseous form,[34,36,37,117,124,132–134] liquid form as a dissolved gas in the catholyte,[8,28–31,109,110,116,124,161] or a mixture of both.[67] Due to the limited solubility of oxygen and its relatively slow diffusion in liquids, a gas diffusion electrode (GDE) is generally favorable in terms of performance. Many other liquid oxidants have also been explored, including hydrogen peroxide,[96,137,162,163] potassium permanganate,[8,49,55,57,131,164,165] and less commonly, sodium hypochlorite (bleach).[95,118]

In order to facilitate ion transport in liquid electrolyte between electrodes, strong all-acidic (*e.g.*, 1 M H_2SO_4) or all-alkaline (*e.g.*, 1 M KOH) media are usually employed as μFC supporting electrolytes, similarly to conventional fuel cells.[132] The supporting electrolytes can either be blended with the reactants or introduced through a separate electrolyte stream. Moreover, the absence of ion selective membrane in μFCs facilitates the use of *mixed*-media conditions, as previously described in Section 3.3. As initially demonstrated by Cohen *et al.*[31] and Choban *et al.*[28], optimizing the pH for each half-cell reaction enables not only improved OCV but also enhanced reaction kinetics, leading to an overall cell performance boost.[138] The mixed-media operation was widely applied to μFCs with various fuels

including H_2,[31,166] aluminum metal,[158,160] and liquid hydrocarbon fuels.[28,138,167] For instance, this operating scheme was utilized by Lu *et al.* to reach high power density output of 1.3 W/cm^2 for a H_2 µFC with an OCV of 1.9 V.[166] Martins *et al.* similarly demonstrated a glycerol µFC with high power density output of 0.3 W/cm^2 and an OCV of 2 V.[118]

The slow kinetics and high activation energy of most fuels and oxidants require the use of catalysts, as detailed in the next subsection. Alternatively, galvanic operation of µFCs has been demonstrated using electroactive redox couples as potential reactant anolytes or catholytes such as vanadium redox species,[7,40,50,64,168–172] iron salts,[106] cerium ions,[139] and organic redox species.[61,167] These liquid phase redox species generally benefit from a lower activation energy and can therefore electrochemically react on bare carbon electrodes at room temperature. These electrolytes notably allow the regeneration of the fuel cell through electrolytic operation mode; such cells are therefore considered as µRFBs or microfluidic electrolyzers, which are further discussed in Section 4.2.

4.1.2 Reaction Kinetics

The choice of catalyst is mainly based on the nature of fuel and oxidant used in a given cell. At the anode, most fuels mentioned in the previous subsection need a catalyst to overcome the activation energy barrier and improve the electrochemical reaction rates and exchange current densities. Most µFC electrodes were based on precious-metal group catalysts, including platinum (Pt), gold, iridium, and palladium (Pd), due to their excellent electrocatalytic activity. Some works using CH_3OH or H_2 as fuel have shown better response with Pt,[129] whereas Pd-based catalysts have proven to improve the cell performance for other fuels such as ethanol, glycerol, and formic acid.[117,125] The electro-oxidation reactions sometimes involve complicated steps which may result in secondary reaction intermediate products. These side products may impact cell performance and life span by causing catalyst poisoning. To overcome this issue, bi-metallic material combinations may be used. For example, combinations of Pt (or Pd) with ruthenium (Ru) at different ratios have been shown to reduce CO poisoning of the Pt active sites and thus enhance alcohol electro-oxidation.[37,161] However, a significant part of the total cost of µFCs can be attributed to the high loading of the mentioned precious-metal catalysts.[96] A resourceful alternative approach to reduce the noble metal content is the synthesis of core-shell catalysts, in which a less costly non-noble metal core is coated with a metal shell with higher electrocatalytic activity. In this regard, other catalyst materials for µFCs have been reported including gold, copper, cobalt, silver, iridium, iron, and nickel.[114,115,119,121,122,173–179] While this approach may result in more rigorous catalyst synthesis processes, it may also be a way of reducing the electrocatalyst cost without compromising the electrocatalytic activity.[115] For the ORR at the cathode, Pt has also been typically applied and shown higher activity than Pd. Pt and gold have also been applied for the

electrochemical reduction of other liquid oxidants such as H_2O_2 and bleach.[95,118,162] Alternatively, a parallel type of so-called biofuel cells use enzymes or microbes to catalyze the electrochemical reaction.[32,70,180,181] These biological catalysts replace metallic ones and although their stability may be limited to a few days, they have gained attention due to their high selectivity and good performance at ambient temperature. Many authors have focused on the use of glucose oxidase and lactate oxidase as enzymes; and *Geobacter sulfurreducens, Shewanella oneiden*sis, *Escherichia coli*, and mixed communities as microbial catalyzers for anodes. Regarding the cathode side, ORR has been achieved with laccase, bilirubin oxidase, and polyphenol oxidase.[150,182,183]

The electrocatalytic activity of a modified electrode not only depends on the reaction rate and the catalyst nature, but also on the size, shape, and dispersion of the catalyst particles. These geometrical characteristics will determine the electrochemically active surface area (ECSA). Regarding µFC catalyst studies, two strategies have been generally reported to increase the ECSA: decreasing the nanoparticle size, which increases the area to volume ratio, and enhancing the dispersion via carbon-based supports. For instance, Arjona *et al.* reported well-ordered and homogeneous cube-shaped Pd nanomaterial catalyst which was obtained without any other intrusive geometries. Tests carried out with three common fuels, methanol, ethanol, and formic acid, led to an improvement over commercial Pd.[67,124,184,185]

When using carbon-based supports, homogeneous catalyst decoration of carbon paper to be used as porous electrodes may be challenging. In this case, the catalyst can alternatively be loaded on the paper surface *in situ*.[98,186] Goulet *et al.* applied carbon nanotubes using flowing deposition on flow-through carbon paper electrodes within a fully assembled cell. They reported a ten-fold increase in the ECSA and corresponding enhancements in the kinetics of the V^{2+} electro-oxidation reaction, leading to 70% increase in power output.[98] Moreover, they demonstrated *in-operando* dynamic deposition of carbon nanotubes on porous carbon paper electrodes. In this technique, the nanotubes were added to the vanadium redox electrolyte such that the flowing deposition occurred continuously during cell operation, dynamically decreasing the pore size and enhancing porous electrode kinetics within the electrolyte flow path.[99] An alternative approach to increase ECSA on porous carbon paper is the utilization of carbon nanofoams.[65,67] In these nanofluidic fuel cells,[65,67,115,187] the reaction kinetics were shown to improve, since the interfacial surface-area-to-volume ratio was increased. However, the relatively low electrical conductivity of carbon foams may considerably impact the ohmic cell resistance and constrain the power density output. The presence of microscale cracks in nanofluidic electrodes may also unbalance the uniformity of flow distribution to favor those cracks. In short, while nanofluidic electrodes have shown benefits for interfacial transport and nanofluidic channels may have benefits for ionic resistance, the microfluidic scale typically offers greater benefits for mass transport

and lower flow resistance, and therefore is the core transport scale. Carbon/graphene aerogels[140,144,188] were recently used by Kwok *et al.*, who reported Pt- and Ru-Pt- decorated graphene aerogels as porous electrodes for μFCs.[189,190]

The electrochemical reaction rate can also benefit from raising the operational temperature of the cell, which reduces the activation overpotential. However, since most μFCs operate effectively at room temperature with negligible self-heating, only limited experimental works have reported temperature effects. Massing *et al.* reported a fast start-up system consisting of an indium tin oxide heating layer implemented on the anode and cathode cover plates. Raising the temperature up to 80°C in 25 s, this system reduced the direct methanol fuel cell start-up time to the order of seconds.[191]

4.1.3 Ohmic Overpotential

As mentioned in Section 2, the combined ohmic cell resistance is influenced by various factors related to the cell design, electrodes, and reactant electrolytes. Whereas the cell resistance may have limited impact on devices operating at low current density, it can be a controlling factor for the overall performance of more optimized cells running at high current and power density. Fundamentally, the liquid electrolytes of microfluidic cells can have a higher ionic conductivity than the corresponding ionomer membranes used in regular electrochemical cells.[13] However, the channel dimensions also play a key role in determining the cell resistance.[192] Various works have applied parametric investigations for the cell design geometries using both experimental and modeling techniques to reduce the cell resistance.[99,171,193–196] A smaller interelectrode spacing was found to reduce the cell resistance, while conversely having a negative impact on the diffusive mixing.[130]

Given the importance of high electrolyte conductivity, strong acidic supporting electrolytes such as H_2SO_4, HCl, and HBr and strong bases such as KOH and NaOH were typically used, as mentioned previously in Section 3.3. The supporting electrolyte concentration can be tuned to optimize the overall cell performance.[49] Ibrahim *et al.* showed a significant increase in the cell resistance when testing organic acids such as citric and oxalic acids in lieu of conventionally used H_2SO_4.[167] In addition, the reactant concentration may indirectly affect the overall ionic conductivity of the electrolyte stream. While a higher reactant concentration is usually favorable for reaction kinetics, mass transport, and energy density, it may also have negative impact on the cell resistance and hinder the performance in certain cases. This may be attributed to the reduced ionic mobility due to the increased electrolyte viscosity and interactions of ions or their weaker dissociations. For example, Martins *et al.* showed an increase in the ohmic cell resistance at higher concentrations of glycerol in a μFC indicating that the ionic mobility was compromised.[116] In other cases, the charge carriers from the supporting electrolyte are consumed in the cell reaction or at the co-laminar interface, *e.g.*, under mixed-media conditions,

causing an increase in the cell resistance. For instance, Goulet *et al.* showed a reduced cell resistance by diluting the active vanadium redox species concentration in the electrolyte to avoid excessive loss of protonic charge carriers.[99]

The electronic resistance of the electrode materials is also important. Porous materials tend to have higher electronic resistance because of their high porosity and tortuosity.[197] As mentioned earlier, despite their kinetic benefits, nano-porous materials such as carbon foams were shown to increase overall cell resistance.[65] Alternatively, the contact resistance of the electrodes can be improved by applying current collectors, reducing the ohmic losses and improving the cell performance.[198] For instance, Lee and Kjeang showed a 79% increase in cell performance by applying gold current collectors that reduced the net ohmic cell resistance by 30%.[88] However, certain technical challenges may need to be considered, as some materials may suffer from corrosion or promote side reactions that may negatively affect the stability of the cell.

4.1.4 Reactant Mass Transport

The use of microfluidics in electrochemical energy conversion provides an opportunity to enhance mass transport by tuning the flows of reactants, products, and electrolyte. A major mass transport limitation in microfluidic fuel cells is the formation of the concentration boundary layer at the electrode surface, as described before in Section 3.[12] It has been demonstrated, both experimentally and computationally, that mass transfer limitations can be reduced by increasing the reactant flow rate which lowers the concentration layer thickness.[64,128,133,165,199] However, these two parameters also determine the fuel cell efficiency in terms of the hydrodynamic stability and fuel utilization, as shown previously in Eq. 30.

In the case of planar electrodes, *e.g.*, in flow-over cell designs, mass transport limitations can be actively mitigated using multiple inlet or outlet channels to replenish depleted reactants. This idea has been explored as a strategy to overcome the limitation of convective mass transport to active sites. This approach greatly enhances the power density, as it assures a high concentration of reactants next to the electrode active area.[53,145,200–202] However, it may require extra energy and manifolding to actively pump the fluid through the multiple inlet channels. Other passive methods have been investigated, such as applying tapered electrodes[203] or channels,[194,204] or introducing herringbone or ridge structures[139,163,205–207] on the bottom of the fluidic channel, imitating the chaotic passive micromixers presented by Stroock *et al.* in 2002.[208] Although more complex microfabrication methods would be required, the integration of such passive mixers demonstrated improved fuel utilization owing to the creation of secondary flows, which refreshed the concentration boundary layer. Using this grooved electrode-based cell design (Figure 6b), Ha and Ahn achieved 14% improvement in peak

power density.[163] Rösing *et al.* reported an innovative approach in which Dean vortices involved in curved channels passively created an additional convective fresh reactant flow.[164] Recently, Zhou *et al.* proposed the incorporation of a titanium capillary tube which acts as a micro-jet that directly injects fuel at the desired position on the anode side (Figure 6c).[134] Other approaches have focused on hydrodynamics where an additional buffer stream may be used to focus the reactants into thin streams close to the electrodes.[50,57,111,165] Using this method, Jayashree *et al.* demonstrated a 38% increase in the fuel utilization per pass (Figure 6d). The authors also discussed the trade-offs between maximizing power density and optimizing fuel utilization.[165] In subsequent works, Xuan *et al.* performed a modeling study based on the experimental data to adjust the buffer-to-fuel flow rate ratio to reduce crossover and increase the fuel utilization while maintaining the power density output.[209] Nonetheless, the limited surface area of the planar electrode configurations resulted in low fuel utilization.

In order to overcome mass transport limitations and maximize faradaic efficiency, some authors have focused on cell architecture optimization using three-dimensional electrodes. In the case of gaseous reactants, employing a breathing electrode configuration have shown significant enhancement in reactant mass transport and overall cell performance because of the orders-of-magnitude higher diffusion coefficient, as discussed in Section 3.1.[38] Jayashree *et al.* first demonstrated the air-breathing concept showing five-fold increase in power density output over the liquid stream with dissolved O_2. The air-breathing electrode has been widely implemented by many other authors since then[36,117,132,202,210,211] and the breathing configuration was applied for other gaseous reactants.[103,104,212–214] For example, Wang *et al.* applied CH_3OH vapor as fuel for a µFC. The cell displayed 30% higher peak power density and 27.5 times higher energy efficiency compared to the liquid feed counterpart, because of the alleviated fuel crossover and eliminated concentration boundary layer.[104]

To promote mass transport in liquid based cells, Kjeang *et al.* pioneered the flow-through porous electrodes configuration, where the reactant liquid is forced into the three-dimensional area of a porous carbon paper electrode.[40] The convective mass transport generated from the flow-through porous electrode configuration significantly mitigated reactant transport limitations and enhanced the overall cell performance.[215,216] Moreover, local reactant depletion was effectively avoided, while high fuel utilization efficiencies close to unity could be achieved. When paired with reactant chemistries with rapid kinetics, the cells with flow-through configuration are therefore often limited by ohmic losses. The flow-through porous electrode configuration has been widely applied in µFCs since then and enabled high power density outputs.[171,172,193,216–220] The flow-through configuration has also been applied with metal-foam electrodes or metal meshes.[140,221] Additionally, zinc metal was demonstrated to be electrodeposited on the pore structure of the porous carbon which would be electrochemically stripped during discharge.[46] Overall, the highest power density performance reported to date by

Goulet *et al.*,[99] of 2.0 W/cm^2, was achieved by the application of *in-operando* flowing deposition on flow-through porous electrodes to concurrently increase active surface area and local mass transport combined with current collectors and cell design optimization to reduce ohmic losses (Figure 6e).

4.1.5 Scaling Approaches

It is important to note that other contributions have been made in this field with the express purpose of meeting the power requirements of target applications. However, scale-up of microfluidic cells can be challenging, in particular for cells that rely on a stable, co-laminar flow to separate the half-cell reactants. Hence, the scalability of a single cell is fundamentally constrained by laminar flow physics and quality.[11,159] For this reason, most efforts to meet the needs of practical applications have been focused on cell stacking strategies.[33,89,181,222] Since the first attempts of vertical and series stacking by Moore *et al.* and Salloum *et al.*, respectively,[169,170] other authors have explored this possibility with the main challenge being to achieve a balanced and uniform flow distribution while keeping a high fuel utilization and low parasitic ionic currents. Ho and Kjeang developed a multiplexing approach in which two cells integrated within the same planar microfluidic chip share a single pair of reactant inlet ports.[223] Kjeang *et al.* proposed another approach to alleviate the volumetric costs of planar stacking, in which they applied a hexagonal array of cylindrical graphite rods as electrodes in a single cavity. The flow area between the rods maintained the microfluidic laminar flow charactersitics.[64] This approach presented scaled power and current outputs and was readily expandable in both vertical and horizontal directions. The approach was expanded upon by other works and similar configurations have been reported using different reactants.[128,133,196] To gain understanding on how the fluidic parallel or series connections affect the µFC performance, Wang *et al.* studied a four-cell array by both experiments and modeling and demonstrated a greater effect of the shunt current losses for HCOOH µFCs when series connections were used.[224] More recently, other stacking strategies such as the circular microfluidic methanol fuel cell presented by Wang *et al.* or the vanadium µFC with multi-layered flow-through electrodes by Li *et al.* have continued exploring the versatility of µFC technology.[214,218]

Overall, as discussed in a recent review by Modestino *et al.*, the scale-up and manufacturability strategies for microfluidic electrochemical cells are important for their practical implementation yet remains challenging.[13] Beside the geometrical constraints, another limitation may be the overhead volume of the system and its support materials over and beyond the electrochemical reaction volume. This would hinder the unprecedented volumetric power densities achieved with microfluidic cells when the total system volume is used for normalization. In order to overcome the scale-up challenges, µFCs therefore need to be designed for scalability. Some cell designs may benefit from the so-called

"areal scaling"[13] in which their various characteristic transport phenomena are co-planar, whereas other cells may benefit from a more conventional multiplexing approach. Any scaling approach, however, needs to balance the distribution of reactants among the different cells within the stack.

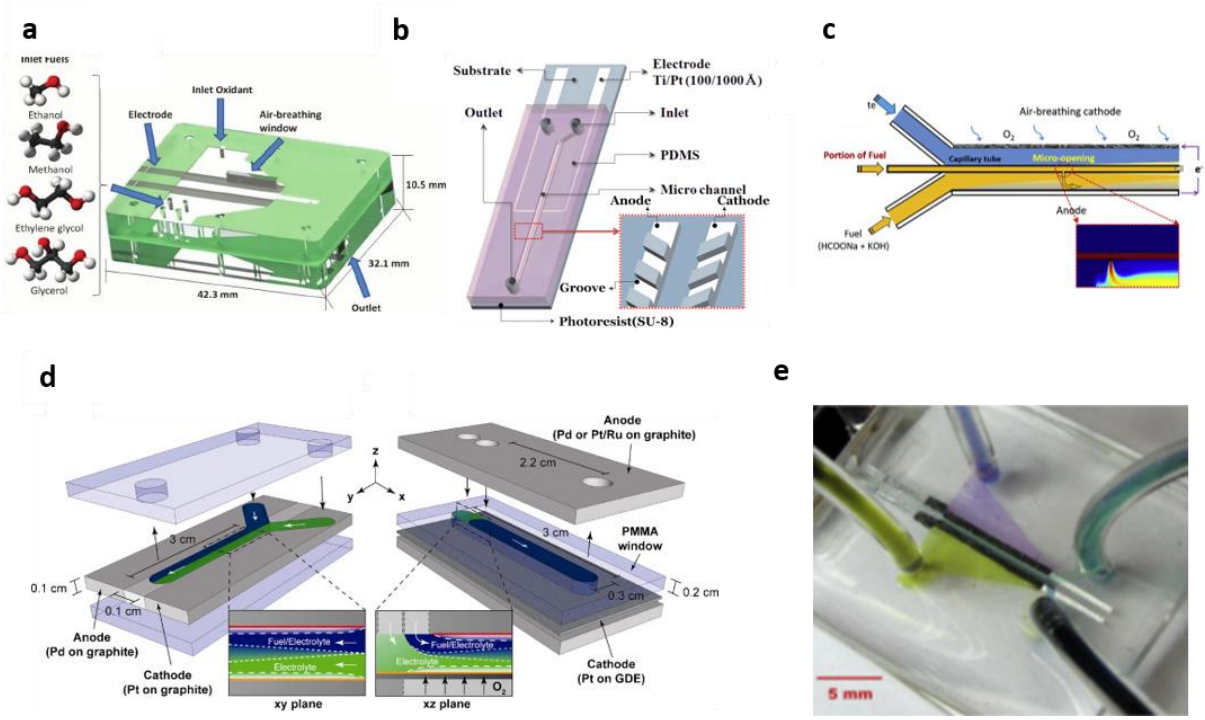

Figure 6. Microfluidic fuel cells: a) a multi-fuel µFC, b) µFC with grooved electrodes for passive mass transport improvement, c) µFC with micro-jet fuel injection, d) µFC designs to study hydrodynamics and fuel utilization, and e) flow-through µFC with *in-operando* flowing deposition. 6a: Adapted from ref. 115 with permission. Copyright 2015 Royal Society of Chemistry. 6b: Reprinted from ref. 163 with permission. Copyright 2014 Elsevier. 6c: Adapted from ref. 134 with permission. Copyright 2020 Elsevier. 6d: Reprinted from ref. 165 with permission. Copyright 2010 Elsevier. 6e: Reprinted from ref. 99 with permission. Copyright 2017 Elsevier.

4.1.6 Capillary-driven µFCs

In contrast to conventional µFCs that rely on active pumping methods to drive the fluids into the microfluidic system, alternative novel ideas that utilize the wicking effect of porous materials have also been explored over the past few years.[16] Microfluidic cells are generally compatible with capillary-driven flow because of their small size and low Reynolds numbers, as described in Section 2. A pioneering work was performed by Esquivel *et al.* in 2014, by reporting the first paper-based µFC developed for integration with lateral flow tests with the possibility of reagents storage for activation by water.[60] As shown in Figure 7a, reactant streams of methanol/KOH fuel and blank KOH supporting electrolyte flowed by capillarity in a Y-shaped paper-based channel and facilitated electrochemical reactions on flow-over and air-breathing electrodes, respectively. Similar to lateral flow strips, the

reactant flow was maintained by the downstream absorbent pad. Copenhaver *et al.* reported a paper-based microfluidic direct formate fuel cell and Galvan *et al.* presented further improvements.[225,226] Similar to these works, many other pump-less microfluidic fuel cells employing paper materials as the main structural component have been reported. Several works have been done to investigate and show the prospects of using various fuels such as HCOOH,[227] ethanol,[228] direct formate,[229] CH_3OH,[230] urea,[143] biofuels,[69,147,231] and vanadium redox reactants in paper-based systems.[232,233] Other works have reported the simple and convenient use of a graphite pencil to draw electrodes for paper-based µFCs.[92–94]

Further developments in paper-based µFC technology have focused on enhancing two main attributes: portability and integrability. Examples of such works are the single-stream paper-based cell using H_2O_2 as both fuel and oxidant presented by Yan *et al.*[234] and the *in-situ* hydrogen generation solution proposed by Esquivel *et al.*, solving the challenges of portable H_2 storage and on-demand release.[235] Recently, Shen *et al.* presented a deeper understanding of the influence of the textural properties of the paper used.[236] In a similar work, the structural design of the microfluidic paper and its leverage on the flow control and fuel efficiency was studied by Navarro-Segarra *et al.*[61] Lastly, although paper membranes remains the most reported material of choice in the construction of capillary-driven µFCs, the concept has been extended to other materials with similar wicking capabilities such as µFCs using cotton thread channels [62,63,237,238] or fabric-based µFC systems.[239] For instance, Liu *et al.* developed a woven-thread based µFC with sodium formate and hydrogen peroxide as fuel and oxidant, respectively (Figure 7b). They reported an OCV of 1.4 V in the cell utilizing mixed-media conditions with an additional neutral Na_2SO_4 electrolyte stream to separate the cathode and anode.[238]

In general, the flexible design and manufacturability of these paper-based cells allows the creation of innovative power source configurations. In this sense, batteries have also been adapted to take advantage of the properties provided by porous substrates. These paper-based batteries usually self-contain the reactant species and rely on the wicking properties of paper for their activation. Usually, they are activated by a drop of water or electrolyte, which is uniformly distributed through the paper microfluidic structure via capillary forces. The activation fluid acts as solvent for the electrolyte and enables the ionic connection between the anode and cathode, which were completely dry before activation – a feature which prevents self-discharge loss. The first example of these batteries was presented by Lee in 2015, when developing a paper-based laminated battery with a magnesium layer as anode and a copper chloride doped filter-paper as cathode.[240] Thom *et al.* demonstrated the feasibility of integrating these batteries with a fluorescence assay.[241] Various origami paper-based batteries have been reported since then, allowing the simplification of conventional fabrication processes.[242–245]

Despite being great examples of the capabilities of paper-based batteries, the power output of the aforementioned single cells was only on the order of microwatts, which is inadequate for most practical applications. Metal-air battery chemistries, such as Al-air and Mg-air,[246] are another promising configuration with high energy density and capability to produce adequate power. Wang *et al.* reported a low-cost paper-based Al-air battery targeting milli-watt level applications. The cell was further improved up to watt-range portable electronics applications.[247,248] The same chemistry was implemented by Shen *et al.* who sandwiched a thin sheet of fibrous paper between an aluminum foil anode and a catalyst coated graphite foil cathode (Figure 7c).[249] Besides the advantages that paper materials offer to batteries, as discussed above, Esquivel *et al.* took advantage of the biodegradable intrinsic capability of cellulose and developed the first biodegradable metal-free paper-based battery, using organic redox reactants (Figure 7d). This novel battery addressed the disposal of primary power sources at the end of their operating life from a more sustainable perspective, and is compatible with the circular economy.[47]

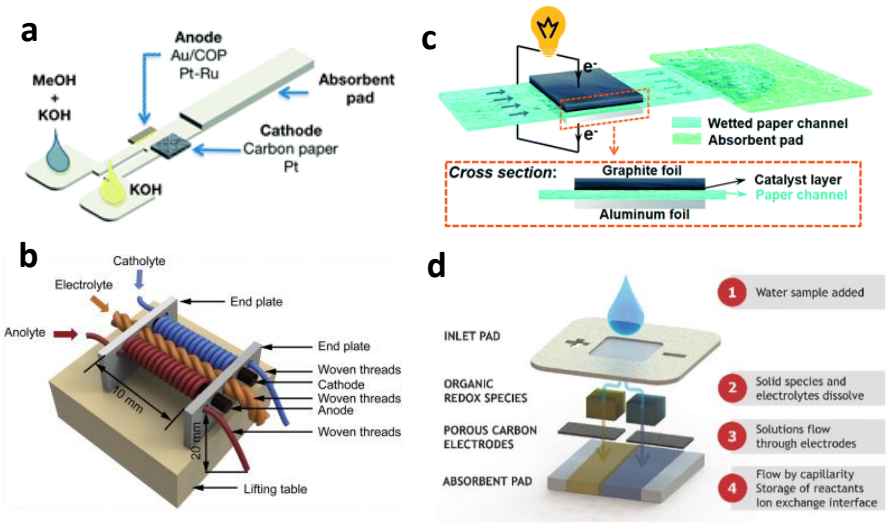

Figure 7: Capillary-driven microfluidic fuel cells: a) paper-based methanol µFC, b) woven thread-based formate µFC, c) aluminum-air paper-based battery, and d) metal-free biodegradable organic flow battery. 7a: Adapted from ref. 60 under License CC BY 3.0. Published 2014 by The Royal Society of Chemistry. 7b: Printed from ref. 238 with permission. Copyright 2018 Elsevier. 7c: Adapted from ref. 249 under License CC BY-NC 3.0. Published 2019 by The Royal Society of Chemistry. 7d: Adapted from ref. 47 under License CC BY-NC 4.0. Published 2017 by John Wiley & Sons.

4.2 Electrolytic Cells

The microfluidic electrochemical energy conversion domain has grown beyond fuel cells and other galvanic cells to include a variety of electrolytic cells, the majority of which can be broadly classified as microfluidic redox flow batteries[250] and microfluidic electrolyzers.[13] This section will summarize the contributions in these areas.

4.2.1 Membrane-less Redox Flow Batteries

As previously explained, redox flow batteries (RFBs) are secondary, rechargeable cells for energy storage applications. Therefore, charging performance under electrolytic mode and cell cycling performance are equally important to discharging performance. In addition, rather than a mere single-pass performance typical of fuel cell mode, a means of closed-loop reactant recirculation may also be included in microfluidic redox flow battery (μRFB) studies. Some works reported research advances related to μRFB reactants that only showed discharge operation, and were thus included in the previous Section 4.1 on galvanic cells.

Preliminary works on μRFBs reported the mathematical modeling of cells during charge and discharge processes and analytically predicted the trade-off between power density and reactant crossover and fuel utilization efficiency.[251] The model was applied by Braff *et al.* in 2013 to predict the performance of a laminar hydrogen-bromine μRFB which eliminated the membrane cost and degradation issues in conventional counterparts. They experimentally demonstrated high peak power density of 795 mW/cm^2 and round-trip voltage efficiency of 92% in the μRFB (Figure 8a).[39] At the same time, the Kjeang group demonstrated a μRFB utilizing vanadium redox species[41] and later demonstrated reactant recirculation in a batch mode using syringe pumps.[252] The cell design was symmetric with dual-pass flow-through porous electrodes (Figure 8b) and achieved high power density of 300 mW/cm^2. However, the reactant crossover hindered the round trip energy efficiency of the μRFB to around 20%.[41] The crossover losses were analyzed during both charge and discharge modes and was attributed to both diffusive mixing and asymmetric splitting of reactant streams at the outlet junction.[252,253] To further address crossover issues, Suss *et al.* proposed the use of a thin, low-porosity layer with sub 1 μm pore diameter as a dispersion blocker that further minimized molecular diffusion of the liquid streams in a hydrogen-bromine μRFB. The results showed an improved power density output of 925 mW/cm^2 and a high cycle efficiency of 96%.[254]

Various other redox flow reactants have been reported in μRFBs. Marma *et al.* reported a H_2/iron μRFB where they investigated the charge and discharge performance by experimental test and one-dimensional modeling.[255] Ibrahim and Kjeang investigated the use of membrane-less cells to alleviate the high cell ASR challenge in RFBs with non-aqueous redox electrolytes. They studied different performance aspects and demonstrated rapid kinetics of the vanadium acetylacetonate system as a benchmark model showing high discharge power density of 550 mW/cm^2 for the first time for non-aqueous electrolytes.[108] Organic quinone redox compounds have also been utilized as reactants.[83,256–258] For example, Karakurt *et al.* presented a flexible μRFB for wearable applications based on non-toxic 2,6-dihydroxyanthraquinone and potassium ferro/ferricyanide redox pairs and showed peak power

density of 0.75 mW/cm^2.[258] The same half-cell reactants were used by Marschewski *et al.* in a miniaturized RFB developed for providing power and heat management, simultaneously. The cell (Figure 8c) used a membrane and investigated interdigitated, tapered, and multiple-pass microfluidic networks for the reactant mass transport.[83] The cell depicted a remarkable power density of 1.4 W/cm^2. Leung *et al.* presented an organic/inorganic membrane-less hybrid RFB based on low-cost zinc and para-benzoquinone species in the negative and positive half-cells, respectively.[256,257] The cell displayed a voltage of 1.52 V and an average energy efficiency of 73% at 30 mA/cm^2 over 12 cycles.

Lastly, there is another class of membrane-less RFBs recently introduced by Navalpotro *et al.*[259–261] which relies on the immiscibility of different solvents used in the two half-cell liquid reactant streams. For example, Bamgbopa *et al.* presented a cyclable membrane-less RFB with aqueous iron(II) sulfate anolyte and an organic catholyte comprising iron(III) acetylacetonate reactant species in water-immiscible ethylacetate solvent and an ionic liquid as supporting catholyte. The cell displayed over 60% discharge capacity and 80% coulombic efficiency after 25 cycles.[262] This class of membrane-less cells are however not the primary focus of this review as the reactant stream separation relies on biphasic separation[263] rather than co-laminar flow and therefore the cells are not necessarily classified as microfluidic. A recent review on this class of RFBs can be found elsewhere.[264]

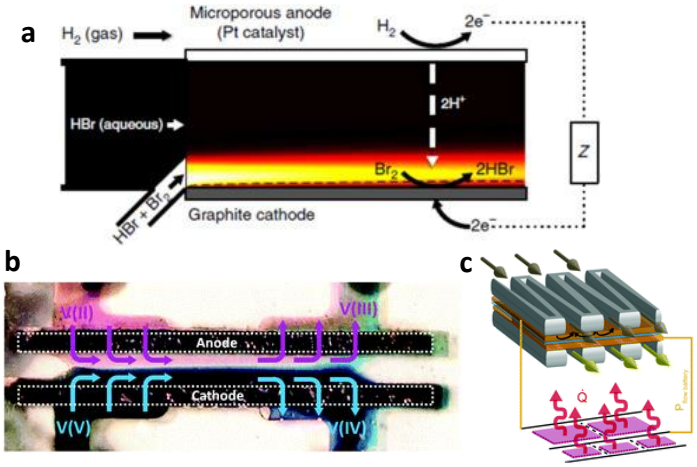

Figure 8: Microfluidic redox flow batteries: a) hydrogen-bromine µRFB with gas diffusion negative electrode and flow-over positive electrode, b) µRFB with flow-through porous electrodes utilizing vanadium redox reactants, and c) 3D printed fluidic networks for miniaturized membrane-based heat-managing RFBs. 8a: adapted from ref. 39 with permission. Copyright 2013 Springer Nature Publishing Group. 8b: reprinted from ref. 41 with permission. Copyright 2013 Royal Society of Chemistry. 8c: adapted from ref. 83 with permission. Copyright 2017 Royal Society of Chemistry.

4.2.2 Membrane-less Electrolyzers

Microfluidic electrolyzers have been reported to offer great advantages such as reduced system complexity and breaking the high ionic resistance paradigm found in benchmark membrane-based

electrolyzers while providing the flexibility of using any electrolyte. This can help optimizing electrolysis performance and efficiency or create new research methodologies for analytical purposes. In the literature, microfluidic electrolyzer works were applied towards electrolytic H_2 generation, CO_2 reduction, and other electrochemical processes, as summarized in this subsection.

H_2 Generation

Hydrogen is an important energy carrier and storage medium to supplement intermittent renewable electricity. At present, most of the hydrogen used worldwide is generated by steam methane reforming, which is not considered green as it generates CO_2 emissions. Electrochemical hydrogen generation by means of water electrolysis is a key path for zero-emission hydrogen production, provided that renewable electricity can be used as energy input. Membrane-less water electrolyzers can reduce system complexity and potentially avoid the high ionic resistance of conventional cells.[13] Hashemi *et al.* first developed the concept of a membrane-less electrolyzer device showing water splitting into hydrogen and oxygen at current densities up to 300 mA/cm^2. The device exhibited reactant conversion efficiencies up to 42% with very low hydrogen gas crossover of 0.4% into the oxidation side during continuous operation.[265] As shown in Figure 9a, the device comprised of two catalyst-decorated parallel plate electrodes separated by a flowing electrolyte. The evolved gases remained close to their respective catalyst surface due to the Segre´–Silberberg effect until downstream collection in separate, dedicated outlets. They also reported modeling and experimental study of a microfluidic hydrogen generator that is vapor-fed by humid air wherein they employed an ionomer thin film to absorb water from the air for transport to the electrodes.[102] Oruc *et al.* reported the design, fabrication, and characterization of a planar microchannel water electrolyzer and studied different parameters such as the channel thickness, operating temperature, and applied potential. The highest hydrogen production rate was observed in a 400 µm tall electrolyzer chamber using pulsed operation at 60°C and a potential of 2.0 V.[266] O'Neil *et al.* 3D printed prototype electrolyzers that achieved electrolysis efficiency of 61.9% and 72.5% in acidic and alkaline solutions, respectively, when operated at 100 mA/cm^2. The prototypes (Figure 9b) employed thin dividers downstream to aid product separation and 2.8% product crossover was measured using *in situ* electrochemical sensors, *in-situ* imaging, and gas chromatography.[267] Rarota *et al.* developed a microfluidic seawater electrolyzer with low power requirements coupled with a series of photovoltaic cells with a Y-shaped junction to facilitate H_2 separation at the outlet.[268] They also developed a solar panel-integrated paper-based device employing graphite from a pencil deposition with reduced graphene oxide coating and sea water electrolyte.[269] Pang *et al.* applied empirical correlations and electrochemical engineering design principles to present a framework using a parallel plate membrane-less electrolyzer model system for evaluating the performance limits and guiding their design optimization. Their analysis

deduced that the efficiencies and current densities of optimized cells constrained to 1% H_2 crossover rates can exceed those of conventional alkaline electrolyzers but are still lower than those achieved by zero-gap PEM electrolyzers.[101] Esposito presented a perspective on the economics of membrane-less electrolyzer technology as a promising approach to drive down electrolyzer capital costs owing to their simple construction and high current densities.[270]

Moreover, some works reported advances on catalyst materials and electrode structures. Campos-Roldán *et al.* presented a unitized regenerative microfluidic cell with alkaline environment operation using platinum group metal-free catalyst material based on NiO-Ni nanostructures supported on carbon nanotubes as a hydrogen bi-functional electrode material.[271,272] They reported power density outputs of 40 mW/cm^2 and 165 mW/cm^2 for fuel cell and electrolyzer modes, respectively. Regarding electrode structures, Hadikhani *et al.* developed a novel porous wall electrolyzer cell. The design resulted in a 58X reduction in H_2 crossover compared to parallel plate electrodes at the same operating conditions.[273] Gillespie *et al.* studied hydrogen generation performance in membrane-less divergent-electrode-flow-through alkaline electrolyzers.[274,275]

Furthermore, the mixed-media operation scheme may also be employed in microfluidic electrolyzers. In the case of hydrogen generation, the reversible (thermodynamic) potential of the cell is reduced to around 0.4 V by utilizing co-laminar acidic and alkaline streams at the hydrogen and oxygen electrodes, respectively. This concept was reported as a switchable unitized regenerative fuel cell by Lu *et al.* which showed an electrolysis onset voltage of only 0.57 V.[166] De *et al.* presented Y-shaped and H-shaped membrane-less reactor designs for water electrolysis.[276] They indicated a reduced applied potential of 1.58 V for asymmetric dual electrolytes compared to 2.2 V for symmetric acidic or alkaline electrolytes at an electrolysis current density of 10 mA/cm^2.

CO_2 Reduction

Significant research efforts have recently been conducted towards the promising electrochemical reduction reaction of carbon dioxide (CO_2RR) to convert it into useful sustainable chemicals or renewable fuels, using clean energy for economic benefits and for closing the carbon cycle.[277–279] Microfluidics based approaches have consequently been reported towards CO_2RR since they may enable elimination of the costly membrane and mitigation of water management issues such as anode dry-out and cathode flooding.[277] Microfluidics also enable higher energy efficiencies, by enabling reduced ionic resistances, higher mass transport, lower thermodynamic equilibrium, and pressurized operation.[280] Notably, many reported membrane-based CO_2 flow reactors also utilized microfluidic approaches for the reactor designs owing to such advantages, even if they were not explicitly reported as microfluidic cells.[75,85,281–283] Microfluidic flow cell designs for CO_2RR have thus been part of recent

reviews and accounts.[280,284–287] Typically, microfluidic CO_2 electrolysis cells utilize two GDEs for both cathode and anode electrodes, separated by a liquid electrolyte microchannel. Whipple *et al.* reported a microfluidic reactor for the CO_2RR and tested several catalysts as well as electrolyte pH effects on reactor efficiency for CO_2 reduction to formic acid.[288] The cell utilized 0.5 M $KHCO_3$ as electrolyte and implemented an oxygen evolution reaction at the anode to balance the electrochemical cell reaction, as shown in Figure 9c. Various numerical electrochemical models of microfluidic electrochemical flow cells were reported for CO_2RR to CO,[289,290] CH_3OH,[291] or formic acid.[292] Wang *et al.* reported that the competing hydrogen evolution reaction and the slow CO_2 diffusion are limiting the cell performance.[293] Wu *et al.* applied a 2D isothermal model to predict polarization curves at different gas flow rates and compositions.[289] Monroe *et al.* showed qualitative agreement in separation efficiencies between a computational model and experimental results in 3D printed laminar flow reactor prototypes for Sn catalyzed CO_2RR into formic acid.[292] Lv *et al.* employed a porous copper electrocatalyst to improve access to catalyst sites for CO_2RR in a microfluidic cell. They reported a current density up to 650 mA/cm^2 with a C2+ product selectivity of 62% and stable operation at 200 mA/cm^2 for more than 2 h. However, they reported flooding and degradation issues related to formation of gaseous products and salt accumulation.[282] Lu *et al.* explored the dual electrolyte or mixed-media advantages offered by microfluidic cells for CO_2RR.[294] They reported six-fold higher reactivity and a significant reduction in anodic potential from 1.7 V to 1 V and an increased cathodic potential from -2.1 V to 0.8 V.[295] Peak faradaic efficiency as high as 95.6% was recorded at 143 mA/cm^2. Moreover, they systematically analyzed the electrolyte flow rate, the microfluidic channel thickness, and the catalyst-to-ionomer ratio effects on maximizing cell performance.[296] They also investigated the dual-electrolyte degradation process from the neutralization reaction and reported an operation scheme for solution recycling.[297]

Other Electrolyzers

Membrane-less microfluidic cells were also reported for the electrolysis reactions of other purposes than H_2 generation and CO_2RR. Talabi *et al.* investigated the use of membrane-less electrolyzers with flow-through mesh electrodes for the simultaneous production of acid and base from aqueous brine solutions.[298] Hashemi *et al.* presented a versatile and membrane-less 3D printed monolithic electrochemical reactor (Figure 9d) for both water splitting and chlor-alkali reaction processes and found product purities of 99% and faradaic efficiencies of 90%.[81] The overall device performance showed 250% higher current density and 37-fold throughput enhancement over their first microfluidic prototype for water electrolysis. Perez *et al.* developed a microfluidic electrochemical reactor for waste-water treatment, comprising flow-through electrodes to maximize mass transport and a very narrow inter-electrode gap to minimize ohmic losses.[44] They successfully removed 100 ppm of

clopyralid contained in a synthetic soil washing effluent completely using 4-10X less electric charge and 6-15X less energy consumption compared to commercial systems. They also assessed the performance of a novel pressurized-jet microfluidic flow-through electrolyzer to produce aqueous solution of H_2O_2, showing feasible production in a 16.5 cm^3 cathode with an instantaneous current efficiency of 100% up to 20 mA/cm^3 corresponding to a H_2O_2 production rate of 13.1 mg/hcm^3.[45] Girenko and Velichenko studied the optimal cathode material for a flow-through coaxial cell applied for the synthesis of medical sodium hypochlorite solutions in a membrane-less electrolyzer for use in human and veterinary purposes.[299]

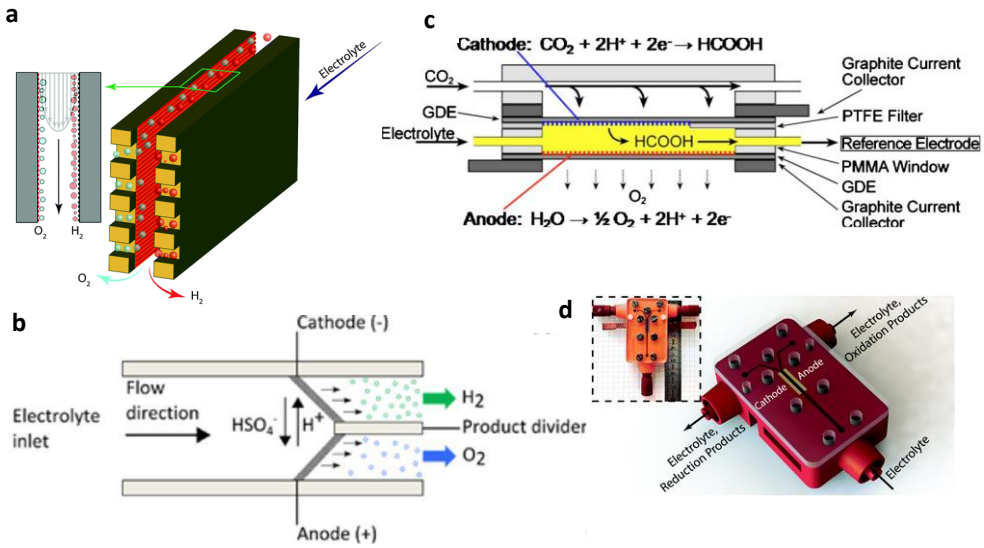

Figure 9: Microfluidic electrolyzers: a) parallel plate microfluidic electrolyzer for hydrogen generation, b) microfluidic electrolyzer employing downstream dividers to aid product separation, c) microfluidic reactor schematic for CO_2 electrolysis into formic acid, and d) a 3D printed versatile microfluidic electrolyzer for brine. 9a: Adapted from ref. 265 with permission. Copyright 2015 Royal Society of Chemistry. 9b: Adapted from ref. 267 under License CC BY-NC-ND 4.0. Published 2016 The Electrochemical Society. 9c: Adapted from ref. 288 with permission. Copyright 2010 The Electrochemical Society. 9d: Reprinted from ref. 81 under License CC BY-NC 3.0. Published 2019 by The Royal Society of Chemistry.

4.3 Emerging Applications

Novel applications that rely on cogeneration or combining dual device functionality in co-laminar flow cells have also emerged. For instance, microfluidics enabled dual functionality for liquid cooling and power generation was envisaged by IBM Corp. for combined powering and cooling of future high-performance computer architectures.[83,300,301] In this concept, redox flow reactants are utilized in microfluidic co-laminar flow arrays to generate power and cooling requirements for computer chips. While the concept is promising, the power density needs of such devices are considerably higher than current state-of-the-art RFB power density outputs. They proposed the applicability of the same

concept for cooling and powering of high-power LEDs and simultaneous cooling and energy storage for solar arrays.

Another dual functionality concept is the simultaneous generation of power and more valuable chemicals. For example, glycerol is a waste by-product from biofuels generation and its oxidation products have higher value.[302,303] Hence, a selective and specific catalyst is of interest to generate higher value products while simultaneously generating power. Isolation of desirable products is however a challenge due to the complex glycerol oxidation process, and a product analyzer is yet to be integrated and applied for full down-stream product analysis. Another example presented by Wouters *et al.* is the cogeneration of nitrobenzene derivatives such as aniline and azoxybenzene in CLFCs.[304,305] They reported 37% conversion at a flow rate of 5 µL/min with an average power density of 0.062 mW/cm^2. Furthermore, Fadakar *et al.* reported a coupled microbial microfluidic flow cell as a self-powered biohydrogen generator.[306]

Photoelectrochemical cells (PECs) are other emerging devices that deploy photo-catalytic redox reactions at one or both electrodes. In these devices, a semiconductor material is employed as photo-electrode in the cell which is photoexcited by sunlight.[307] These cells however have mass transport challenges as reviewed by Modestino *et al.* for solar hydrogen generation.[308] Microfluidics (or optofluidics) offers several prospective benefits for PECs, including high surface-to-volume ratio, enhanced reaction rates, and enhanced mass transfer and photon transfer because of the uniform light distribution.[309] This has inspired many researchers to develop microfluidic photoelectrochemical cells (µPECs) for different applications such as converting organic pollutants into electricity.[310–312] For example, Li *et al.* assembled a PDMS galvanic µPEC (fuel cell) comprising of a TiO_2 photoanode and a Pt air-breathing cathode for glucose oxidation and oxygen reduction, respectively, producing a peak power density of 0.58 mW/cm^2.[311,313] Guima *et al.* reported the combination of fuel cell and photocatalysis in the same device employing a mixed-media 3D printed µFC with PtO_x/Pt dispersed on a $BiVO_4$ photoanode which produced a maximum power density of 0.48 mW/cm^2 using pollutant-model rhodamine B as fuel.[80] Kwok *et al.* presented a dual-fuel µFC using CH_3OH and photoproduced H_2 employing Pt/Pt25 as photo-catalyst showing ten-fold increase in peak power density when the system was exposed to simulated solar light.[105,314] Ovando-Medina *et al.* presented an air-breathing photo-microfluidic fuel cell with ZnO/Au composite as photoanode and human blood as direct source of glucose.[315] They demonstrated a 1.5X increase in power density in visible light vs. darkness. Similarly, Dector *et al.* evaluated a photo-assisted µFC with TiO_2-Ni as photoanode and human urine as a fuel. The cell displayed an OCV of 0.7 V and maximum power density of 0.09 mW/cm^2.[316] Photo-assisted catalysis has also been reported for microfluidic electrolysis cells and applied towards the generation of different chemicals such as H_2O_2,[317] chlorine,[318] H_2,[308] or liquid fuels.[319] Kalamaras *et al.* applied a

range of CuO-based thin films as photocathodes in a continuous flow microfluidic photoelectrochemical cell reactor for the production of liquid fuels from the electrolysis of CO_2 saturated aqueous $NaHCO_3$ solution.[319]

4.4 Analytical Tools

An alternative avenue for microfluidics aided electrochemical energy conversion is to apply the microfluidic cells as analytical tools. Examples of analyses reported to date include screening of new catalyst materials,[320] studying electrochemical reactions,[321] characterizing electrode material properties, characterizing flow conditions,[322] or measuring electrochemical characteristics.[107] Microfluidics serves as a powerful technology for creating electrochemical cells that may represent conventional counterparts in a simple, low-cost, precise, and versatile way with rapid prototyping and enable the possibility of flow imaging and flow visualization. In these cases, the outcomes of the works utilizing microfluidic devices may be directly translatable and relevant to conventional electrochemical energy conversion systems. In this regard, it is noteworthy that many of the µFCs covered in previous sections may thus serve as analytical devices even though they were originally developed for other uses such as power sources or electrolyzers. For example, the results of testing new methods or novel electrocatalyst or photocatalyst materials in microfluidic flow cells can be applied towards the development of large-scale electrochemical cells. Some works in the literature have expressly designed and utilized microfluidic cells for such analytical purposes. For example, Brushett *et al.* reported an alkaline H_2/O_2 microfluidic fuel cell as a platform for cathode catalyst characterization, which was also later applied towards the anode and the electrode preparation techniques.[323,324] Jhong *et al.* utilized a microfluidic platform to study the cathode electrode performance for the ORR and CO_2RR and its dependence on the catalyst layer preparation methods comparing hand-painting, air-brushing, and screen-printing.[97] Modestino *et al.* developed an integrated microfluidic test-bed for mass-transport and catalysis research in energy conversion devices via water electrolysis, and suggested the use of the same system for fuel cell and photo-electrolyzer research.[325]

In the case of electrolyzers, the generated gaseous products (*e.g.*, H_2 and O_2) makes the microfluidic system design and operation more challenging than for all-liquid µFCs.[270] This is because the gas evolution may result in blockage of electroactive sites, thus slowing down the reaction, impacting mass transport, or promoting the mixing of products.[326,327] This is typically more evident at low flow rates, when the bubbles may fill the microchannel, resulting in increased ionic resistance which would result in voltage instability.[265,328] Therefore, microfluidic analytical tools were widely applied towards gas evolution reactions and bubble formations.[329–333] Arbabi *et al.* utilized microfluidic platforms to visualize bubble transport in electrolyzer gas diffusion layers to investigate its impact on multiphase flow (Figure 10a).[329] In order to keep the bubbles small at low flow rates, Hadikhani *et al.* analyzed the

use of surfactants as additives in the electrolyte, showing inhibited bubble coalescence, faster detachment, and increased hydrogen throughput.[331] Davis *et al.* utilized high speed video camera to investigate the bubble dynamics in gas evolving electrodes of membrane-less electrolyzers.[332] Their method determined the current density distributions along the electrode by detecting and quantifying the downstream gas formation.

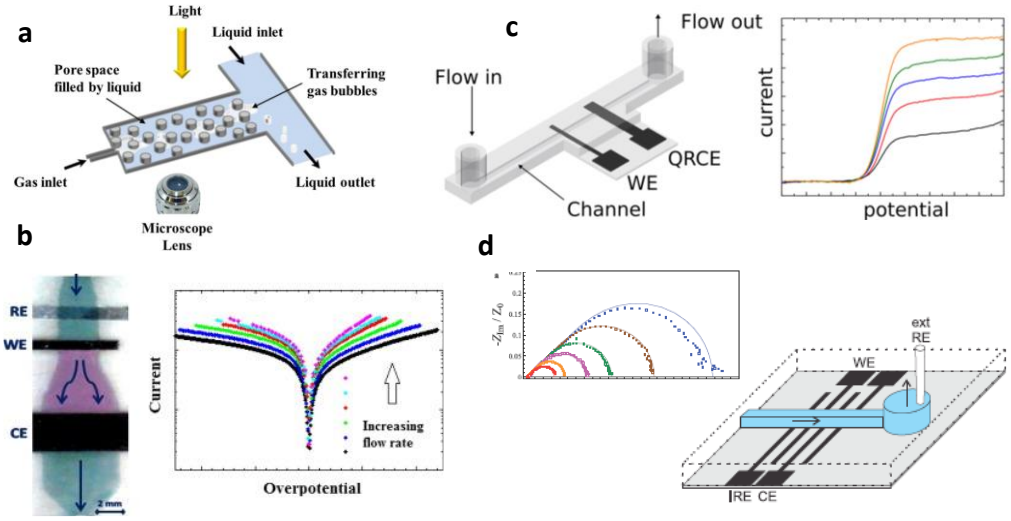

Figure 10. Microfluidic electrochemical cells as analytical tools: a) bubble visualization in electrolyzers, b) kinetic measurements in flow-through porous electrodes, c) hydrodynamic electrochemistry measurements, and d) mass-transport impedance measurements. 10a: Adapted from ref. 329 with permission. Copyright 2011 Elsevier. 10b: Reprinted from ref. 107 with permission. Copyright 2015 Elsevier. 10c: Adapted from ref. 71 with permission. Copyright 2019 Elsevier. 10d: Adapted from ref. 334 with permission. Copyright 2016 Elsevier.

For RFB works, some microfluidic analytical studies focused on analyzing the diffusion issues in µRFBs that hinder the cell efficiency.[253,335] For example, Ibrahim *et al.* presented an analytical cell design that was based on the original µRFB design by Lee *et al.*[41] with dual-pass architecture. The analytical cell was used to investigate cell performance and crossover losses during both discharge and charge modes. The analysis confirmed the impact of crossover on the round-trip cell efficiency and showed a trade-off of reactant conversion efficiency and crossover losses at the operating flow rates.[253] The same analytical cell design was applied to investigate the influence of parasitic shunt current losses that occur in cell arrays that have fluidic ionic connection through the electrolyte and electronic connection through their series connection, the results of which can be adopted for large-scale RFBs.[336] Other microfluidic analytical cells have focused on measuring electrochemical parameters and development of electrode modifications related to RFBs. Goulet *et al.* developed an analytical three-electrode flow cell (Figure 10b) to measure electrochemical kinetics of redox reactants using Tafel slope of IR-compensated polarization at a flow rate that is fast enough to decouple mass transport from reaction kinetics within flow-through porous electrodes.[107] The rate constant data extracted from

this cell demonstrated that the negative electrode has significantly slower kinetics than the positive electrode in vanadium RFBs using flow-through porous electrodes, which has critical implications for larger-scale cells and systems. They also applied the cell to quantify enhancements in the kinetics on porous electrodes that are *in-situ* decorated with carbon nanotubes, showing enhancements in the ECSA.[98] Furthermore, the same cell design was employed to study the importance of wetting of porous electrodes[66] and to measure reaction kinetics of non-aqueous vanadium acetylacetonate electrolytes on flow-through porous electrodes.[108]

Similar works were also reported using microfluidic tools for other hydrodynamic electrochemical analyses. Kjeang *et al.* developed a novel electrochemical velocimetry approach in a microfluidic analytical cell to measure local flow rates.[322] Snowden *et al.* fabricated microfluidic cells using microstereo-lithography for electrochemical flow detection by measuring the transport-limited current response of an oxidation reaction, which was in agreement with the well-established Levich equation and mass transport simulation models.[337] Similarly, O'Neil *et al.* used hydrodynamic electrochemistry to characterize a single-step 3D printed microfluidic cell (Figure 10c), which behaved according to the Levich equation.[71] Dumitrescu *et al.* applied a dual-electrode microfluidic electrochemical flow cell for examining the kinetics of electrocatalysts, indicating major advantages in mass transport over the standard rotating ring disk electrode technique.[320] Holm *et al.* demonstrated numerical results that were in good agreement with experimental results in a microfluidic cell for estimating mass-transport impedance (Figure 10d) in channel and double channel electrodes.[334,338] The validated model was applied to test validity of empirical and analytical approximations. In general, it can be observed that the broad results of these latter analytical studies on electrochemical fundamentals such as reaction kinetics and mass transport are also applicable for conventional electrochemical energy conversion devices. In addition to their simple design and rapid fabrication, demonstrations in microfluidic cells serve as a better representation of real flow cell operation than conventional three-electrode electrochemical characterization in stationary cells or commonly used characterization cells such as H-cells with stagnant flow and/or planar electrodes.

Lastly, the research fields of microfluidics and electrochemistry are also frequently linked for electrochemical sensing purposes for which microfluidic analytical devices may be constructively employed. Examples of such contributions include microfluidic sensors or detectors that rely on electrochemical sensing[339–342] applied for sensing labeled particles[343] or detecting analytes such as lactate,[153,344] dopamine,[345,346] or toxins.[347]. These works however do not focus on energy conversion and are therefore generally beyond the scope of this review. For further information on electrochemical sensing aided by microfluidics, the reader is referred to alternate review articles that cover more general lab-on-a-chip or micro-total-analysis-systems available elsewhere.[348–350]

5 - Opportunities

As shown in the previous section, the research field of microfluidic electrochemical energy conversion has experienced major growth over the past two decades since its inception in 2002. On the device perspective, the field started with membrane-less microfluidic fuel cell applications and has expanded to include a wide variety of other electrochemical flow cells such as paper-based fuel cells, redox flow batteries, metal-air batteries, hybrid flow cells, electrolyzers, and photoelectrochemical cells. Figure 5 illustrates the evolution of contributions covered in the different research areas since 2002. The figure shows the significant dominance of research outcomes from galvanic cells throughout the entire period as well as the more recent, post 2014 expansion of research outcomes from electrolytic cells and other emerging cell concepts. It also captures the gradual rise of paper-based microfluidic electrochemical cells in the last decade, which as of 2020 represent up to one third of the annual contributions in this field. On the practical utility perspective, most microfluidic fuel cell works were focused on power sources for portable applications or off-grid systems, owing to their simplicity and low cost. In this regard, the power density outputs of the cells – a figure of merit that drove the field for many years - has significantly evolved to reach levels that are comparable to or even exceed those of conventional cells. This is a competitive feature for microfluidic cells and may entice further research in new directions that benefit from ultra-high power density, such as combined powering and cooling of microelectronics. Notably, high power density also generally translates into opportunities for high voltage efficiency and high overall energy conversion efficiency, which are important figures or merit for redox flow batteries, although such reports have been less common to date. Despite encouraging progress, some of the challenges discussed by Goulet and Kjeang in 2014 to make the technology commercially viable have still not been adequately addressed, such as the physical constraints of scale-up. In this regard, the scale-up guidelines discussed by Modestino *et al.* categorized the scaling approaches into areal and multiplexing, in which areal scale-up can readily benefit from current manufacturing techniques. Emerging manufacturing techniques such as the production of "*cellular fluidics*" may also aid practical scaling of microfluidic devices. In these cells, precise control and uniform distribution of reactants can be programmed in a way that enables high through-put production of scalable cells with more structured packaging and less support materials to enable high volumetric power densities. Other challenges discussed by Goulet and Kjeang in 2014 are the stability of the co-laminar interface, and perhaps more importantly, reactant recharging, recovery, or recycling as well as device durability and system integration. Targeted research to address these gaps is therefore still required – and recommended for future work. Furthermore, the effect of the balance of plant (pumps,

tanks, piping, etc.) on overall system energy density and complexity has only occasionally been considered, despite its impact on the practical implementation of portable solutions. To date, these shortcomings have been a major constraint for technology commercialization in this sector and have so far rendered the technology more suitable for stationary power solutions such as redox flow batteries, where subsystems for electrolyte handling and ancillary devices are already established. In some cases, microfluidic cells may capitalize on opportunities for increased device lifetime, for instance in the upcoming generation of organic redox flow cells, as the use of organic species originating from natural sources are known to cause membrane degradation. Commercial development of microfluidic electrochemical cells also stands to benefit from more explicit technology – application pairing, which is a commonly used strategy for commercialization of conventional battery technologies.

Notably, microfluidic strategies have found an interesting niche in paper-based devices in which cells are developed with wicking materials able to drive fluid flow by capillary forces. Generally, these power sources are intended for single-use applications offering added benefits for disposability. Despite their limited capacity defined by the saturation of the paper substrate, the devices may be engineered to match their target application needs, such as running a sample test or a series of tests. An example of such work is the lateral flow paper-based fuel cell proposed for powering lateral flow diagnostic assays, where it can be integrated within manufacturing processes and be activated by the same sample or analyte used. While the concept was demonstrated with methanol, it could eventually harvest reactant fuels from the biological analytes, enabling self-powered autonomous diagnostic devices. It is also noteworthy that unlike conventional cells, paper-based microfluidic fuel cells and batteries can be completely biodegradable or even compostable, given that a fully integrated device can be designed and fabricated without use of plastics, metals, and toxic materials. This is a timely research direction considering the severe environmental concerns and toxicity associated with battery and other e-waste as well as plastic pollution in aquifers, oceans, and biological systems.

Besides, the collective knowledge generated by the microfluidic flow cell research community over the past 20 years has also been redirected towards new applications. In this regard, the development of microfluidic analytical tools, as described in Section 4.4, is considered an important opportunity for microfluidic flow cells, since microfluidics is the ideal tool for efficient mass transport within electrochemical cells. Therefore, the use of such analytical tools is increasing, with key applications towards assessing catalysts and electrode materials, visualizing flow distribution, measuring electrochemical diagnostics, characterizing different applied methods, and isolating specific components or analytes from unwanted interferences. Alternatively, microfluidic analytical cells can also serve as rapid validation tools for computational materials screening results from modeling or artificial intelligence techniques for catalysts, photo-catalysts, or redox reactants, for example. Some

of these tools may however benefit from having standardized cell formats with demonstrated utility, which is subject to further research and investigation. Hence, microfluidics technology may enable tremendous analytical opportunities for improved electrochemical energy conversion by providing effective mass transport in a way that resembles full-scale applications found in fuel cells, flow batteries, electrolysis cells, and photoelectrochemical cells.

Lastly, the inherent advantages of membrane-less cell architectures can be very useful for the recently developed microfluidic electrolyzers, as they have advantages of simple structures and low costs with high purity and separation efficiencies of products. These devices may also be less sensitive to interface stability and therefore more amenable for two-dimensional scale-up without compromising the transport processes, if carefully engineered. The gas bubble generation may impose technical limitations to the operation in microfluidic systems, but efficient control has been shown in the contributions. This may therefore trigger commercialization activities towards renewable hydrogen production, CO_2 electro-reduction, and other electrolytic processes. There is also a plethora of untapped research opportunities on the use of microfluidics technology for electrolytic and hybrid cells that are likely to extend well beyond hydrogen and CO_2. The recent surge in interest in 'power-to-x' (or P2X) technologies for constructive electrochemical conversion of surplus renewable electricity is ripe for research on microfluidics augmented systems, particularly in locations or applications that may not benefit from direct electrification. This includes producing other chemicals, feedstocks, or fuels (*e.g.*, green ammonia), running certain processes (*e.g.*, capacitive desalination), or even cogeneration. For instance, it can be envisioned that microfluidic P2X cells may find important utility for distributed on- or off-grid capture and use of renewable energy on small to medium scales. These microfluidic P2X cells would benefit from a multitude of microfluidic advantages gathered from the collective knowledge on various microfluidic electrochemical cells, enabling unprecedented efficiencies, flow control, product selectivity, and precise local product separation. As a research community, it is important to continue exploring innovative use of microfluidics for novel electrochemical energy conversion systems, for which the true benefits of microfluidics may not yet have been realized or fully exploited. Overall, the use of microfluidic tools, devices, and systems is anticipated to continue its growth and utility for electrochemical energy conversion in many years to come.

Short biographies

- Dr. Omar A. Ibrahim earned a B.Sc. and M.Sc. in Mechanical Engineering from Alexandria University, Egypt and received his PhD in 2018 in Mechatronic Systems Engineering at Simon Fraser University, Canada, in the Fuel Cell Research Laboratory, under the supervision of Prof. Erik Kjeang. He was awarded a convocation medal for his doctoral thesis entitled "Practical advances in microfluidic electrochemical energy conversion". During his PhD, he co-invented a biodegradable power source for environmental sensors, which was recognized and awarded seed grant from the Bill & Melinda Gates Foundation. He was also a visiting researcher at IBM Research – Zurich under a Mitacs award. His research focuses on microfluidics, energy systems, and sustainability and he has 25+ scientific contributions. Currently, he is a product development scientist and a Marie Curie fellow at Fuelium SL, Spain, working on developing sustainable battery systems.
- Marina Navarro-Segarra received her Bachelor's degree in Physics from the Autonomous University of Barcelona in 2017. She also holds an MSc in Electrochemistry from the University of Barcelona. Currently, she is developing her doctorate studies in Electrochemistry at the Microelectronics Institute of Barcelona, IMB-CNM (CSIC). Her research is focused on the development of sustainable electrochemical power sources for portable devices.
- Pardis Sadeghi received her Bachelor's degree in Chemical Engineering from University of Tehran, Iran in 2018. She is currently a Master's student in Mechatronic Systems Engineering at Simon Fraser University, Canada. She is a research assistant in the SFU Fuel Cell Research Laboratory working on modeling and simulation of paper-based microfluidic flow batteries under the supervision of Prof. Erik Kjeang. She expects to defend her MSc thesis in Fall 2021.
- Dr. Neus Sabaté obtained her PhD in Physics in 2003. She is an ICREA Research Professor and leader of the Self-Powered Engineered Devices Group at the Microelectronics Institute of Barcelona (IMB-CNM). She has co-authored more than 100 papers in journals and conferences and submitted 15 patents. In 2006 she started a research line in silicon microfabricated fuel cells that evolved to the biodegradable electrochemical power sources she develops today. In 2015 she obtained an ERC-Consolidator Grant to develop single-use paper fuel cells as key components of a new generation of affordable and efficient point-of-care devices. She also co-founded Fuelium SL, a company that commercializes paper batteries for single use applications.
- Dr. Juan Pablo Esquivel is currently a Tenured Scientist at the IMB-CNM (CSIC) and has recently been appointed as Ikerbasque Research Associate at BCMaterials. He is also co-founder and Scientific Advisor of the spin-off company Fuelium. He has a PhD in Electronics Engineering from the Autonomous University of Barcelona and was a Senior Fellow at the University of Washington, under a Marie Curie Fellowship. His work is focused on the development of paper-based fuel cells and biodegradable batteries for autonomous diagnostic devices, combining engineering, electrochemistry, paper microfluidics, and printed electronics technologies with sustainability principles and a strong product-oriented approach. He has received several international prizes and distinctions for his work, has authored more than 100 scientific contributions and is inventor of 12 patents.
- Dr. Erik Kjeang is an Associate Professor in Mechatronic Systems Engineering at Simon Fraser University (SFU) in Vancouver, Canada and Canada Research Chair in Fuel Cell Science and Technology Development. Dr. Kjeang obtained a Ph.D. in Mechanical Engineering from the University of Victoria, Canada and an M.Sc. in Energy Engineering from Umeå University, Sweden. Prior to joining SFU, Dr. Kjeang worked as a research engineer at Ballard Power Systems. He has 17 years of experience with fuel cell research, focusing on electrode and cell design – with or without membranes. Dr. Kjeang is also a recognized expert on fuel cell

durability and recently contributed technology for enhancing and predicting membrane lifetime in fuel cell buses in collaboration with Ballard. His lab at SFU features Canada's first facility for multi-length scale X-ray tomography, which is optimal for visualization of electrochemical cells. He has raised more than $20M in funding and authored 120 peer-reviewed journal publications and 6 patents.

Acknowledgments

Funding for this research was provided by the Natural Sciences and Engineering Research Council of Canada, Canada Foundation for Innovation, British Columbia Knowledge Development Fund, and ERC Consolidator Grant (SUPERCELL – GA.648518). This research was undertaken, in part, thanks to funding from the Canada Research Chairs program. O.I. acknowledges partial funding of this research through the Marie Skłodowska-Curie European Fellowship within the European Union's H2020 Framework Programme (Grant agreement ID: 101033075 – SPRICE). The authors thank Carles Tortosa for his support in the preparation of graphical material.

List of Abbreviations

Symbol/Abbreviation	Definition
ASR	Area-specific resistance
CLFC	Co-laminar flow cell
CNC	Computer numerical control
CO_2RR	Carbon dioxide reduction reaction
ECSA	Electrochemically active surface area
EIS	Electrochemical impedance spectroscopy
GDE	Gas diffusion electrode
OCV	Open-circuit voltage
ORR	Oxygen reduction reaction
PDMS	Poly(dimethylsiloxane)
PEC	Photoelectrochemical cell
PEM	Polymer electrolyte membrane
PMMA	Poly(methyl methacrylate)
PLA	Polylactic acid
RFB	Redox flow battery
µFC	Microfluidic fuel cell
µPEC	Microfluidic photoelectrochemical cell
µRFB	Microfluidic redox flow battery

References

(1) Schleussner, C.-F.; Rogelj, J.; Schaeffer, M.; Lissner, T.; Licker, R.; Fischer, E. M.; Knutti, R.; Levermann, A.; Frieler, K.; Hare, W. Science and Policy Characteristics of the Paris Agreement Temperature Goal. *Nat. Clim. Change* **2016**, *6*, 827–835. https://doi.org/10.1038/nclimate3096.

(2) Zou, C.; Zhao, Q.; Zhang, G.; Xiong, B. Energy Revolution: From a Fossil Energy Era to a New Energy Era. *Nat. Gas Ind. B* **2016**, *3*, 1–11. https://doi.org/10.1016/j.ngib.2016.02.001.

(3) Bouckaert, S.; Fernandez Pales, A.; McGlade, C.; Remme, U.; Wanner, B.; Varro, L.; D'Ambrosio, D.; Spencer, T. Net Zero by 2050: A Roadmap for the Global Energy Sector. *International Energy Agency*. Paris, France 2021, pp 1–224.

(4) Liu, R. S.; Zhang, L.; Sun, X.; Liu, H.; Zhang, J. Electrochemical Technologies for Energy Storage and Conversion, 2 Volume Set. John Wiley & Sons: Weinheim, Germany 2011, pp 1–43. https://doi.org/10.1002/9783527639496.

(5) Nguyen, N.; Wereley, S.; Shaegh, S. A. M. Fundamentals and Applications of Microfluidics. Artech House: Boston 2019, pp 1–576. https://doi.org/http://doi.wiley.com/10.1002/1521-3773%252820010316%252940%253A6%253C9823%253A%253AAID-ANIE9823%253E3.3.CO%253B2-C.

(6) Convery, N.; Gadegaard, N. 30 Years of Microfluidics. *Micro and Nano Engineering* **2019**, *2*, 76–91. https://doi.org/10.1016/j.mne.2019.01.003.

(7) Ferrigno, R.; Stroock, A. D.; Clark, T. D.; Mayer, M.; Whitesides, G. M. Membraneless Vanadium Redox Fuel Cell Using Laminar Flow. *J. Am. Chem. Soc.* **2002**, *124*, 12930–12931. https://doi.org/10.1021/ja020812q.

(8) Choban, E. R.; Markoski, L. J.; Wieckowski, A.; Kenis, P. J. A. Microfluidic Fuel Cell Based on Laminar Flow. *J. Power Sources* **2004**, *128*, 54–60. https://doi.org/DOI 10.1016/j.jpowsour.2003.11.052.

(9) Kjeang, E. Microfluidic Fuel Cells and Batteries. Springer International Publishing: Cham 2014, pp 1–76. https://doi.org/10.1007/978-3-319-06346-1.

(10) Kjeang, E.; Djilali, N.; Sinton, D. Microfluidic Fuel Cells: A Review. *J. Power Sources* **2009**, *186*, 353–369. https://doi.org/DOI 10.1016/j.jpowsour.2008.10.011.

(11) Goulet, M.-A.; Kjeang, E. Co-Laminar Flow Cells for Electrochemical Energy Conversion. *J. Power Sources* **2014**, *260*, 186–196. https://doi.org/10.1016/j.jpowsour.2014.03.009.

(12) Nasharudin, M. N.; Kamarudin, S. K.; Hasran, U. A.; Masdar, M. S. Mass Transfer and Performance of Membrane-Less Micro Fuel Cell: A Review. *Int. J. Hydrog. Energy* **2014**, *39*, 1039–1055. https://doi.org/10.1016/j.ijhydene.2013.09.135.

(13) Modestino, M. A.; Fernandez Rivas, D.; Hashemi, S. M. H.; Gardeniers, J. G. E.; Psaltis, D. The Potential for Microfluidics in Electrochemical Energy Systems. *Energy Environ. Sci.* **2016**, *9*, 3381–3391. https://doi.org/10.1039/c6ee01884j.

(14) Hanapi, I. H.; Kamarudin, S. K.; Zainoodin, A. M.; Hasran, U. A. Membrane-less Micro Fuel Cell System Design and Performance: An Overview. *Int. J. Energy Res.* **2019**, *43*, 8956–8972. https://doi.org/10.1002/er.4804.

(15) Wang, Y.; Luo, S.; Kwok, H. Y. H.; Pan, W.; Zhang, Y.; Zhao, X.; Leung, D. Y. C. Microfluidic Fuel Cells with Different Types of Fuels: A Prospective Review. *Renew. Sustain. Energy Rev.* **2021**, *141*, 110806. https://doi.org/10.1016/j.rser.2021.110806.

(16) Shen, L.; Zhang, G.; Etzold, B. J. M. Paper-Based Microfluidics for Electrochemical Applications. *ChemElectroChem* **2020**, *7*, 10–30. https://doi.org/10.1002/celc.201901495.

(17) Newman, J.; Thomas-Alyea, K. E. Electrochemical Systems. John Wiley & Sons: Hoboken, NJ 2004, pp 1–635.

(18) Mench, M. M. Fuel Cell Engines. *Fuel Cell Engines*. John Wiley & Sons, Inc.: Hoboken, NJ January 1, 2008, pp 1–515. https://doi.org/10.1002/9780470209769.

(19) Zhang, H.; Zhang, H.; Li, X.; Zhang, J. Redox Flow Batteries: Fundamentals and Applications. CRC Press: Boca Raton, FL 2017, pp 1–444. https://doi.org/10.1201/9781315152684.

(20) Soloveichik, G. L. Flow Batteries: Current Status and Trends. *Chem. Rev.* **2015**, *115*, 11533–11558. https://doi.org/10.1021/cr500720t.

(21) Shah, A. A.; Watt-Smith, M. J.; Walsh, F. C. A Dynamic Performance Model for Redox-Flow Batteries Involving Soluble Species. *Electrochim. Acta* **2008**, *53*, 8087–8100. https://doi.org/10.1016/j.electacta.2008.05.067.

(22) Bird, R. B.; Lightfoot, E. N.; Stewart, W. E. Transport Phenomena. John Wiley and Sons, Inc.: New York 2007, pp 1–897.

(23) Barton, J. L.; Brushett, F. R. A One-Dimensional Stack Model for Redox Flow Battery Analysis and Operation. *Batteries* **2019**, *5*, 25. https://doi.org/10.3390/batteries5010025.

(24) Fu, E.; Downs, C. Progress in the Development and Integration of Fluid Flow Control Tools in Paper Microfluidics. *Lab Chip* **2017**, *17*, 614–628. https://doi.org/10.1039/C6LC01451H.

(25) Washburn, E. W. The Dynamics of Capillary Flow. *Phys. Rev.* **1921**, *17*, 273–283. https://doi.org/10.1103/PhysRev.17.273.

(26) Lucas, R. Rate of Capillary Ascension of Liquids. *Kolloid-Zeitschrift* **1918**, *23*, 15–22. https://doi.org/10.1007/BF01461107.

(27) Richards, L. A. Capillary Conduction Of Liquids Through Porous Mediums. *Physics* **1931**, *1*, 318–333. https://doi.org/10.1063/1.1745010.

(28) Choban, E. R.; Spendelow, J. S.; Gancs, L.; Wieckowski, A.; Kenis, P. J. A. Membraneless Laminar Flow-Based Micro Fuel Cells Operating in Alkaline, Acidic, and Acidic/Alkaline Media. *Electrochim. Acta* **2005**, *50*, 5390–5398. https://doi.org/10.1016/j.electacta.2005.03.019.

(29) Choban, E. R.; Waszczuk, P.; Kenis, P. J. A. Characterization of Limiting Factors in Laminar Flow-Based Membraneless Microfuel Cells. *Electrochem. Solid-State Lett.* **2005**, *8*, A348. https://doi.org/10.1149/1.1921131.

(30) Cohen, J. L.; Westly, D. A.; Pechenik, A.; Abruña, H. D. Fabrication and Preliminary Testing of a Planar Membraneless Microchannel Fuel Cell. *J. Power Sources* **2005**, *139*, 96–105. https://doi.org/10.1016/j.jpowsour.2004.06.072.

(31) Cohen, J. L.; Volpe, D. J.; Westly, D. A.; Pechenik, A.; Abruña, H. D. A Dual Electrolyte H 2/O 2 Planar Membraneless Microchannel Fuel Cell System with Open Circuit Potentials in Excess of 1.4 V. *Langmuir* **2005**, *21*, 3544–3550. https://doi.org/10.1021/la0479307.

(32) Zebda, A.; Renaud, L.; Cretin, M.; Pichot, F.; Innocent, C.; Ferrigno, R.; Tingry, S. A Microfluidic Glucose Biofuel Cell to Generate Micropower from Enzymes at Ambient Temperature. *Electrochem. commun.* **2009**, *11*, 592–595. https://doi.org/10.1016/j.elecom.2008.12.036.

(33) Lee, S. H.; Ahn, Y. A Laminar Flow-Based Single Stack of Flow-over Planar Microfluidic Fuel Cells. *J. Power Sources* **2017**, *351*, 67–73. https://doi.org/10.1016/j.jpowsour.2017.03.102.

(34) Jayashree, R. S.; Gancs, L.; Choban, E. R.; Primak, A.; Natarajan, D.; Markoski, L. J.; Kenis, P. J. A. Air-Breathing Laminar Low-Based Microfluidic Fuel Cell. *J. Am. Chem. Soc.* **2005**, *127*, 16758–16759. https://doi.org/10.1021/ja054599k.

(35) Tominaka, S.; Ohta, S.; Obata, H.; Momma, T.; Osaka, T. On-Chip Fuel Cell: Micro Direct Methanol Fuel Cell of an Air-Breathing, Membraneless, and Monolithic Design. *J. Am. Chem. Soc.* **2008**, *130*, 10456–10457. https://doi.org/10.1021/ja8024214.

(36) Shaegh, S. A. M.; Nguyen, N. T.; Chan, S. H. Air-Breathing Microfluidic Fuel Cell with Fuel Reservoir. *J. Power Sources* **2012**, *209*, 312–317. https://doi.org/10.1016/j.jpowsour.2012.02.115.

(37) Jayashree, R. S.; Egas, D.; Spendelow, J. S.; Natarajan, D.; Markoski, L. J.; Kenis, P. J. A. Air-Breathing Laminar Flow-Based Direct Methanol Fuel Cell with Alkaline Electrolyte. *Electrochem. Solid-State Lett.* **2006**, *9*, A252. https://doi.org/10.1149/1.2185836.

(38) Xuan, J.; Leung, D. Y. C.; Wang, H.; Leung, M. K. H.; Wang, B.; Ni, M. Air-Breathing Membraneless Laminar Flow-Based Fuel Cells: Do They Breathe Enough Oxygen? *Appl. Energy* **2013**, *104*, 400–407. https://doi.org/10.1016/j.apenergy.2012.10.063.

(39) Braff, W. A.; Bazant, M. Z.; Buie, C. R. Membrane-Less Hydrogen Bromine Flow Battery. *Nat. Commun.* **2013**, *4*, 2346. https://doi.org/10.1038/ncomms3346.

(40) Kjeang, E.; Michel, R.; Harrington, D. A.; Djilali, N.; Sinton, D. A Microfluidic Fuel Cell with Flow-through Porous Electrodes. *J. Am. Chem. Soc.* **2008**, *130*, 4000–4006. https://doi.org/10.1021/ja078248c.

(41) Lee, J. W.; Goulet, M.-A.; Kjeang, E. Microfluidic Redox Battery. *Lab Chip* **2013**, *13*, 2504–2507. https://doi.org/10.1039/c3lc50499a.

(42) Davis, J. T.; Qi, J.; Fan, X.; Bui, J. C.; Esposito, D. v. Floating Membraneless PV-Electrolyzer Based on Buoyancy-Driven Product Separation. *Int. J. Hydrog. Energy* **2018**, *43*, 1224–1238. https://doi.org/10.1016/j.ijhydene.2017.11.086.

(43) Rajaei, H.; Rajora, A.; Haverkort, J. W. Design of Membraneless Gas-Evolving Flow-through Porous Electrodes. *J. Power Sources* **2021**, *491*, 229364. https://doi.org/10.1016/j.jpowsour.2020.229364.

(44) Pérez, J. F.; Llanos, J.; Sáez, C.; López, C.; Cañizares, P.; Rodrigo, M. A. Development of an Innovative Approach for Low-Impact Wastewater Treatment: A Microfluidic Flow-through Electrochemical Reactor. *Chem. Eng. J.* **2018**, *351*, 766–772. https://doi.org/10.1016/j.cej.2018.06.150.

(45) Pérez, J. F.; Llanos, J.; Sáez, C.; López, C.; Cañizares, P.; Rodrigo, M. A. Towards the Scale up of a Pressurized-Jet Microfluidic Flow-through Reactor for Cost-Effective Electro-Generation of H2O2. *J. Clean. Prod.* **2019**, *211*, 1259–1267. https://doi.org/10.1016/j.jclepro.2018.11.225.

(46) Ortiz-Ortega, E.; Díaz-Patiño, L.; Bejar, J.; Trejo, G.; Guerra-Balcázar, M.; Espinosa-Magaña, F.; Álvarez-Contreras, L.; Arriaga, L. G.; Arjona, N. A Flow-Through Membraneless Microfluidic Zinc–Air Cell. *ACS Appl. Mater. Interfaces* **2020**, *12*, 41185–41199. https://doi.org/10.1021/acsami.0c08525.

(47) Esquivel, J. P.; Alday, P.; Ibrahim, O. A.; Fernández, B.; Kjeang, E.; Sabaté, N. A Metal-Free and Biotically Degradable Battery for Portable Single-Use Applications. *Adv. Energy Mater.* **2017**, *7*, 1700275. https://doi.org/10.1002/aenm.201700275.

(48) Hayes, J. R.; Engstrom, A. M.; Friesen, C. Orthogonal Flow Membraneless Fuel Cell. *J. Power Sources* **2008**, *183*, 257–259. https://doi.org/10.1016/j.jpowsour.2008.04.061.

(49) Salloum, K. S.; Hayes, J. R.; Friesen, C. A.; Posner, J. D. Sequential Flow Membraneless Microfluidic Fuel Cell with Porous Electrodes. *J. Power Sources* **2008**, *180*, 243–252. https://doi.org/10.1016/j.jpowsour.2007.12.116.

(50) Salloum, K. S.; Posner, J. D. Counter Flow Membraneless Microfluidic Fuel Cell. *J. Power Sources* **2010**, *195*, 6941–6944. https://doi.org/10.1016/j.jpowsour.2010.03.096.

(51) Park, H. B.; Lee, K. H.; Sung, H. J. Performance of H-Shaped Membraneless Micro Fuel Cells. *J. Power Sources* **2013**, *226*, 266–271. https://doi.org/10.1016/j.jpowsour.2012.11.003.

(52) Park, H. B.; Ahmed, D. H.; Lee, K. H.; Sung, H. J. An H-Shaped Design for Membraneless Micro Fuel Cells. *Electrochim. Acta* **2009**, *54*, 4416–4425. https://doi.org/10.1016/j.electacta.2009.03.018.

(53) Tanveer, M.; Kim, K. Y. Performance Analysis of a Micro Laminar Flow Fuel Cell with Multiple Inlets of a Bridge-Shaped Microchannel. *J. Power Sources* **2018**, *399*, 8–17. https://doi.org/10.1016/j.jpowsour.2018.07.057.

(54) Lopez-Montesinos, P. O.; Desai, A. v.; Kenis, P. J. A. A Three-Dimensional Numerical Model of a Micro Laminar Flow Fuel Cell with a Bridge-Shaped Microchannel Cross-Section. *J. Power Sources* **2014**, *269*, 542–549. https://doi.org/10.1016/j.jpowsour.2014.06.127.

(55) López-Montesinos, P. O.; Yossakda, N.; Schmidt, A.; Brushett, F. R.; Pelton, W. E.; Kenis, P. J. A. Design, Fabrication, and Characterization of a Planar, Silicon-Based, Monolithically Integrated Micro Laminar Flow Fuel Cell with a Bridge-Shaped Microchannel Cross-Section. *J. Power Sources* **2011**, *196*, 4638–4645. https://doi.org/10.1016/j.jpowsour.2011.01.037.

(56) Tanveer, M.; Kim, K.-Y. Effects of Bridge-Shaped Microchannel Geometry on the Performance of a Micro Laminar Flow Fuel Cell. *Micromachines* **2019**, *10*, 822. https://doi.org/10.3390/mi10120822.

(57) Sun, M. H.; Velve Casquillas, G.; Guo, S. S.; Shi, J.; Ji, H.; Ouyang, Q.; Chen, Y. Characterization of Microfluidic Fuel Cell Based on Multiple Laminar Flow. *Microelectron. Eng.* **2007**, *84*, 1182–1185. https://doi.org/10.1016/j.mee.2007.01.175.

(58) Sharifi, F.; Ghobadian, S.; Cavalcanti, F. R.; Hashemi, N. Paper-Based Devices for Energy Applications. *Renew. Sustain. Energy Rev.* **2015**, *52*, 1453–1472. https://doi.org/10.1016/j.rser.2015.08.027.

(59) Nguyen, T. H.; Fraiwan, A.; Choi, S. Paper-Based Batteries: A Review. *Biosens. Bioelectron.* **2014**, *54*, 640–649. https://doi.org/10.1016/j.bios.2013.11.007.

(60) Esquivel, J. P.; del Campo, F. J.; Gómez de la Fuente, J. L.; Rojas, S.; Sabaté, N. Microfluidic Fuel Cells on Paper: Meeting the Power Needs of next Generation Lateral Flow Devices. *Energy Environ. Sci.* **2014**, *7*, 1744–1749. https://doi.org/10.1039/C3EE44044C.

(61) Navarro-Segarra, M.; Alday, P. P.; Garcia, D.; Ibrahim, O. A.; Kjeang, E.; Sabaté, N.; Esquivel, J. P. An Organic Redox Flow Cell-Inspired Paper-Based Primary Battery. *ChemSusChem* **2020**, *13*, 2394–2401. https://doi.org/10.1002/cssc.201903511.

(62) Wu, R.; Ye, D.; Chen, R.; Zhang, B.; Zhu, X.; Guo, H.; Liu, Z. A Membraneless Microfluidic Fuel Cell with Continuous Multistream Flow through Cotton Threads. *Int. J. Energy Res.* **2020**, *44*, 2243–2251. https://doi.org/10.1002/er.5085.

(63) Wang, S.; Ye, D.; Liu, Z.; Chen, R.; Zhu, X.; Zhang, B.; Wu, R.; Liao, Q. A Direct Formate Microfluidic Fuel Cell with Cotton Thread-Based Electrodes. *Int. J. Hydrog. Energy* **2020**, *45*, 27665–27674. https://doi.org/10.1016/j.ijhydene.2020.07.115.

(64) Kjeang, E.; McKechnie, J.; Sinton, D.; Djilali, N. Planar and Three-Dimensional Microfluidic Fuel Cell Architectures Based on Graphite Rod Electrodes. *J. Power Sources* **2007**, *168*, 379–390. https://doi.org/10.1016/j.jpowsour.2007.02.087.

(65) Lee, J. W.; Kjeang, E. Nanofluidic Fuel Cell. *J. Power Sources* **2013**, *242*, 472–477. https://doi.org/10.1016/j.jpowsour.2013.05.129.

(66) Goulet, M. A.; Skyllas-Kazacos, M.; Kjeang, E. The Importance of Wetting in Carbon Paper Electrodes for Vanadium Redox Reactions. *Carbon* **2016**, *101*, 390–398. https://doi.org/10.1016/j.carbon.2016.02.011.

(67) Ortiz-Ortega, E.; Goulet, M. A.; Lee, J. W.; Guerra-Balcázar, M.; Arjona, N.; Kjeang, E.; Ledesma-García, J.; Arriaga, L. G. A Nanofluidic Direct Formic Acid Fuel Cell with a Combined Flow-through and Air-Breathing Electrode for High Performance. *Lab Chip* **2014**, *14*, 4596–4598. https://doi.org/10.1039/c4lc01010h.

(68) Shyu, J.-C.; Wang, P.-Y.; Lee, C.-L.; Chang, S.-C.; Sheu, T.-S.; Kuo, C.-H.; Huang, K.-L.; Yang, Z.-Y. Fabrication and Test of an Air-Breathing Microfluidic Fuel Cell. *Energies* **2015**, *8*, 2082–2096. https://doi.org/10.3390/en8032082.

(69) González-Guerrero, M. J.; del Campo, F. J.; Esquivel, J. P.; Leech, D.; Sabaté, N. Paper-Based Microfluidic Biofuel Cell Operating under Glucose Concentrations within Physiological Range. *Biosens. Bioelectron.* **2017**, *90*, 475–480. https://doi.org/10.1016/j.bios.2016.09.062.

(70) González-Guerrero, M. J.; del Campo, F. J.; Esquivel, J. P.; Giroud, F.; Minteer, S. D.; Sabaté, N. Paper-Based Enzymatic Microfluidic Fuel Cell: From a Two-Stream Flow Device to a Single-

Stream Lateral Flow Strip. *J. Power Sources* **2016**, *326*, 410–416. https://doi.org/10.1016/j.jpowsour.2016.07.014.

(71) O'Neil, G. D.; Ahmed, S.; Halloran, K.; Janusz, J. N.; Rodríguez, A.; Terrero Rodríguez, I. M. Single-Step Fabrication of Electrochemical Flow Cells Utilizing Multi-Material 3D Printing. *Electrochem. commun.* **2019**, *99*, 56–60. https://doi.org/10.1016/j.elecom.2018.12.006.

(72) Lee, C.-Y.; Taylor, A. C.; Nattestad, A.; Beirne, S.; Wallace, G. G. 3D Printing for Electrocatalytic Applications. *Joule* **2019**, *3*, 1835–1849. https://doi.org/10.1016/j.joule.2019.06.010.

(73) Ambrosi, A.; Shi, R. R. S.; Webster, R. D. 3D-Printing for Electrolytic Processes and Electrochemical Flow Systems. *J. Mater. Chem. A* **2020**, *8*, 21902–21929. https://doi.org/10.1039/D0TA07939A.

(74) Hashemi, S. M. H.; Babic, U.; Hadikhani, P.; Psaltis, D. The Potentials of Additive Manufacturing for Mass Production of Electrochemical Energy Systems. *Curr. Opin. Electrochem.* **2020**, *20*, 54–59. https://doi.org/10.1016/j.coelec.2020.02.008.

(75) Corral, D.; Feaster, J. T.; Sobhani, S.; DeOtte, J. R.; Lee, D. U.; Wong, A. A.; Hamilton, J.; Beck, V. A.; Sarkar, A.; Hahn, C.; et al. Advanced Manufacturing for Electrosynthesis of Fuels and Chemicals from CO_2. *Energy Environ. Sci.* **2021**, *14*, 3064–3074. https://doi.org/10.1039/D0EE03679J.

(76) Weisgrab, G.; Ovsianikov, A.; Costa, P. F. Functional 3D Printing for Microfluidic Chips. *Adv. Mater. Technol.* **2019**, *4*, 1900275. https://doi.org/10.1002/admt.201900275.

(77) Bhattacharjee, N.; Urrios, A.; Kang, S.; Folch, A. The Upcoming 3D-Printing Revolution in Microfluidics. *Lab Chip* **2016**, *16*, 1720–1742. https://doi.org/10.1039/C6LC00163G.

(78) Yazdi, A. A.; Popma, A.; Wong, W.; Nguyen, T.; Pan, Y.; Xu, J. 3D Printing: An Emerging Tool for Novel Microfluidics and Lab-on-a-Chip Applications. *Microfluid. Nanofluidics* **2016**, *20*, 50. https://doi.org/10.1007/s10404-016-1715-4.

(79) Channon, R. B.; Joseph, M. B.; Macpherson, J. v. Additive Manufacturing for Electrochemical (Micro)Fluidic Platforms. *Electrochem. Soc. Interface* **2016**, *25*, 63–68. https://doi.org/10.1149/2.F06161if.

(80) Guima, K.-E.; Gomes, L. E.; Alves Fernandes, J.; Wender, H.; Martins, C. A. Harvesting Energy from an Organic Pollutant Model Using a New 3D-Printed Microfluidic Photo Fuel Cell. *ACS Appl. Mater. Interfaces* **2020**, *12*, 54563–54572. https://doi.org/10.1021/acsami.0c14464.

(81) H. Hashemi, S. M.; Karnakov, P.; Hadikhani, P.; Chinello, E.; Litvinov, S.; Moser, C.; Koumoutsakos, P.; Psaltis, D. A Versatile and Membrane-Less Electrochemical Reactor for the Electrolysis of Water and Brine. *Energy Environ. Sci.* **2019**, *12*, 1592–1604. https://doi.org/10.1039/C9EE00219G.

(82) Guima, K.-E.; Coelho, P.-H. L.; Trindade, M. A. G.; Martins, C. A. 3D-Printed Glycerol Microfluidic Fuel Cell. *Lab Chip* **2020**, *20*, 2057–2061. https://doi.org/10.1039/D0LC00351D.

(83) Marschewski, J.; Brenner, L.; Ebejer, N.; Ruch, P.; Michel, B.; Poulikakos, D.; Li, X.; Zhang, Y.-B.; Jiang, J.; Yaghi, O. M.; et al. 3D-Printed Fluidic Networks for High-Power-Density Heat-Managing Miniaturized Redox Flow Batteries. *Energy Environ. Sci.* **2017**, *10*, 780–787. https://doi.org/10.1039/C6EE03192G.

(84) Dudukovic, N. A.; Fong, E. J.; Gemeda, H. B.; DeOtte, J. R.; Cerón, M. R.; Moran, B. D.; Davis, J. T.; Baker, S. E.; Duoss, E. B. Cellular Fluidics. *Nature* **2021**, *595*, 58–65. https://doi.org/10.1038/s41586-021-03603-2.

(85) Wicks, J.; Jue, M. L.; Beck, V. A.; Oakdale, J. S.; Dudukovic, N. A.; Clemens, A. L.; Liang, S.; Ellis, M. E.; Lee, G.; Baker, S. E.; et al. 3D-Printable Fluoropolymer Gas Diffusion Layers for CO_2 Electroreduction. *Adv. Mater.* **2021**, *33*, 2003855. https://doi.org/10.1002/adma.202003855.

(86) Bui, J. C.; Davis, J. T.; Esposito, D. v. 3D-Printed Electrodes for Membraneless Water Electrolysis. *Sustain. Energy Fuels* **2020**, *4*, 213–225. https://doi.org/10.1039/C9SE00710E.

(87) Beck, V. A.; Ivanovskaya, A. N.; Chandrasekaran, S.; Forien, J.-B.; Baker, S. E.; Duoss, E. B.; Worsley, M. A. Inertially Enhanced Mass Transport Using 3D-Printed Porous Flow-through Electrodes with Periodic Lattice Structures. *Proc. Natl. Acad. Sci.* **2021**, *118*, e2025562118. https://doi.org/10.1073/pnas.2025562118.

(88) Lee, J. W.; Kjeang, E. Chip-Embedded Thin Film Current Collector for Microfluidic Fuel Cells. *Int. J. Hydrog. Energy* **2012**, *37*, 9359–9367. https://doi.org/10.1016/j.ijhydene.2012.02.155.

(89) Wang, Y.; Leung, D. Y. C. A High-Performance Aluminum-Feed Microfluidic Fuel Cell Stack. *J. Power Sources* **2016**, *336*, 427–436. https://doi.org/10.1016/j.jpowsour.2016.11.009.

(90) Rao, L. T.; Dubey, S. K.; Javed, A.; Goel, S. Statistical Performance Analysis and Robust Design of Paper Microfluidic Membraneless Fuel Cell With Pencil Graphite Electrodes. *J. Electrochem. Energy Convers. Storage* **2020**, *17*, 031015. https://doi.org/10.1115/1.4045979.

(91) Dossi, N.; Toniolo, R.; Pizzariello, A.; Impellizzieri, F.; Piccin, E.; Bontempelli, G. Pencil-Drawn Paper Supported Electrodes as Simple Electrochemical Detectors for Paper-Based Fluidic Devices. *Electrophoresis* **2013**, *34*, 2085–2091. https://doi.org/10.1002/elps.201200425.

(92) Rao, L. T.; Rewatkar, P.; Dubey, S. K.; Javed, A.; Goel, S. Automated Pencil Electrode Formation Platform to Realize Uniform and Reproducible Graphite Electrodes on Paper for Microfluidic Fuel Cells. *Sci. Rep.* **2020**, *10*, 11675. https://doi.org/10.1038/s41598-020-68579-x.

(93) Arun, R. K.; Halder, S.; Chanda, N.; Chakraborty, S. A Paper Based Self-Pumping and Self-Breathing Fuel Cell Using Pencil Stroked Graphite Electrodes. *Lab Chip* **2014**, *14*, 1661–1664. https://doi.org/10.1039/C4LC00029C.

(94) Arun, R. K.; Gupta, V.; Singh, P.; Biswas, G.; Chanda, N. Selection of Graphite Pencil Grades for the Design of Suitable Electrodes for Stacking Multiple Single-Inlet Paper-Pencil Fuel Cells. *ChemistrySelect* **2019**, *4*, 152–159. https://doi.org/10.1002/slct.201802960.

(95) Kjeang, E.; Michel, R.; Harrington, D. A.; Sinton, D.; Djilali, N. An Alkaline Microfluidic Fuel Cell Based on Formate and Hypochlorite Bleach. *Electrochim. Acta* **2008**, *54*, 698–705. https://doi.org/10.1016/j.electacta.2008.07.009.

(96) Sung, W.; Choi, J. W. A Membraneless Microscale Fuel Cell Using Non-Noble Catalysts in Alkaline Solution. *J. Power Sources* **2007**, *172*, 198–208. https://doi.org/10.1016/j.jpowsour.2007.07.012.

(97) Jhong, H.-R. (Molly); Brushett, F. R.; Yin, L.; Stevenson, D. M.; Kenis, P. J. A. Combining Structural and Electrochemical Analysis of Electrodes Using Micro-Computed Tomography and a Microfluidic Fuel Cell. *J. Electrochem. Soc.* **2012**, *159*, B292–B298. https://doi.org/10.1149/2.033203jes.

(98) Goulet, M. A.; Habisch, A.; Kjeang, E. In Situ Enhancement of Flow-through Porous Electrodes with Carbon Nanotubes via Flowing Deposition. *Electrochim. Acta* **2016**, *206*, 36–44. https://doi.org/10.1016/j.electacta.2016.04.147.

(99) Goulet, M.-A.; Ibrahim, O. A.; Kim, W. H. J.; Kjeang, E. Maximizing the Power Density of Aqueous Electrochemical Flow Cells with in Operando Deposition. *J. Power Sources* **2017**, *339*, 80–85. https://doi.org/10.1016/j.jpowsour.2016.11.053.

(100) Hashemi, S. M. H.; Neuenschwander, M.; Hadikhani, P.; Modestino, M. A.; Psaltis, D. Membrane-Less Micro Fuel Cell Based on Two-Phase Flow. *J. Power Sources* **2017**, *348*, 212–218. https://doi.org/10.1016/j.jpowsour.2017.02.079.

(101) Pang, X.; Davis, J. T.; Harvey, A. D.; Esposito, D. v. Framework for Evaluating the Performance Limits of Membraneless Electrolyzers. *Energy Environ. Sci.* **2020**, *13*, 3663–3678. https://doi.org/10.1039/D0EE02268C.

(102) Modestino, M. A.; Dumortier, M.; Hosseini Hashemi, S. M.; Haussener, S.; Moser, C.; Psaltis, D. Vapor-Fed Microfluidic Hydrogen Generator. *Lab Chip* **2015**, *15*, 2287–2296. https://doi.org/10.1039/C5LC00259A.

(103) Ouyang, T.; Lu, J.; Zhao, Z.; Chen, J.; Xu, P. New Insight on the Mechanism of Vibration Effects in Vapor-Feed Microfluidic Fuel Cell. *Energy* **2021**, *225*, 120207. https://doi.org/10.1016/j.energy.2021.120207.

(104) Wang, Y.; Leung, D. Y. C.; Xuan, J.; Wang, H. A Vapor Feed Methanol Microfluidic Fuel Cell with High Fuel and Energy Efficiency. *Appl. Energy* **2015**, *147*, 456–465. https://doi.org/10.1016/j.apenergy.2015.03.028.

(105) Kwok, Y. H.; Wang, Y.; Wu, M.; Li, F.; Zhang, Y.; Zhang, H.; Leung, D. Y. C. A Dual Fuel Microfluidic Fuel Cell Utilizing Solar Energy and Methanol. *J. Power Sources* **2019**, *409*, 58–65. https://doi.org/10.1016/j.jpowsour.2018.10.095.

(106) Liu, C.; Liao, Q.; Zhu, X.; Yang, Y. Investigating the Composition of Iron Salts on the Performance of Microfluidic Fuel Cells. *Ind. Eng. Chem. Res.* **2018**, *57*, 1756–1762. https://doi.org/10.1021/acs.iecr.7b04636.

(107) Goulet, M. A.; Eikerling, M.; Kjeang, E. Direct Measurement of Electrochemical Reaction Kinetics in Flow-through Porous Electrodes. *Electrochem. commun.* **2015**, *57*, 14–17. https://doi.org/10.1016/j.elecom.2015.04.019.

(108) Ibrahim, O. A.; Kjeang, E. Leveraging Co-Laminar Flow Cells for Non-Aqueous Electrochemical Systems. *J. Power Sources* **2018**, *402*, 7–14. https://doi.org/10.1016/j.jpowsour.2018.09.013.

(109) Mitrovski, S. M.; Nuzzo, R. G. A Passive Microfluidic Hydrogen-Air Fuel Cell with Exceptional Stability and High Performance. *Lab Chip* **2006**, *6*, 353–361. https://doi.org/10.1039/b513829a.

(110) Mitrovski, S. M.; Elliott, L. C. C.; Nuzzo, R. G. Microfluidic Devices for Energy Conversion: Planar Integration and Performance of a Passive, Fully Immersed H_2O_2 Fuel Cell. *Langmuir* **2004**, 20, 6974–6976 https://doi.org/10.1021/la048417w.

(111) Jayashree, R. S.; Mitchell, M.; Natarajan, D.; Markoski, L. J.; Kenis, P. J. A. Microfluidic Hydrogen Fuel Cell with a Liquid Electrolyte. *Langmuir* **2007**, *23*, 6871–6874. https://doi.org/10.1021/la063673p.

(112) Huo, W.; Zhou, Y.; Zhang, H.; Zou, Z.; Yang, H. Microfluidic Direct Methanol Fuel Cell with Ladder-Shaped Microchannel for Decreased Methanol Crossover. *Int. J. Electrochem. Sci.* **2013**, *8*, 4827–4838.

(113) Hollinger, A. S.; Maloney, R. J.; Jayashree, R. S.; Natarajan, D.; Markoski, L. J.; Kenis, P. J. A. Nanoporous Separator and Low Fuel Concentration to Minimize Crossover in Direct Methanol Laminar Flow Fuel Cells. *J. Power Sources* **2010**, *195*, 3523–3528. https://doi.org/10.1016/j.jpowsour.2009.12.063.

(114) Armenta-González, A. J.; Carrera-Cerritos, R.; Moreno-Zuria, A.; Álvarez-Contreras, L.; Ledesma-García, J.; Cuevas-Muñiz, F. M.; Arriaga, L. G. An Improved Ethanol Microfluidic Fuel Cell Based on a PdAg/MWCNT Catalyst Synthesized by the Reverse Micelles Method. *Fuel* **2016**, *167*, 240–247. https://doi.org/10.1016/j.fuel.2015.11.057.

(115) Maya-Cornejo, J.; Ortiz-Ortega, E.; Álvarez-Contreras, L.; Arjona, N.; Guerra-Balcázar, M.; Ledesma-García, J.; Arriaga, L. G. Copper-Palladium Core-Shell as an Anode in a Multi-Fuel Membraneless Nanofluidic Fuel Cell: Toward a New Era of Small Energy Conversion Devices. *Chem. Commun.* **2015**, *51*, 2536–2539. https://doi.org/10.1039/c4cc08529a.

(116) Martins, C. A.; Ibrahim, O. A.; Pei, P.; Kjeang, E. Towards a Fuel-Flexible Direct Alcohol Microfluidic Fuel Cell with Flow-through Porous Electrodes: Assessment of Methanol, Ethylene Glycol and Glycerol Fuels. *Electrochim. Acta* **2018**, *271*, 537–543. https://doi.org/10.1016/j.electacta.2018.03.197.

(117) Panjiara, D.; Pramanik, H. Electrooxidation Study of Glycerol on Synthesized Anode Electrocatalysts Pd/C and Pd-Pt/C in a Y-Shaped Membraneless Air-Breathing Microfluidic Fuel Cell for Power Generation. *Ionics* **2020**, *26*, 2435–2452. https://doi.org/10.1007/s11581-019-03385-8.

(118) Martins, C. A.; Ibrahim, O. A.; Pei, P.; Kjeang, E. “bleaching” Glycerol in a Microfluidic Fuel Cell to Produce High Power Density at Minimal Cost. *Chem. Commun.* **2017**, *54*, 192–195. https://doi.org/10.1039/c7cc08190a.

(119) Martins, C. A.; Ibrahim, O. A.; Pei, P.; Kjeang, E. In Situ Decoration of Metallic Catalysts in Flow-through Electrodes: Application of Fe/Pt/C for Glycerol Oxidation in a Microfluidic Fuel Cell. *Electrochim. Acta* **2019**, *305*, 47–55. https://doi.org/10.1016/j.electacta.2019.03.018.

(120) Raj kumar, T.; Gnana kumar, G.; Manthiram, A. Biomass-Derived 3D Carbon Aerogel with Carbon Shell-Confined Binary Metallic Nanoparticles in CNTs as an Efficient Electrocatalyst for Microfluidic Direct Ethylene Glycol Fuel Cells. *Adv. Energy Mater.* **2019**, *9*, 1803238. https://doi.org/10.1002/aenm.201803238.

(121) López–Coronel, A.; Ortiz–Ortega, E.; Torres–Pacheco, L. J.; Guerra–Balcázar, M.; Arriaga, L. G.; Álvarez–Contreras, L.; Arjona, N. High Performance of Pd and PdAg with Well–defined Facets in Direct Ethylene Glycol Microfluidic Fuel Cells. *Electrochim. Acta* **2019**, *320*, 134622. https://doi.org/10.1016/j.electacta.2019.134622.

(122) Arjona, N.; Palacios, A.; Moreno Zuria, A.; Guerra-Balcázar, M.; Ledesma García, J.; Arriaga, L. G. AuPd/Polyaniline as the Anode in an Ethylene Glycol Microfluidic Fuel Cell Operated at Room Temperature. *Chem. Commun.* **2014**, *50*, 8151–8153. https://doi.org/10.1039/c4cc03288h.

(123) Moreno-Zuria, A.; Dector, A.; Cuevas-Muñiz, F. M.; Esquivel, J. P.; Sabaté, N.; Ledesma-García, J.; Arriaga, L. G.; Chávez-Ramírez, A. U. Direct Formic Acid Microfluidic Fuel Cell Design and Performance Evolution. *J. Power Sources* **2014**, *269*, 783–788. https://doi.org/10.1016/j.jpowsour.2014.07.049.

(124) Déctor, A.; Esquivel, J. P.; González, M. J.; Guerra-Balcázar, M.; Ledesma-García, J.; Sabaté, N.; Arriaga, L. G. Formic Acid Microfluidic Fuel Cell Evaluation in Different Oxidant Conditions. *Electrochim. Acta* **2013**, *92*, 31–35. https://doi.org/10.1016/j.electacta.2012.12.134.

(125) Morales-Acosta, D.; Rodríguez G., H.; Godinez, L. A.; Arriaga, L. G. Performance Increase of Microfluidic Formic Acid Fuel Cell Using Pd/MWCNTs as Catalyst. *J. Power Sources* **2010**, *195*, 1862–1865. https://doi.org/10.1016/j.jpowsour.2009.10.007.

(126) Erickson, E. M.; Mitrovski, S. M.; Gewirth, A. A.; Nuzzo, R. G. Optimization of a Permeation-Based Microfluidic Direct Formic Acid Fuel Cell (DFAFC). *Electrophoresis* **2011**, *32*, 947–956. https://doi.org/10.1002/elps.201000472.

(127) Xu, H.; Zhang, H.; Wang, H.; Leung, D. Y. C.; Zhang, L.; Cao, J.; Jiao, K.; Xuan, J. Counter-Flow Formic Acid Microfluidic Fuel Cell with High Fuel Utilization Exceeding 90%. *Appl. Energy* **2015**, *160*, 930–936. https://doi.org/10.1016/j.apenergy.2015.01.101.

(128) Zhu, X.; Zhang, B.; Ye, D. D.; Li, J.; Liao, Q. Air-Breathing Direct Formic Acid Microfluidic Fuel Cell with an Array of Cylinder Anodes. *J. Power Sources* **2014**, *247*, 346–353. https://doi.org/10.1016/j.jpowsour.2013.08.119.

(129) Ma, J.; Gago, A. S.; Alonso-Vante, N. Performance Study of Platinum Nanoparticles Supported onto MWCNT in a Formic Acid Microfluidic Fuel Cell System. *J. Electrochem. Soc.* **2013**, *160*, F859–F866. https://doi.org/10.1149/2.101308jes.

(130) García-Cuevas, R. A.; Cervantes, I.; Arriaga, L. G.; Diaz-Diaz, I. A. Toward Geometrical Design Improvement of Membraneless Fuel Cells: Numerical Study. *Int. J. Hydrog. Energy* **2013**, *38*, 14791–14800. https://doi.org/10.1016/j.ijhydene.2013.09.014.

(131) Liu, C.; Liu, H.; Liu, L. Potassium Permanganate as an Oxidant for a Microfluidic Direct Formate Fuel Cell. *Int. J. Electrochem. Sci.* **2019**, *14*, 4557–4570. https://doi.org/10.20964/2019.05.01.

(132) Zhang, B.; Ye, D. D.; Li, J.; Zhu, X.; Liao, Q. Air-Breathing Microfluidic Fuel Cells with a Cylinder Anode Operating in Acidic and Alkaline Media. *Electrochim. Acta* **2015**, *177*, 264–269. https://doi.org/10.1016/j.electacta.2015.03.080.

(133) Ye, D. D.; Zhang, B.; Zhu, X.; Sui, P. C.; Djilali, N.; Liao, Q. Computational Modeling of Alkaline Air-Breathing Microfluidic Fuel Cells with an Array of Cylinder Anodes. *J. Power Sources* **2015**, *288*, 150–159. https://doi.org/10.1016/j.jpowsour.2015.04.087.

(134) Zhou, Y.; Zhang, B.; Zhu, X.; Ye, D. D.; Chen, R.; Zhang, T.; Gong, X. L.; Liao, Q. Enhancing Fuel Transport in Air-Breathing Microfluidic Fuel Cells by Immersed Fuel Micro-Jet. *J. Power Sources* **2020**, *445*, 227326. https://doi.org/10.1016/j.jpowsour.2019.227326.

(135) Yang, Y.; Xue, Y.; Zhang, H.; Chang, H. Flexible H2O2 Microfluidic Fuel Cell Using Graphene/Prussian Blue Catalyst for High Performance. *Chem. Eng. J.* **2019**, *369*, 813–817. https://doi.org/10.1016/j.cej.2019.03.134.

(136) Hasegawa, S.; Shimotani, K.; Kishi, K.; Watanabe, H. Electricity Generation from Decomposition of Hydrogen Peroxide. *Electrochem. Solid-State Lett.* **2005**, *8*, A119. https://doi.org/10.1149/1.1849112.

(137) Yang, Y.; Xue, Y.; Huang, F.; Zhang, H.; Tao, K.; Zhang, R.; Shen, Q.; Chang, H. A Facile Microfluidic Hydrogen Peroxide Fuel Cell with High Performance: Electrode Interface and Power-Generation Properties. *ACS Appl. Energy Mater.* **2018**, *1*, 5328–5335. https://doi.org/10.1021/acsaem.8b00943.

(138) Brushett, F. R.; Jayashree, R. S.; Zhou, W. P.; Kenis, P. J. A. Investigation of Fuel and Media Flexible Laminar Flow-Based Fuel Cells. *Electrochim. Acta* **2009**, *54*, 7099–7105. https://doi.org/10.1016/j.electacta.2009.07.011.

(139) Mota, N. da; Finkelstein, D. A.; Kirtland, J. D.; Rodriguez, C. A.; Stroock, A. D.; Abruña, H. D. Membraneless, Room-Temperature, Direct Borohydride/Cerium Fuel Cell with Power Density of over 0.25 W/Cm 2. *J. Am. Chem. Soc.* **2012**, *134*, 6076–6079. https://doi.org/10.1021/ja211751k.

(140) Guo, S.; Sun, J.; Zhang, Z.; Sheng, A.; Gao, M.; Wang, Z.; Zhao, B.; Ding, W. Study of the Electrooxidation of Borohydride on a Directly Formed CoB/Ni-Foam Electrode and Its Application in Membraneless Direct Borohydride Fuel Cells. *J. Mater. Chem. A* **2017**, *5*, 15879–15890. https://doi.org/10.1039/c7ta03464d.

(141) Durga, S.; Ponmani, K.; Kiruthika, S.; Muthukumaran, B. Electrochemical Oxidation of Hydrazine in Membraneless Fuel Cells. *J. Electrochem. Sci. Technol.* **2014**, *5*, 73–81. https://doi.org/10.33961/jecst.2014.5.3.73.

(142) Rao, L. T.; Dubey, S. K.; Javed, A.; Goel, S. Development of Membraneless Paper-pencil Microfluidic Hydrazine Fuel Cell. *Electroanalysis* **2020**, *32*, 2581–2588. https://doi.org/10.1002/elan.202060191.

(143) Chino, I.; Muneeb, O.; Do, E.; Ho, V.; Haan, J. L. A Paper Microfluidic Fuel Cell Powered by Urea. *J. Power Sources* **2018**, *396*, 710–714. https://doi.org/10.1016/j.jpowsour.2018.06.082.

(144) Zhang, H.; Wang, Y.; Wu, Z.; Leung, D. Y. C. A Direct Urea Microfluidic Fuel Cell with Flow-through Ni-Supported-Carbon- Nanotube-Coated Sponge as Porous Electrode. *J. Power Sources* **2017**, *363*, 61–69. https://doi.org/10.1016/j.jpowsour.2017.07.055.

(145) Yang, Y.; Ye, D.; Liao, Q.; Zhang, P.; Zhu, X.; Li, J.; Fu, Q. Enhanced Biofilm Distribution and Cell Performance of Microfluidic Microbial Fuel Cells with Multiple Anolyte Inlets. *Biosens. Bioelectron.* **2016**, *79*, 406–410. https://doi.org/10.1016/j.bios.2015.12.067.

(146) Dector, A.; Escalona-Villalpando, R. A.; Dector, D.; Vallejo-Becerra, V.; Chávez-Ramírez, A. U.; Arriaga, L. G.; Ledesma-García, J. Perspective Use of Direct Human Blood as an Energy Source in Air-Breathing Hybrid Microfluidic Fuel Cells. *J. Power Sources* **2015**, *288*, 70–75. https://doi.org/10.1016/j.jpowsour.2015.04.089.

(147) Hernández Rivera, J.; Ortega Díaz, D.; Amaya Cruz, D. M.; Rodríguez-Reséndiz, J.; Olivares Ramírez, J. M.; Dector, A.; Dector, D.; Galindo, R.; Esparza Ponce, H. E. A Paper-Based Microfluidic Fuel Cell Using Soft Drinks as a Renewable Energy Source. *Energies* **2020**, *13*, 2443. https://doi.org/10.3390/en13102443.

(148) Escalona-Villalpando, R. A.; Dector, A.; Dector, D.; Moreno-Zuria, A.; Durón-Torres, S. M.; Galván-Valencia, M.; Arriaga, L. G.; Ledesma-García, J. Glucose Microfluidic Fuel Cell Using Air as Oxidant. *Int. J. Hydrog. Energy* **2016**, *41*, 23394–23400. https://doi.org/10.1016/j.ijhydene.2016.04.238.

(149) Dector, A.; Cuevas-Muñiz, F. M.; Guerra-Balcázar, M.; Godínez, L. A.; Ledesma-García, J.; Arriaga, L. G. Glycerol Oxidation in a Microfluidic Fuel Cell Using Pd/C and Pd/MWCNT Anodes Electrodes. *Int. J. Hydrog. Energy* **2013**, *38*, 12617–12622. https://doi.org/10.1016/j.ijhydene.2012.12.030.

(150) Lee, J. wook; Kjeang, E. A Perspective on Microfluidic Biofuel Cells. *Biomicrofluidics* **2010**, *4*, 041301. https://doi.org/10.1063/1.3515523.

(151) Yang, W.; Lee, K. K.; Choi, S. A Laminar-Flow Based Microbial Fuel Cell Array. *Sens. Actuators B Chem.* **2017**, *243*, 292–297. https://doi.org/10.1016/j.snb.2016.11.155.

(152) Jiang, H.; Ali, Md. A.; Xu, Z.; Halverson, L. J.; Dong, L. Integrated Microfluidic Flow-Through Microbial Fuel Cells. *Sci. Rep.* **2017**, *7*, 41208. https://doi.org/10.1038/srep41208.

(153) Garcia, S. O.; Ulyanova, Y. v; Figueroa-Teran, R.; Bhatt, K. H.; Singhal, S.; Atanassov, P. Wearable Sensor System Powered by a Biofuel Cell for Detection of Lactate Levels in Sweat. *ECS J. Solid State Sci. Technol.* **2016**, *5*, M3075–M3081. https://doi.org/10.1149/2.0131608jss.

(154) Zebda, A.; Renaud, L.; Cretin, M.; Innocent, C.; Pichot, F.; Ferrigno, R.; Tingry, S. Electrochemical Performance of a Glucose/Oxygen Microfluidic Biofuel Cell. *J. Power Sources* **2009**, *193*, 602–606. https://doi.org/10.1016/j.jpowsour.2009.04.066.

(155) Parkhey, P.; Sahu, R. Microfluidic Microbial Fuel Cells: Recent Advancements and Future Prospects. *Int. J. Hydrog. Energy* **2021**, *46*, 3105–3123. https://doi.org/10.1016/j.ijhydene.2020.07.019.

(156) Chen, B.; Leung, D. Y. C.; Xuan, J.; Wang, H. A High Specific Capacity Membraneless Aluminum-Air Cell Operated with an Inorganic/Organic Hybrid Electrolyte. *J. Power Sources* **2016**, *336*, 19–26. https://doi.org/10.1016/j.jpowsour.2016.10.051.

(157) Rao, L. T.; Dubey, S. K.; Javed, A.; Goel, S. Metal-Free Al-Air Microfluidic Paper Fuel Cell to Power Portable Electronic Devices. *Int. J. Energy Res.* **2021**, *45*, 7070–7081. https://doi.org/10.1002/er.6292.

(158) Chen, B.; Leung, D. Y. C.; Xuan, J.; Wang, H. A Mixed-PH Dual-Electrolyte Microfluidic Aluminum–Air Cell with High Performance. *Appl. Energy* **2017**, *185*, 1303–1308. https://doi.org/10.1016/j.apenergy.2015.10.029.

(159) Chen, B.; Leung, D. Y. C.; Wang, H.; Xuan, J. Scaling Up Microfluidic Aluminum-Air Cell with Electrochemical Impedance Spectroscopy (EIS) Assisted Performance Analysis. *J. Electrochem. Soc.* **2016**, *163*, F1032–F1037. https://doi.org/10.1149/2.0501609jes.

(160) Feng, S.; Yang, G.; Zheng, D.; Wang, L.; Wang, W.; Wu, Z.; Liu, F. A Dual-Electrolyte Aluminum/Air Microfluidic Cell with Enhanced Voltage, Power Density and Electrolyte Utilization via a Novel Composite Membrane. *J. Power Sources* **2020**, *478*, 228960. https://doi.org/10.1016/j.jpowsour.2020.228960.

(161) Li, A.; Chan, S. H.; Nguyen, N. T. A Laser-Micromachined Polymeric Membraneless Fuel Cell. *J. Micromech. Microeng.* **2007**, *17*, 1107–1113. https://doi.org/10.1088/0960-1317/17/6/002.

(162) Kjeang, E.; Brolo, A. G.; Harrington, D. a.; Djilali, N.; Sinton, D. Hydrogen Peroxide as an Oxidant for Microfluidic Fuel Cells. *J. Electrochem. Soc.* **2007**, *154*, B1220. https://doi.org/10.1149/1.2784185.

(163) Ha, S. M.; Ahn, Y. Laminar Flow-Based Micro Fuel Cell Utilizing Grooved Electrode Surface. *J. Power Sources* **2014**, *267*, 731–738. https://doi.org/10.1016/j.jpowsour.2014.06.005.

(164) Rösing, W.; Schildhauer, T.; König, J.; Cierpka, C. Passive Control of the Concentration Boundary Layer in Microfluidic Fuel Cells Using Dean Vortices. *Microfluid. Nanofluidics* **2019**, *23*, 110. https://doi.org/10.1007/s10404-019-2274-2.

(165) Jayashree, R. S.; Yoon, S. K.; Brushett, F. R.; Lopez-Montesinos, P. O.; Natarajan, D.; Markoski, L. J.; Kenis, P. J. A. On the Performance of Membraneless Laminar Flow-Based Fuel Cells. *J. Power Sources* **2010**, *195*, 3569–3578. https://doi.org/10.1016/j.jpowsour.2009.12.029.

(166) Lu, X.; Xuan, J.; Leung, D. Y. C.; Zou, H.; Li, J.; Wang, H.; Wang, H. A Switchable PH-Differential Unitized Regenerative Fuel Cell with High Performance. *J. Power Sources* **2016**, *314*, 76–84. https://doi.org/10.1016/j.jpowsour.2016.02.092.

(167) Ibrahim, O. A.; Alday, P.; Sabaté, N.; Esquivel, J. P.; Kjeang, E. Evaluation of Redox Chemistries for Single-Use Biodegradable Capillary Flow Batteries. *J. Electrochem. Soc.* **2017**, *164*, A2448–A2456. https://doi.org/10.1149/2.0971712jes.

(168) Kjeang, E.; Proctor, B. T.; Brolo, A. G.; Harrington, D. A.; Djilali, N.; Sinton, D. High-Performance Microfluidic Vanadium Redox Fuel Cell. *Electrochim. Acta* **2007**, *52*, 4942–4946. https://doi.org/10.1016/j.electacta.2007.01.062.

(169) Moore, S.; Sinton, D.; Erickson, D. A Plate-Frame Flow-through Microfluidic Fuel Cell Stack. *J. Power Sources* **2011**, *196*, 9481–9487. https://doi.org/10.1016/j.jpowsour.2011.07.024.

(170) Salloum, K. S.; Posner, J. D. A Membraneless Microfluidic Fuel Cell Stack. *J. Power Sources* **2011**, *196*, 1229–1234. https://doi.org/10.1016/j.jpowsour.2010.08.069.

(171) Krishnamurthy, D.; Johansson, E. O.; Lee, J. W.; Kjeang, E. Computational Modeling of Microfluidic Fuel Cells with Flow-through Porous Electrodes. *J. Power Sources* **2011**, *196*, 10019–10031. https://doi.org/10.1016/j.jpowsour.2011.08.024.

(172) Lee, J. W.; Hong, J. K.; Kjeang, E. Electrochemical Characteristics of Vanadium Redox Reactions on Porous Carbon Electrodes for Microfluidic Fuel Cell Applications. *Electrochim. Acta* **2012**, *83*, 430–438. https://doi.org/10.1016/j.electacta.2012.07.104.

(173) Arun, R. K.; Anjali; Sardar, M.; Singh, P.; Jha, B. M.; Chanda, N. A Spiral Shaped Regenerative Microfluidic Fuel Cell with Ni-C Based Porous Electrodes. *Int. J. Energy Res.* **2019**, *43*, 8834–8840. https://doi.org/10.1002/er.4841.

(174) Zhang, H. M.; Wang, Y. F.; Kwok, Y. H.; Wu, Z. C.; Xia, D. H.; Leung, D. Y. C. A Direct Ammonia Microfluidic Fuel Cell Using NiCu Nanoparticles Supported on Carbon Nanotubes as an Electrocatalyst. *ChemSusChem* **2018**, *11*, 2889–2897. https://doi.org/10.1002/cssc.201801232.

(175) Whipple, D. T.; Jayashree, R. S.; Egas, D.; Alonso-Vante, N.; Kenis, P. J. A. Ruthenium Cluster-like Chalcogenide as a Methanol Tolerant Cathode Catalyst in Air-Breathing Laminar Flow Fuel Cells. *Electrochim. Acta* **2009**, *54*, 4384–4388. https://doi.org/10.1016/j.electacta.2009.03.013.

(176) Gago, A. S.; Morales-Acosta, D.; Arriaga, L. G.; Alonso-Vante, N. Carbon Supported Ruthenium Chalcogenide as Cathode Catalyst in a Microfluidic Formic Acid Fuel Cell. *J. Power Sources* **2011**, *196*, 1324–1328. https://doi.org/10.1016/j.jpowsour.2010.08.109.

(177) Morales-Acosta, D.; Morales-Acosta, M. D.; Godinez, L. A.; Álvarez-Contreras, L.; Duron-Torres, S. M.; Ledesma-García, J.; Arriaga, L. G. PdCo Supported on Multiwalled Carbon Nanotubes as an Anode Catalyst in a Microfluidic Formic Acid Fuel Cell. *J. Power Sources* **2011**, *196*, 9270–9275. https://doi.org/10.1016/j.jpowsour.2011.07.064.

(178) Zhong, H.; Tian, R.; Gong, X.; Li, D.; Tang, P.; Alonso-Vante, N.; Feng, Y. Advanced Bifunctional Electrocatalyst Generated through Cobalt Phthalocyanine Tetrasulfonate Intercalated Ni2Fe-Layered Double Hydroxides for a Laminar Flow Unitized Regenerative Micro-Cell. *J. Power Sources* **2017**, *361*, 21–30. https://doi.org/10.1016/j.jpowsour.2017.06.057.

(179) Estrada-Solís, M. J.; Abrego-Martínez, J. C.; Moreno-Zuria, A.; Arriaga, L. G.; Sun, S.; Cuevas-Muñiz, F. M.; Mohamedi, M. Use of a Bilayer Platinum-Silver Cathode to Selectively Perform the Oxygen Reduction Reaction in a High Concentration Mixed-Reactant Microfluidic Direct Ethanol Fuel Cell. *Int. J. Hydrog. Energy* **2019**, *44*, 18372–18381. https://doi.org/10.1016/j.ijhydene.2019.05.078.

(180) González-Guerrero, M. J.; Esquivel, J. P.; Sánchez-Molas, D.; Godignon, P.; Muñoz, F. X.; del Campo, F. J.; Giroud, F.; Minteer, S. D.; Sabaté, N. Membraneless Glucose/O2 Microfluidic Enzymatic Biofuel Cell Using Pyrolyzed Photoresist Film Electrodes. *Lab Chip* **2013**, *13*, 2972–2979. https://doi.org/10.1039/c3lc50319d.

(181) Galindo-de-la-Rosa, J.; Arjona, N.; Moreno-Zuria, A.; Ortiz-Ortega, E.; Guerra-Balcázar, M.; Ledesma-García, J.; Arriaga, L. G. Evaluation of Single and Stack Membraneless Enzymatic Fuel Cells Based on Ethanol in Simulated Body Fluids. *Biosens. Bioelectron.* **2017**, *92*, 117–124. https://doi.org/10.1016/j.bios.2017.02.010.

(182) Yang, Y.; Liu, T.; Tao, K.; Chang, H. Generating Electricity on Chips: Microfluidic Biofuel Cells in Perspective. *Ind. Eng. Chem. Res.* **2018**, *57*, 2746–2758. https://doi.org/10.1021/acs.iecr.8b00037.

(183) Rewatkar, P.; Hitaishi, V. P.; Lojou, E.; Goel, S. Enzymatic Fuel Cells in a Microfluidic Environment: Status and Opportunities. A Mini Review. *Electrochem. commun.* **2019**, *107*, 106533. https://doi.org/10.1016/j.elecom.2019.106533.

(184) Arjona, N.; Guerra-Balcázar, M.; Ortiz-Frade, L.; Osorio-Monreal, G.; Álvarez-Contreras, L.; Ledesma-García, J.; Arriaga, L. G. Electrocatalytic Activity of Well-Defined and Homogeneous Cubic-Shaped Pd Nanoparticles. *J. Mater. Chem. A* **2013**, *1*, 15524–15529. https://doi.org/10.1039/c3ta13891g.

(185) Arjona, N.; Goulet, M. A.; Guerra-Balćazar, M.; Ledesma-García, J.; Kjeang, E.; Arriaga, L. G. Direct Formic Acid Microfluidic Fuel Cell with Pd Nanocubes Supported on Flow-through Microporous Electrodes. *ECS Electrochem. Lett.* **2015**, *4*, F24–F28. https://doi.org/10.1149/2.0031504eel.

(186) Martins, C. A.; Pei, P.; Tellis, M.; Ibrahim, O. A.; Kjeang, E. Graphene-Oxide-Modified Metal-Free Cathodes for Glycerol/Bleach Microfluidic Fuel Cells. *ACS Appl. Nano Mater.* **2020**, *3*, 8286–8293. https://doi.org/10.1021/acsanm.0c01722.

(187) Gurrola, M. P.; Ortiz-Ortega, E.; Farias-Zuñiga, C.; Chávez-Ramírez, A. U.; Ledesma-García, J.; Arriaga, L. G. Evaluation and Coupling of a Membraneless Nanofluidic Device for Low-Power Applications. *J. Power Sources* **2016**, *307*, 244–250. https://doi.org/10.1016/j.jpowsour.2015.12.091.

(188) Zhou, Y.; Zhu, X.; Zhang, B.; Ye, D. D.; Chen, R.; Liao, Q. High Performance Formic Acid Fuel Cell Benefits from Pd–PdO Catalyst Supported by Ordered Mesoporous Carbon. *Int. J. Hydrog. Energy* **2020**, *45*, 29235–29245. https://doi.org/10.1016/j.ijhydene.2020.07.169.

(189) Kwok, Y. H.; Tsang, A. C. H.; Wang, Y.; Leung, D. Y. C. Ultra-Fine Pt Nanoparticles on Graphene Aerogel as a Porous Electrode with High Stability for Microfluidic Methanol Fuel Cell. *J. Power Sources* **2017**, *349*, 75–83. https://doi.org/10.1016/j.jpowsour.2017.03.030.

(190) Kwok, Y. H.; Wang, Y. F.; Tsang, A. C. H.; Leung, D. Y. C. Graphene-Carbon Nanotube Composite Aerogel with Ru@Pt Nanoparticle as a Porous Electrode for Direct Methanol Microfluidic Fuel Cell. *Appl. Energy* **2018**, *217*, 258–265. https://doi.org/10.1016/j.apenergy.2018.02.141.

(191) Massing, J.; van der Schoot, N.; Kähler, C. J.; Cierpka, C. A Fast Start up System for Microfluidic Direct Methanol Fuel Cells. *Int. J. Hydrog. Energy* **2019**, *44*, 26517–26529. https://doi.org/10.1016/j.ijhydene.2019.08.107.

(192) Wang, Y.; Leung, D. Y. C.; Zhang, H.; Xuan, J.; Wang, H. Numerical and Experimental Comparative Study of Microfluidic Fuel Cells with Different Flow Configurations: Co-Flow vs. Counter-Flow Cell. *Appl. Energy* **2017**, *203*, 535–548. https://doi.org/10.1016/j.apenergy.2017.06.070.

(193) Xu, Q.; She, Y.; Li, L. Model-Based Analysis of Geometrical Effects in Microfluidic Fuel Cell with Flow-through Porous Electrodes. *Int. J. Mod. Phys. B* **2020**, *34*, 2040022. https://doi.org/10.1142/S0217979220400226.

(194) Tanveer, M.; Kim, K.-Y. Effects of Geometric Configuration of the Channel and Electrodes on the Performance of a Membraneless Micro-Fuel Cell. *Energy Convers. Manag.* **2017**, *136*, 372–381. https://doi.org/10.1016/j.enconman.2017.01.027.

(195) Sprague, I. B.; Byun, D.; Dutta, P. Effects of Reactant Crossover and Electrode Dimensions on the Performance of a Microfluidic Based Laminar Flow Fuel Cell. *Electrochim. Acta* **2010**, *55*, 8579–8589. https://doi.org/10.1016/j.electacta.2010.07.035.

(196) Deng, B.; Ye, D.; Zhang, B.; Zhu, X.; Chen, R.; Liao, Q. Current Density Distribution in Air-Breathing Microfluidic Fuel Cells with an Array of Graphite Rod Anodes. *Int. J. Hydrog. Energy* **2021**, *46*, 2960–2968. https://doi.org/10.1016/j.ijhydene.2020.07.035.

(197) Li, L.; Bei, S.; Xu, Q.; Zheng, K.; Zheng, Y. Role of Electrical Resistance and Geometry of Porous Electrodes in the Performance of Microfluidic Fuel Cells. *Int. J. Energy Res.* **2018**, *42*, 1277–1286. https://doi.org/10.1002/er.3927.

(198) Li, L.; Fan, W.; Xuan, J.; Leung, M. K. H.; Zheng, K.; She, Y. Optimal Design of Current Collectors for Microfluidic Fuel Cell with Flow-through Porous Electrodes: Model and Experiment. *Appl. Energy* **2017**, *206*, 413–424. https://doi.org/10.1016/j.apenergy.2017.08.175.

(199) Chang, M. H.; Chen, F.; Fang, N. S. Analysis of Membraneless Fuel Cell Using Laminar Flow in a Y-Shaped Microchannel. *J. Power Sources* **2006**, *159*, 810–816. https://doi.org/10.1016/j.jpowsour.2005.11.066.

(200) Yoon, S. K.; Fichtl, G. W.; Kenis, P. J. A. Active Control of the Depletion Boundary Layers in Microfluidic Electrochemical Reactors. *Lab Chip* **2006**, *6*, 1516–1524. https://doi.org/10.1039/b609289f.

(201) Lee, J.; Keng, G. L.; Palmore, G. T. R.; Tripathi, A. Optimization of Microfluidic Fuel Cells Using Transport Principles. *Anal. Chem.* **2007**, *79*, 7301–7307. https://doi.org/10.1021/ac070812e.

(202) Zhu, X.; Zhou, Y.; Ye, D.-D.; Chen, R.; Zhang, T.; Liao, Q. Discrete-Holes Film Fueling Anode Heads for High Performance Air-Breathing Microfluidic Fuel Cell. *J. Power Sources* **2021**, *482*, 228966. https://doi.org/10.1016/j.jpowsour.2020.228966.

(203) Bazylak, A.; Sinton, D.; Djilali, N. Improved Fuel Utilization in Microfluidic Fuel Cells: A Computational Study. *J. Power Sources* **2005**, *143*, 57–66. https://doi.org/10.1016/j.jpowsour.2004.11.029.

(204) Ebrahimi Khabbazi, A.; Richards, A. J.; Hoorfar, M. Numerical Study of the Effect of the Channel and Electrode Geometry on the Performance of Microfluidic Fuel Cells. *J. Power Sources* **2010**, *195*, 8141–8151. https://doi.org/10.1016/j.jpowsour.2010.06.094.

(205) D'Alessandro, J.; Fodor, P. S. Use of Grooved Microchannels to Improve the Performance of Membrane-Less Fuel Cells. *Fuel Cells* **2014**, *14*, 818–826. https://doi.org/10.1002/fuce.201400047.

(206) Lee, S. W.; Ahn, Y. Influence of Electrode Groove Geometry on the Passive Control of the Depletion Layer in Microfluidic Fuel Cells. *J. Micromech. Microeng.* **2015**, *25*, 127001. https://doi.org/10.1088/0960-1317/25/12/127001.

(207) Marschewski, J.; Ruch, P.; Ebejer, N.; Huerta Kanan, O.; Lhermitte, G.; Cabrol, Q.; Michel, B.; Poulikakos, D. On the Mass Transfer Performance Enhancement of Membraneless Redox Flow Cells with Mixing Promoters. *Int. J. Heat Mass Transfer* **2017**, *106*, 884–894. https://doi.org/10.1016/j.ijheatmasstransfer.2016.10.030.

(208) Stroock, A. D.; Dertinger, S. K. W.; Ajdari, A.; Mezić, I.; Stone, H. A.; Whitesides, G. M. Chaotic Mixer for Microchannels. *Science* **2002**, *295*, 647–651. https://doi.org/10.1126/science.1066238.

(209) Xuan, J.; Leung, M. K. H.; Leung, D. Y. C.; Ni, M.; Wang, H. Hydrodynamic Focusing in Microfluidic Membraneless Fuel Cells: Breaking the Trade-off between Fuel Utilization and Current Density. *Int. J. Hydrog. Energy* **2011**, *36*, 11075–11084. https://doi.org/10.1016/j.ijhydene.2011.05.150.

(210) Xuan, J.; Wang, H.; Leung, D. Y. C.; Leung, M. K. H.; Xu, H.; Zhang, L.; Shen, Y. Theoretical Graetz-Damköhler Modeling of an Air-Breathing Microfluidic Fuel Cell. *J. Power Sources* **2013**, *231*, 1–5. https://doi.org/10.1016/j.jpowsour.2012.12.090.

(211) Shaegh, S. A. M.; Nguyen, N.-T.; Chan, S. H. An Air-Breathing Microfluidic Formic Acid Fuel Cell with a Porous Planar Anode: Experimental and Numerical Investigations. *J. Micromech. Microeng.* **2010**, *20*, 105008. https://doi.org/10.1088/0960-1317/20/10/105008.

(212) Wang, Y.; Leung, D. Y. C.; Zhang, H.; Xuan, J.; Wang, H. Numerical Investigation and Optimization of Vapor-Feed Microfluidic Fuel Cells with High Fuel Utilization. *Electrochim. Acta* **2018**, *261*, 127–136. https://doi.org/10.1016/j.electacta.2017.12.132.

(213) Ouyang, T.; Lu, J.; Chen, J.; Xu, P.; Tian, Z. Q. Innovation of Vapor-Feed Microfluidic Fuel Cell with Novel Geometric Configuration and Operation Parameters Optimization. *Int. J. Hydrog. Energy* **2021**, *46*, 15976–15990. https://doi.org/10.1016/j.ijhydene.2021.02.099.

(214) Wang, Y.; Leung, D. Y. C. A Circular Stacking Strategy for Microfluidic Fuel Cells with Volatile Methanol Fuel. *Appl. Energy* **2016**, *184*, 659–669. https://doi.org/10.1016/j.apenergy.2016.11.019.

(215) Fuerth, D.; Bazylak, A. Up-Scaled Microfluidic Fuel Cells With Porous Flow-Through Electrodes. *J. Fluids Eng.* **2013**, *135*, 021102. https://doi.org/10.1115/1.4023449.

(216) Zhang, B.; Ye, D. D.; Sui, P. C.; Djilali, N.; Zhu, X. Computational Modeling of Air-Breathing Microfluidic Fuel Cells with Flow-over and Flow-through Anodes. *J. Power Sources* **2014**, *259*, 15–24. https://doi.org/10.1016/j.jpowsour.2014.02.076.

(217) Li, L.; Zheng, K.; Ni, M.; Leung, M. K. H.; Xuan, J. Partial Modification of Flow-through Porous Electrodes in Microfluidic Fuel Cell. *Energy* **2015**, *88*, 563–571. https://doi.org/10.1016/j.energy.2015.05.085.

(218) Li, L.; Nikiforidis, G.; Leung, M. K. H.; Daoud, W. A. Vanadium Microfluidic Fuel Cell with Novel Multi-Layer Flow-through Porous Electrodes: Model, Simulations and Experiments. *Appl. Energy* **2016**, *177*, 729–739. https://doi.org/10.1016/j.apenergy.2016.05.072.

(219) Wang, H. N.; Zhu, X.; Zhang, B.; Ye, D. D.; Chen, R.; Liao, Q.; Sui, P. C.; Djilali, N. Two-Phase Computational Modelling of a Membraneless Microfluidic Fuel Cell with a Flow-through Porous Anode. *J. Power Sources* **2019**, *420*, 88–98. https://doi.org/10.1016/j.jpowsour.2019.02.081.

(220) Tanveer, M.; Kim, K. A Membraneless Microfluidic Fuel Cell with a Hollow Flow Channel and Porous Flow-through Electrodes. *Int. J. Energy Res.* **2021**, *45*, 8536–8550. https://doi.org/10.1002/er.6390.

(221) Yang, Y.; Ye, D.; Zhu, X.; Liao, Q.; Li, J.; Chen, R. Boosting Power Density of Microfluidic Biofuel Cell with Porous Three-Dimensional Graphene@nickel Foam as Flow-through Anode. *Int. J. Hydrog. Energy* **2018**, *43*, 18516–18520. https://doi.org/10.1016/j.ijhydene.2018.08.052.

(222) Li, L.; Bei, S.; Liu, R.; Xu, Q.; Zheng, K.; She, Y.; He, Y. Design of a Radial Vanadium Redox Microfluidic Fuel Cell: A New Way to Break the Size Limitation. *Int. J. Energy Res.* **2019**, *43*, 3028–3037. https://doi.org/10.1002/er.4473.

(223) Ho, B.; Kjeang, E. Planar Multiplexing of Microfluidic Fuel Cells. *J. Fluids Eng.* **2013**, *135*, 021304.

(224) Wang, H.; Gu, S.; Leung, D. Y. C.; Xu, H.; Leung, M. K. H.; Zhang, L.; Xuan, J. Development and Characteristics of a Membraneless Microfluidic Fuel Cell Array. *Electrochim. Acta* **2014**, *135*, 467–477. https://doi.org/10.1016/j.electacta.2014.04.165.

(225) Copenhaver, T. S.; Purohit, K. H.; Domalaon, K.; Pham, L.; Burgess, B. J.; Manorothkul, N.; Galvan, V.; Sotez, S.; Gomez, F. A.; Haan, J. L. A Microfluidic Direct Formate Fuel Cell on Paper. *Electrophoresis* **2015**, *36*, 1825–1829. https://doi.org/10.1002/elps.201400554.

(226) Galvan, V.; Domalaon, K.; Tang, C.; Sotez, S.; Mendez, A.; Jalali-Heravi, M.; Purohit, K.; Pham, L.; Haan, J.; Gomez, F. A. An Improved Alkaline Direct Formate Paper Microfluidic Fuel Cell. *Electrophoresis* **2016**, *37*, 504–510. https://doi.org/10.1002/elps.201500360.

(227) Lal, S.; Janardhanan, V. M.; Deepa, M.; Sagar, A.; Sahu, K. C. Low Cost Environmentally Benign Porous Paper Based Fuel Cells for Micro-Nano Systems. *J. Electrochem. Soc.* **2015**, *162*, F1402–F1407. https://doi.org/10.1149/2.0251514jes.

(228) Chandra, S.; Lal, S.; Janardhanan, V. M.; Sahu, K. C.; Deepa, M. Ethanol Based Fuel Cell on Paper Support. *J. Power Sources* **2018**, *396*, 725–733. https://doi.org/10.1016/j.jpowsour.2018.06.068.

(229) Purohit, K. H.; Emrani, S.; Rodriguez, S.; Liaw, S. S.; Pham, L.; Galvan, V.; Domalaon, K.; Gomez, F. A.; Haan, J. L. A Microfluidic Galvanic Cell on a Single Layer of Paper. *J. Power Sources* **2016**, *318*, 163–169. https://doi.org/10.1016/j.jpowsour.2016.03.109.

(230) Lal, S.; Deepa, M.; Sahu, K. C.; Janardhanan, V. M. Methanol-Based Fuel Cell on Paper Support with N-Doped Graphene Oxide/Nickel Cobaltite Composite Catalyst. *J. Electrochem. Soc.* **2019**, *166*, F190–F197. https://doi.org/10.1149/2.0301904jes.

(231) del Torno-de Román, L.; Navarro, M.; Hughes, G.; Esquivel, J. P.; Milton, R. D.; Minteer, S. D.; Sabaté, N. Improved Performance of a Paper-Based Glucose Fuel Cell by Capillary Induced Flow. *Electrochim. Acta* **2018**, *282*, 336–342. https://doi.org/10.1016/j.electacta.2018.05.074.

(232) Jung, D. G.; Ahn, Y. Microfabricated Paper-Based Vanadium Co-Laminar Flow Fuel Cell. *J. Power Sources* **2020**, *451*, 227801. https://doi.org/10.1016/j.jpowsour.2020.227801.

(233) Pasala, V.; Ramanujam, K. Flexible Paper-Based Borohydride-Vanadium Fuel Cell for Powering Micro-Nanosystems. *Ionics* **2017**, *23*, 1811–1817. https://doi.org/10.1007/s11581-017-1987-z.

(234) Yan, X.; Xu, A.; Zeng, L.; Gao, P.; Zhao, T. A Paper-Based Microfluidic Fuel Cell with Hydrogen Peroxide as Fuel and Oxidant. *Energy Technol.* **2018**, *6*, 140-143. https://doi.org/10.1002/ente.201700470.

(235) Esquivel, J. P.; Buser, J. R.; Lim, C. W.; Rojas, S.; Yager, P. Single-Use Paper-Based Hydrogen Fuel Cells for Point-of-Care Diagnostic Applications. *J. Power Sources* **2017**, *342*, 442–451. https://doi.org/10.1016/j.jpowsour.2016.12.085.

(236) Shen, L. L.; Zhang, G. R.; Venter, T.; Biesalski, M.; Etzold, B. J. M. Towards Best Practices for Improving Paper-Based Microfluidic Fuel Cells. *Electrochim. Acta* **2019**, *298*, 389–399. https://doi.org/10.1016/j.electacta.2018.12.077.

(237) Liu, Z.; Ye, D.; Chen, R.; Zhang, B.; Zhu, X.; Liao, Q. A Dual-Functional Three-Dimensional Herringbone-like Electrode for a Membraneless Microfluidic Fuel Cell. *J. Power Sources* **2019**, *438*, 227058. https://doi.org/10.1016/j.jpowsour.2019.227058.

(238) Liu, Z.; Ye, D.; Chen, R.; Zhang, B.; Zhu, X.; Li, J.; Liao, Q. A Woven Thread-Based Microfluidic Fuel Cell with Graphite Rod Electrodes. *Int. J. Hydrog. Energy* **2018**, *43*, 22467–22473. https://doi.org/10.1016/j.ijhydene.2018.10.086.

(239) Domalaon, K.; Tang, C.; Mendez, A.; Bernal, F.; Purohit, K.; Pham, L.; Haan, J.; Gomez, F. A. Fabric-Based Alkaline Direct Formate Microfluidic Fuel Cells. *Electrophoresis* **2017**, *38,* 1224-1231. https://doi.org/10.1002/elps.201600306.

(240) Lee, K. B. Urine-Activated Paper Batteries for Biosystems. *J. Micromech. Microeng.* **2005**, *15*, S210. https://doi.org/10.1088/0960-1317/15/9/S06.

(241) Thom, N. K.; Yeung, K.; Pillion, M. B.; Phillips, S. T. "Fluidic Batteries" as Low-Cost Sources of Power in Paper-Based Microfluidic Devices. *Lab Chip* **2012**, *12*, 1768-1770. https://doi.org/10.1039/c2lc40126f.

(242) Zhang, X.; Li, J.; Chen, C.; Lou, B.; Zhang, L.; Wang, E. A Self-Powered Microfluidic Origami Electrochemiluminescence Biosensing Platform. *Chem. Commun.* **2013**, *49*, 3866–3868. https://doi.org/10.1039/c3cc40905h.

(243) Koo, Y.; Sankar, J.; Yun, Y. High Performance Magnesium Anode in Paper-Based Microfluidic Battery, Powering on-Chip Fluorescence Assay. *Biomicrofluidics* **2014**, *8*, 054104. https://doi.org/10.1063/1.4894784.

(244) Chen, S.-S.; Hu, C.-W.; Yu, I.-F.; Liao, Y.-C.; Yang, J.-T. Origami Paper-Based Fluidic Batteries for Portable Electrophoretic Devices. *Lab Chip* **2014**, *14*, 2124–2130. https://doi.org/10.1039/c4lc00091a.

(245) Lee, H.; Choi, S. An Origami Paper-Based Bacteria-Powered Battery. *Nano Energy* **2015**, *15*, 549–557. https://doi.org/http://dx.doi.org/10.1016/j.nanoen.2015.05.019.

(246) Wang, Y.; Pan, W.; Luo, S.; Zhao, X.; Kwok, H. Y. H.; Leung, D. Y. C. Integrating Micro Metal-air Batteries in Lateral Flow Test for Point-of-care Applications. *Int. J. Energy Res.* **2020**, 1–10. https://doi.org/10.1002/er.5953.

(247) Wang, Y.; Kwok, H. Y. H.; Pan, W.; Zhang, H.; Lu, X.; Leung, D. Y. C. Parametric Study and Optimization of a Low-Cost Paper-Based Al-Air Battery with Corrosion Inhibition Ability. *Appl. Energy* **2019**, *251*, 113342. https://doi.org/10.1016/j.apenergy.2019.113342.

(248) Wang, Y.; Kwok, H.; Pan, W.; Zhang, H.; Leung, D. Y. C. Innovative Paper-Based Al-Air Batteries as a Low-Cost and Green Energy Technol. for the Miniwatt Market. *J. Power Sources* **2019**, *414*, 278–282. https://doi.org/10.1016/j.jpowsour.2019.01.018.

(249) Shen, L.-L.; Zhang, G.-R.; Biesalski, M.; Etzold, B. J. M. Paper-Based Microfluidic Aluminum–Air Batteries: Toward next-Generation Miniaturized Power Supply. *Lab Chip* **2019**, *19*, 3438–3447. https://doi.org/10.1039/C9LC00574A.

(250) Bamgbopa, M. O.; Almheiri, S.; Sun, H. Prospects of Recently Developed Membraneless Cell Designs for Redox Flow Batteries. *Renew. Sustain. Energy Rev.* **2017**, *70*, 506–518. https://doi.org/10.1016/j.rser.2016.11.234.

(251) Braff, W. A.; Buie, C. R.; Bazant, M. Z. Boundary Layer Analysis of Membraneless Electrochemical Cells. *J. Electrochem. Soc.* **2013**, *160*, A2056–A2063. https://doi.org/10.1149/2.052311jes.

(252) Goulet, M.-A.; Kjeang, E. Reactant Recirculation in Electrochemical Co-Laminar Flow Cells. *Electrochim. Acta* **2014**, *140*, 217–224. https://doi.org/10.1016/j.electacta.2014.03.092.

(253) Ibrahim, O. A.; Goulet, M. A.; Kjeang, E. In-Situ Characterization of Symmetric Dual-Pass Architecture of Microfluidic Co-Laminar Flow Cells. *Electrochim. Acta* **2016**, *187*, 277–285. https://doi.org/10.1016/j.electacta.2015.11.081.

(254) Suss, M. E.; Conforti, K.; Gilson, L.; Buie, C. R.; Bazant, M. Z. Membraneless Flow Battery Leveraging Flow-through Heterogeneous Porous Media for Improved Power Density and Reduced Crossover. *RSC Adv.* **2016**, *6*, 100209–100213. https://doi.org/10.1039/C6RA22608F.

(255) Marma, K.; Kolli, J.; Cho, K. T. Membrane-Less Hydrogen Iron Redox Flow Battery. *J. Electrochem. Energy Convers. Storage* **2019**, *16*, 011005. https://doi.org/10.1115/1.4040329.

(256) Leung, P. K.; Martin, T.; Shah, A. A.; Mohamed, M. R.; Anderson, M. A.; Palma, J. Membrane-Less Hybrid Flow Battery Based on Low-Cost Elements. *J. Power Sources* **2017**, *341*, 36–45. https://doi.org/10.1016/j.jpowsour.2016.11.062.

(257) Leung, P. K.; Martin, T.; Shah, A. A.; Anderson, M. A.; Palma, J. Membrane-Less Organic–Inorganic Aqueous Flow Batteries with Improved Cell Potential. *Chem. Commun.* **2016**, *52*, 14270–14273. https://doi.org/10.1039/C6CC07692K.

(258) Karakurt, I.; Elwood, J.; Li, X.; Beker, L.; Sweet, E.; Cai, W.; Lin, L. Membraneless Microfluidic Redox Battery for Wearable Electronics Applications. In *Proceedings of 19th International Conference on Solid-State Sensors, Actuators and Microsystems (TRANSDUCERS)*; IEEE: Kaohsiung, Taiwan, 18-22 June, 2017; pp 1820–1823. https://doi.org/10.1109/TRANSDUCERS.2017.7994423.

(259) Navalpotro, P.; Palma, J.; Anderson, M.; Marcilla, R. A Membrane-Free Redox Flow Battery with Two Immiscible Redox Electrolytes. *Angew. Chem. Int. Ed.* **2017**, *56*, 12460–12465. https://doi.org/10.1002/anie.201704318.

(260) Navalpotro, P.; Sierra, N.; Trujillo, C.; Montes, I.; Palma, J.; Marcilla, R. Exploring the Versatility of Membrane-Free Battery Concept Using Different Combinations of Immiscible Redox Electrolytes. *ACS Appl. Mater. Interfaces* **2018**, *10*, 41246–41256. https://doi.org/10.1021/acsami.8b11581.

(261) Navalpotro, P.; Trujillo, C.; Montes, I.; Neves, C. M. S. S.; Palma, J.; Freire, M. G.; Coutinho, J. A. P.; Marcilla, R. Critical Aspects of Membrane-Free Aqueous Battery Based on Two Immiscible Neutral Electrolytes. *Energy Storage Mater.* **2020**, *26*, 400–407. https://doi.org/10.1016/j.ensm.2019.11.011.

(262) Bamgbopa, M. O.; Shao-Horn, Y.; Hashaikeh, R.; Almheiri, S. Cyclable Membraneless Redox Flow Batteries Based on Immiscible Liquid Electrolytes: Demonstration with All-Iron Redox Chemistry. *Electrochim. Acta* **2018**, *267*, 41–50. https://doi.org/10.1016/j.electacta.2018.02.063.

(263) Gong, K.; Xu, F.; Lehrich, M. G.; Ma, X.; Gu, S.; Yan, Y. Exploiting Immiscible Aqueous-Nonaqueous Electrolyte Interface toward a Membraneless Redox-Flow Battery Concept. *J. Electrochem. Soc.* **2017**, *164*, A2590–A2593. https://doi.org/10.1149/2.1241712jes.

(264) Molina-Osorio, A. F.; Gamero-Quijano, A.; Peljo, P.; Scanlon, M. D. Membraneless Energy Conversion and Storage Using Immiscible Electrolyte Solutions. *Curr. Opin. Electrochem.* **2020**, *21*, 100–108. https://doi.org/10.1016/j.coelec.2020.01.013.

(265) H. Hashemi, S. M.; Modestino, M. A.; Psaltis, D. A Membrane-Less Electrolyzer for Hydrogen Production across the PH Scale. *Energy Environ. Sci.* **2015**, *8*, 2003–2009. https://doi.org/10.1039/C5EE00083A.

(266) Oruc, M. E.; Desai, A. v.; Nuzzo, R. G.; Kenis, P. J. A. Design, Fabrication, and Characterization of a Proposed Microchannel Water Electrolyzer. *J. Power Sources* **2016**, *307*, 122–128. https://doi.org/10.1016/J.JPOWSOUR.2015.12.062.

(267) O'Neil, G. D.; Christian, C. D.; Brown, D. E.; Esposito, D. v. Hydrogen Production with a Simple and Scalable Membraneless Electrolyzer. *J. Electrochem. Soc.* **2016**, *163*, F3012–F3019. https://doi.org/10.1149/2.0021611jes.

(268) Rarotra, S.; Mandal, T. K.; Bandyopadhyay, D. Microfluidic Electrolyzers for Production and Separation of Hydrogen from Sea Water Using Naturally Abundant Solar Energy. *Energy Technol.* **2017**, *5*, 1208–1217. https://doi.org/10.1002/ente.201600512.

(269) Rarotra, S.; Shahid, S.; De, M.; Mandal, T. K.; Bandyopadhyay, D. Graphite/RGO Coated Paper μ-Electrolyzers for Production and Separation of Hydrogen and Oxygen. *Energy* **2021**, *228*, 120490. https://doi.org/10.1016/j.energy.2021.120490.

(270) Esposito, D. v. Membraneless Electrolyzers for Low-Cost Hydrogen Production in a Renewable Energy Future. *Joule* **2017**, *1*, 651–658. https://doi.org/10.1016/j.joule.2017.07.003.

(271) Campos-Roldán, C. A.; Zhong, H.; Unni, S. M.; González-Huerta, R. de G.; Feng, Y.; Alonso-Vante, N. Unitized Regenerative Alkaline Microfluidic Cell Based on Platinum Group Metal-Free Electrode Materials. *ACS Appl. Energy Mater.* **2020**, *3*, 7397–7403. https://doi.org/10.1021/acsaem.0c00788.

(272) Campos-Roldán, C. A.; Calvillo, L.; Boaro, M.; de Guadalupe González-Huerta, R.; Granozzi, G.; Alonso-Vante, N. NiO–Ni/CNT as an Efficient Hydrogen Electrode Catalyst for a Unitized Regenerative Alkaline Microfluidic Cell. *ACS Appl. Energy Mater.* **2020**, *3*, 4746–4755. https://doi.org/10.1021/acsaem.0c00375.

(273) Hadikhani, P.; Hashemi, S. M. H.; Schenk, S. A.; Psaltis, D. A Membrane-Less Electrolyzer with Porous Walls for High Throughput and Pure Hydrogen Production. *Sustain. Energy Fuels* **2021**, *5*, 2419–2432. https://doi.org/10.1039/D1SE00255D.

(274) Gillespie, M. I.; van der Merwe, F.; Kriek, R. J. Performance Evaluation of a Membraneless Divergent Electrode-Flow-through (DEFT) Alkaline Electrolyser Based on Optimisation of Electrolytic Flow and Electrode Gap. *J. Power Sources* **2015**, *293*, 228–235. https://doi.org/10.1016/j.jpowsour.2015.05.077.

(275) Gillespie, M. I.; Kriek, R. J. Hydrogen Production from a Rectangular Horizontal Filter Press Divergent Electrode-Flow-Through (DEFT^{TM}) Alkaline Electrolysis Stack. *J. Power Sources* **2017**, *372*, 252–259. https://doi.org/10.1016/j.jpowsour.2017.10.080.

(276) De, B. S.; Singh, A.; Elias, A.; Khare, N.; Basu, S. An Electrochemical Neutralization Energy-Assisted Membrane-Less Microfluidic Reactor for Water Electrolysis. *Sustain. Energy Fuels* **2020**, *4*, 6234–6244. https://doi.org/10.1039/D0SE01474E.

(277) Fan, L.; Xia, C.; Yang, F.; Wang, J.; Wang, H.; Lu, Y. Strategies in Catalysts and Electrolyzer Design for Electrochemical CO_2 Reduction toward C_{2+} Products. *Sci. Adv.* **2020**, *6*, eaay3111. https://doi.org/10.1126/sciadv.aay3111.

(278) Albo, J.; Alvarez-Guerra, M.; Castaño, P.; Irabien, A. Towards the Electrochemical Conversion of Carbon Dioxide into Methanol. *Green Chem.* **2015**, *17*, 2304–2324. https://doi.org/10.1039/C4GC02453B.

(279) Bevilacqua, M.; Filippi, J.; Miller, H. A.; Vizza, F. Recent Technological Progress in CO_2 Electroreduction to Fuels and Energy Carriers in Aqueous Environments. *Energy Technol.* **2015**, *3*, 197–210. https://doi.org/10.1002/ente.201402166.

(280) Yang, Y.; Li, F. Reactor Design for Electrochemical CO2 Conversion toward Large-Scale Applications. *Curr. Opin. Green Sustain. Chem.* **2021**, *27*, 100419. https://doi.org/10.1016/j.cogsc.2020.100419.

(281) Wu, J.; Ma, S.; Sun, J.; Gold, J. I.; Tiwary, C.; Kim, B.; Zhu, L.; Chopra, N.; Odeh, I. N.; Vajtai, R.; et al. A Metal-Free Electrocatalyst for Carbon Dioxide Reduction to Multi-Carbon Hydrocarbons and Oxygenates. *Nat. Commun.* **2016**, *7*, 13869. https://doi.org/10.1038/ncomms13869.

(282) Lv, J.; Jouny, M.; Luc, W.; Zhu, W.; Zhu, J.; Jiao, F. A Highly Porous Copper Electrocatalyst for Carbon Dioxide Reduction. *Adv. Mater.* **2018**, *30*, 1803111. https://doi.org/10.1002/adma.201803111.

(283) Lu, X.; Wu, Y.; Yuan, X.; Huang, L.; Wu, Z.; Xuan, J.; Wang, Y.; Wang, H. High-Performance Electrochemical CO $_2$ Reduction Cells Based on Non-Noble Metal Catalysts. *ACS Energy Lett.* **2018**, *3*, 2527–2532. https://doi.org/10.1021/acsenergylett.8b01681.

(284) Liang, S.; Altaf, N.; Huang, L.; Gao, Y.; Wang, Q. Electrolytic Cell Design for Electrochemical CO2 Reduction. *J. CO2 Util.* **2020**, *35*, 90–105. https://doi.org/10.1016/j.jcou.2019.09.007.

(285) Weekes, D. M.; Salvatore, D. A.; Reyes, A.; Huang, A.; Berlinguette, C. P. Electrolytic CO2 Reduction in a Flow Cell. *Acc. Chem. Res.* **2018**, *51*, 910–918. https://doi.org/10.1021/acs.accounts.8b00010.

(286) Endrődi, B.; Bencsik, G.; Darvas, F.; Jones, R.; Rajeshwar, K.; Janáky, C. Continuous-Flow Electroreduction of Carbon Dioxide. *Prog. Energy Combust. Sci.* **2017**, *62*, 133–154. https://doi.org/10.1016/j.pecs.2017.05.005.

(287) Lin, R.; Guo, J.; Li, X.; Patel, P.; Seifitokaldani, A. Electrochemical Reactors for CO2 Conversion. *Catalysts* **2020**, *10*, 473. https://doi.org/10.3390/catal10050473.

(288) Whipple, D. T.; Finke, E. C.; Kenis, P. J. A. Microfluidic Reactor for the Electrochemical Reduction of Carbon Dioxide: The Effect of PH. *Electrochem. Solid-State Lett.* **2010**, *13*, B109. https://doi.org/10.1149/1.3456590.

(289) Wu, K.; Birgersson, E.; Kim, B.; Kenis, P. J. A.; Karimi, I. A. Modeling and Experimental Validation of Electrochemical Reduction of CO_2 to CO in a Microfluidic Cell. *J. Electrochem. Soc.* **2015**, *162*, F23–F32. https://doi.org/10.1149/2.1021414jes.

(290) Wu, K.; Birgersson, E.; Kenis, P. J. A.; Karimi, I. A. Modeling and Simulating Electrochemical Reduction of CO2 in a Microfluidic Cell. *Comput. Aided Chem. Eng.* **2014**, *34*, 639–644. https://doi.org/10.1016/B978-0-444-63433-7.50091-2.

(291) Kotb, Y.; Fateen, S.-E. K.; Albo, J.; Ismail, I. Modeling of a Microfluidic Electrochemical Cell for the Electro-Reduction of CO_2 to CH_3OH. *J. Electrochem. Soc.* **2017**, *164*, E391–E400. https://doi.org/10.1149/2.0741713jes.

(292) Monroe, M. M.; Lobaccaro, P.; Lum, Y.; Ager, J. W. Membraneless Laminar Flow Cell for Electrocatalytic CO_2 Reduction with Liquid Product Separation. *J. Phys. D: Appl. Phys.* **2017**, *50*, 154006. https://doi.org/10.1088/1361-6463/aa6359.

(293) Wang, H.; Leung, D. Y. C.; Xuan, J. Modeling of a Microfluidic Electrochemical Cell for CO2 Utilization and Fuel Production. *Appl. Energy* **2013**, *102*, 1057–1062. https://doi.org/10.1016/j.apenergy.2012.06.020.

(294) Lu, X.; Leung, D. Y. C.; Wang, H.; Xuan, J. Microfluidics-Based PH-Differential Reactor for CO2 Utilization: A Mathematical Study. *Appl. Energy* **2018**, *227*, 525–532. https://doi.org/10.1016/j.apenergy.2017.08.191.

(295) Lu, X.; Leung, D. Y. C.; Wang, H.; Maroto-Valer, M. M.; Xuan, J. A PH-Differential Dual-Electrolyte Microfluidic Electrochemical Cells for CO2 Utilization. *Renew. Energy* **2016**, *95*, 277–285. https://doi.org/10.1016/j.renene.2016.04.021.

(296) Lu, X.; Leung, D. Y. C.; Wang, H.; Xuan, J. A High Performance Dual Electrolyte Microfluidic Reactor for the Utilization of CO2. *Appl. Energy* **2017**, *194*, 549–559. https://doi.org/10.1016/j.apenergy.2016.05.091.

(297) Lu, X.; Leung, D. Y. C.; Wang, H.; Xuan, J. Characterization of a Microfluidic Reactor for CO2 Conversion with Electrolyte Recycling. *Renew. Energy* **2017**, *102*, 15–20. https://doi.org/10.1016/j.renene.2016.10.025.

(298) Talabi, O. O.; Dorfi, A. E.; O'Neil, G. D.; Esposito, D. v. Membraneless Electrolyzers for the Simultaneous Production of Acid and Base. *Chem. Commun.* **2017**, *53*, 8006–8009. https://doi.org/10.1039/C7CC02361H.

(299) Girenko, D. v.; Velichenko, A. B. Selection of the Optimal Cathode Material to Synthesize Medical Sodium Hypochlorite Solutions in a Membraneless Electrolyzer. *Surf. Eng. Appl. Electrochem.* **2018**, *54*, 88–95. https://doi.org/10.3103/S1068375518010052.

(300) Sridhar, A.; Sabry, M. M.; Ruch, P.; Atienza, D.; Michel, B. PowerCool: Simulation of Integrated Microfluidic Power Generation in Bright Silicon MPSoCs. In *IEEE/ACM International Conference on Computer-Aided Design (ICCAD)*; San Jose, CA, USA, 2-6 November, 2014; pp 527–534. https://doi.org/10.1109/ICCAD.2014.7001401.

(301) Andreev, A. A.; Sridhar, A.; Sabry, M. M.; Zapater, M.; Ruch, P.; Michel, B.; Atienza, D. PowerCool: Simulation of Cooling and Powering of 3D MPSoCs with Integrated Flow Cell Arrays. *IEEE Trans. Comput.* **2018**, *67*, 73–85. https://doi.org/10.1109/TC.2017.2695179.

(302) Martins, C. A.; Fernández, P. S.; Camara, G. A. Alternative Uses for Biodiesel Byproduct: Glycerol as Source of Energy and High Valuable Chemicals. *Green Energy and Technology*. Springer International Publishing: Cham 2018, pp 159–186. https://doi.org/10.1007/978-3-319-73552-8_7.

(303) Velázquez-Hernández, I.; Zamudio, E.; Rodríguez-Valadez, F. J.; García-Gómez, N. A.; Álvarez-Contreras, L.; Guerra-Balcázar, M.; Arjona, N. Electrochemical Valorization of Crude Glycerol in Alkaline Medium for Energy Conversion Using Pd, Au and PdAu Nanomaterials. *Fuel* **2020**, *262*, 116556. https://doi.org/10.1016/j.fuel.2019.116556.

(304) Wouters, B.; Hereijgers, J.; de Malsche, W.; Breugelmans, T.; Hubin, A. Electrochemical Characterisation of a Microfluidic Reactor for Cogeneration of Chemicals and Electricity. *Electrochim. Acta* **2016**, *210*, 337–345. https://doi.org/10.1016/j.electacta.2016.05.187.

(305) Wouters, B.; Hereijgers, J.; de Malsche, W.; Breugelmans, T.; Hubin, A. Performance Study of a Microfluidic Reactor for Cogeneration of Chemicals and Electricity. *Chem. Eng. Res. Des.* **2019**, *142*, 336–345. https://doi.org/10.1016/j.cherd.2018.12.023.

(306) Fadakar, A.; Mardanpour, M. M.; Yaghmaei, S. The Coupled Microfluidic Microbial Electrochemical Cell as a Self-Powered Biohydrogen Generator. *J. Power Sources* **2020**, *451*, 227817. https://doi.org/10.1016/j.jpowsour.2020.227817.

(307) Li, M.; Liu, Y.; Dong, L.; Shen, C.; Li, F.; Huang, M.; Ma, C.; Yang, B.; An, X.; Sand, W. Recent Advances on Photocatalytic Fuel Cell for Environmental Applications—The Marriage of Photocatalysis and Fuel Cells. *Sci. Total Environ.* **2019**, *668*, 966–978. https://doi.org/10.1016/j.scitotenv.2019.03.071.

(308) Modestino, M. A.; Hashemi, S. M. H.; Haussener, S. Mass Transport Aspects of Electrochemical Solar-Hydrogen Generation. *Energy Environ. Sci.* **2016**, *9*, 1533–1551. https://doi.org/10.1039/C5EE03698D.

(309) Zhang, H.; Wang, H.; Leung, M. K. H.; Xu, H.; Zhang, L.; Xuan, J. Understanding the Performance of Optofluidic Fuel Cells: Experimental and Theoretical Analyses. *Chem. Eng. J.* **2016**, *283*, 1455–1464. https://doi.org/10.1016/j.cej.2015.08.124.

(310) Wang, N.; Zhang, X.; Wang, Y.; Yu, W.; Chan, H. L. W. Microfluidic Reactors for Photocatalytic Water Purification. *Lab Chip* **2014**, *14*, 1074–1082. https://doi.org/10.1039/C3LC51233A.

(311) Li, L.; Wang, G.; Chen, R.; Zhu, X.; Wang, H.; Liao, Q.; Yu, Y. Optofluidics Based Micro-Photocatalytic Fuel Cell for Efficient Wastewater Treatment and Electricity Generation. *Lab Chip* **2014**, *14*, 3368. https://doi.org/10.1039/C4LC00595C.

(312) Galindo-de-la-Rosa, J.; Álvarez, A.; Gurrola, M. P.; Rodríguez-Morales, J. A.; Oza, G.; Arriaga, L. G.; Ledesma-García, J. Alcohol Dehydrogenase Immobilized on TiO_2 Nanotubes for Ethanol Microfluidic Fuel Cells. *ACS Sustain. Chem. Eng.* **2020**, *8*, 10900–10910. https://doi.org/10.1021/acssuschemeng.0c03219.

(313) Li, L.; Xue, S.; Chen, R.; Liao, Q.; Zhu, X.; Wang, Z.; He, X.; Feng, H.; Cheng, X. Performance Characteristics of a Membraneless Solar Responsive Photocatalytic Fuel Cell with an Air-Breathing Cathode under Different Fuels and Electrolytes and Air Conditions. *Electrochim. Acta* **2015**, *182*, 280–288. https://doi.org/10.1016/j.electacta.2015.09.090.

(314) Kwok, Y. H.; Wang, Y.; Zhang, Y.; Zhang, H.; Li, F.; Pan, W.; Leung, D. Y. C. Boosting Cell Performance and Fuel Utilization Efficiency in a Solar Assisted Methanol Microfluidic Fuel Cell. *Int. J. Hydrog. Energy* **2020**, *45*, 21796–21807. https://doi.org/10.1016/j.ijhydene.2020.05.163.

(315) Ovando-Medina, V. M.; Dector, A.; Antonio-Carmona, I. D.; Romero-Galarza, A.; Martínez-Gutiérrez, H.; Olivares-Ramírez, J. M. A New Type of Air-Breathing Photo-Microfluidic Fuel Cell Based on ZnO/Au Using Human Blood as Energy Source. *Int. J. Hydrog. Energy* **2019**, *44*, 31423–31433. https://doi.org/10.1016/j.ijhydene.2019.10.003.

(316) Dector, D.; Ortega-Díaz, D.; Olivares-Ramírez, J. M.; Dector, A.; Pérez-Bueno, J. J.; Fernández, D.; Amaya-Cruz, D. M.; Reyes-Rojas, A. Harvesting Energy from Real Human Urine in a Photo-Microfluidic Fuel Cell Using TiO2–Ni Anode Electrode. *Int. J. Hydrog. Energy* **2021**, *46*, 26163–26173. https://doi.org/10.1016/j.ijhydene.2021.02.148.

(317) Hu, S. Membrane-Less Photoelectrochemical Devices for H_2O_2 Production: Efficiency Limit and Operational Constraint. *Sustain. Energy Fuels* **2019**, *3*, 101–114. https://doi.org/10.1039/C8SE00329G.

(318) Elmas, S.; Ambroz, F.; Chugh, D.; Nann, T. Microfluidic Chip for the Photocatalytic Production of Active Chlorine. *Langmuir* **2016**, *32*, 4952–4958. https://doi.org/10.1021/acs.langmuir.6b00748.

(319) Kalamaras, E.; Belekoukia, M.; Tan, J. Z. Y.; Xuan, J.; Maroto-Valer, M. M.; Andresen, J. M. A Microfluidic Photoelectrochemical Cell for Solar-Driven CO_2 Conversion into Liquid Fuels with CuO-Based Photocathodes. *Faraday Discuss.* **2019**, *215*, 329–344. https://doi.org/10.1039/C8FD00192H.

(320) Dumitrescu, I.; Yancey, D. F.; Crooks, R. M. Dual-Electrode Microfluidic Cell for Characterizing Electrocatalysts. *Lab Chip* **2012**, *12*, 986. https://doi.org/10.1039/c2lc21181e.

(321) Andersen, N. I.; Artyushkova, K.; Matanović, I.; Hickey, D. P.; Minteer, S. D.; Atanassov, P. Spectro-Electrochemical Microfluidic Platform for Monitoring Multi-Step Cascade Reactions. *ChemElectroChem* **2019**, *6*, 246–251. https://doi.org/10.1002/celc.201800578.

(322) Kjeang, E.; Roesch, B.; McKechnie, J.; Harrington, D. A.; Djilali, N.; Sinton, D. Integrated Electrochemical Velocimetry for Microfluidic Devices. *Microfluid. Nanofluidics* **2007**, *3*, 403–416. https://doi.org/10.1007/s10404-006-0128-1.

(323) Brushett, F. R.; Zhou, W.-P.; Jayashree, R. S.; Kenis, P. J. A. Alkaline Microfluidic Hydrogen-Oxygen Fuel Cell as a Cathode Characterization Platform. *J. Electrochem. Soc.* **2009**, *156*, B565. https://doi.org/10.1149/1.3083226.

(324) Brushett, F. R.; Naughton, M. S.; Ng, J. W. D.; Yin, L.; Kenis, P. J. A. Analysis of Pt/C Electrode Performance in a Flowing-Electrolyte Alkaline Fuel Cell. *Int. J. Hydrog. Energy* **2012**, *37*, 2559–2570. https://doi.org/10.1016/j.ijhydene.2011.10.078.

(325) Modestino, M. A.; Diaz-Botia, C. A.; Haussener, S.; Gomez-Sjoberg, R.; Ager, J. W.; Segalman, R. A. Integrated Microfluidic Test-Bed for Energy Conversion Devices. *Phys. Chem. Chem. Phys.* **2013**, *15*, 7050. https://doi.org/10.1039/c3cp51302e.

(326) Angulo, A.; van der Linde, P.; Gardeniers, H.; Modestino, M.; Fernández Rivas, D. Influence of Bubbles on the Energy Conversion Efficiency of Electrochemical Reactors. *Joule* **2020**, *4*, 555–579. https://doi.org/10.1016/j.joule.2020.01.005.

(327) Li, Y.; Yang, G.; Yu, S.; Kang, Z.; Mo, J.; Han, B.; Talley, D. A.; Zhang, F.-Y. In-Situ Investigation and Modeling of Electrochemical Reactions with Simultaneous Oxygen and Hydrogen Microbubble Evolutions in Water Electrolysis. *Int. J. Hydrog. Energy* **2019**, *44*, 28283–28293. https://doi.org/10.1016/j.ijhydene.2019.09.044.

(328) Hadikhani, P.; Hashemi, S. M. H.; Balestra, G.; Zhu, L.; Modestino, M. A.; Gallaire, F.; Psaltis, D. Inertial Manipulation of Bubbles in Rectangular Microfluidic Channels. *Lab Chip* **2018**, *18*, 1035–1046. https://doi.org/10.1039/C7LC01283G.

(329) Arbabi, F.; Kalantarian, A.; Abouatallah, R.; Wang, R.; Wallace, J. S.; Bazylak, A. Feasibility Study of Using Microfluidic Platforms for Visualizing Bubble Flows in Electrolyzer Gas Diffusion Layers. *J. Power Sources* **2014**, *258*, 142–149. https://doi.org/10.1016/j.jpowsour.2014.02.042.

(330) Yang, G.; Yu, S.; Li, Y.; Li, K.; Ding, L.; Xie, Z.; Wang, W.; Dohrmann, Y.; Zhang, F.-Y. A Simple Convertible Electrolyzer in Membraneless and Membrane-Based Modes for Understanding Water Splitting Mechanism. *J. Power Sources* **2021**, *487*, 229353. https://doi.org/10.1016/j.jpowsour.2020.229353.

(331) Hadikhani, P.; H. Hashemi, S. M.; Psaltis, D. The Impact of Surfactants on the Inertial Separation of Bubbles in Microfluidic Electrolyzers. *J. Electrochem. Soc.* **2020**, *167*, 134504. https://doi.org/10.1149/1945-7111/abb6ca.

(332) Davis, J. T.; Brown, D. E.; Pang, X.; Esposito, D. v. High Speed Video Investigation of Bubble Dynamics and Current Density Distributions in Membraneless Electrolyzers. *J. Electrochem. Soc.* **2019**, *166*, F312–F321. https://doi.org/10.1149/2.0961904jes.

(333) Shyu, J. C.; Huang, C. L. Characterization of Bubble Formation in Microfluidic Fuel Cells Employing Hydrogen Peroxide. *J. Power Sources* **2011**, *196*, 3233–3238. https://doi.org/10.1016/j.jpowsour.2010.12.005.

(334) Ibáñez, S. E.; Quintero, A. E.; García-Salaberri, P. A.; Vera, M. Effects of the Diffusive Mixing and Self-Discharge Reactions in Microfluidic Membraneless Vanadium Redox Flow Batteries. *Int. J. Heat Mass Transfer* **2021**, *170*, 121022. https://doi.org/10.1016/j.ijheatmasstransfer.2021.121022.

(335) Ibrahim, O. A.; Goulet, M.-A.; Kjeang, E. Microfluidic Electrochemical Cell Array in Series: Effect of Shunt Current. *J. Electrochem. Soc.* **2015**, *162*, F639–F644. https://doi.org/10.1149/2.0211507jes.

(336) Snowden, M. E.; King, P. H.; Covington, J. A.; Macpherson, J. v.; Unwin, P. R. Fabrication of Versatile Channel Flow Cells for Quantitative Electroanalysis Using Prototyping. *Anal. Chem.* **2010**, *82*, 3124–3131. https://doi.org/10.1021/ac100345v.

(337) Holm, T.; Ingdal, M.; Fanavoll, E. v.; Sunde, S.; Seland, F.; Harrington, D. A. Mass-Transport Impedance at Channel Electrodes: Accurate and Approximate Solutions. *Electrochim. Acta* **2016**, *202*, 84–89. https://doi.org/10.1016/j.electacta.2016.03.096.

(338) Holm, T.; Ingdal, M.; Strobl, J. R.; Fanavoll, E. v.; Sunde, S.; Seland, F.; Harrington, D. A. Generator-Sensor Impedance at Double Channel Electrodes. *Electrochim. Acta* **2017**, *229*, 452–457. https://doi.org/10.1016/j.electacta.2017.01.075.

(339) Kimlinger, M. J.; Martin, R. S. The Use of a 3D-Printed Microfluidic Device and Pressure Mobilization for Integrating Capillary Electrophoresis with Electrochemical Detection. *Electroanalysis* **2018**, *30*, 2241–2249. https://doi.org/10.1002/elan.201800367.

(340) Munshi, A. S.; Martin, R. S. Microchip-Based Electrochemical Detection Using a 3-D Printed Wall-Jet Electrode Device. *Analyst* **2016**, *141*, 862–869. https://doi.org/10.1039/C5AN01956G.

(341) Trindade, M. A. G.; Martins, C. A.; Angnes, L.; Herl, T.; Raith, T.; Matysik, F.-M. New Electrochemical Flow-Cell Configuration Integrated into a Three-Dimensional Microfluidic Platform: Improving Analytical Application in the Presence of Air Bubbles. *Anal. Chem.* **2018**, *90*, 10917–10926. https://doi.org/10.1021/acs.analchem.8b02438.

(342) Munshi, A. S.; Chen, C.; Townsend, A. D.; Martin, R. S. Use of 3D Printing and Modular Microfluidics to Integrate Cell Culture, Injections and Electrochemical Analysis. *Anal. Methods* **2018**, *10*, 3364–3374. https://doi.org/10.1039/C8AY00829A.

(343) Walgama, C.; Nguyen, M. P.; Boatner, L. M.; Richards, I.; Crooks, R. M. Hybrid Paper and 3D-Printed Microfluidic Device for Electrochemical Detection of Ag Nanoparticle Labels. *Lab Chip* **2020**, *20*, 1648–1657. https://doi.org/10.1039/D0LC00276C.

(344) Ortega, L.; Llorella, A.; Esquivel, J. P.; Sabaté, N. Paper-Based Batteries as Conductivity Sensors for Single-Use Applications. *ACS Sens.* **2020**, *5*, 1743–1749. https://doi.org/10.1021/acssensors.0c00405.

(345) Sansuk, S.; Bitziou, E.; Joseph, M. B.; Covington, J. A.; Boutelle, M. G.; Unwin, P. R.; Macpherson, J. v. Ultrasensitive Detection of Dopamine Using a Carbon Nanotube Network Microfluidic Flow Electrode. *Anal. Chem.* **2013**, *85*, 163–169. https://doi.org/10.1021/ac3023586.

(346) Erkal, J. L.; Selimovic, A.; Gross, B. C.; Lockwood, S. Y.; Walton, E. L.; McNamara, S.; Martin, R. S.; Spence, D. M. 3D Printed Microfluidic Devices with Integrated Versatile and Reusable Electrodes. *Lab Chip* **2014**, *14*, 2023–2032. https://doi.org/10.1039/C4LC00171K.

(347) Dávila, D.; Esquivel, J. P.; Sabaté, N.; Mas, J. Silicon-Based Microfabricated Microbial Fuel Cell Toxicity Sensor. *Biosens. Bioelectron.* **2011**, *26*, 2426–2430. https://doi.org/10.1016/j.bios.2010.10.025.

(348) Fernández-la-Villa, A.; Pozo-Ayuso, D. F.; Castaño-Álvarez, M. Microfluidics and Electrochemistry: An Emerging Tandem for next-Generation Analytical Microsystems. *Curr. Opin. Electrochem.* **2019**, *15*, 175–185. https://doi.org/10.1016/j.coelec.2019.05.014.

(349) Wongkaew, N.; Simsek, M.; Griesche, C.; Baeumner, A. J. Functional Nanomaterials and Nanostructures Enhancing Electrochemical Biosensors and Lab-on-a-Chip Performances: Recent Progress, Applications, and Future Perspective. *Chem. Rev.* **2019**, *119*, 120–194. https://doi.org/10.1021/acs.chemrev.8b00172.

(350) Kudr, J.; Zitka, O.; Klimanek, M.; Vrba, R.; Adam, V. Microfluidic Electrochemical Devices for Pollution Analysis–A Review. *Sens. Actuators B Chem.* **2017**, *246*, 578–590. https://doi.org/10.1016/j.snb.2017.02.052.

A table of contents (TOC) graphic